QUATERNARY FAULTING IN CLAYTON VALLEY, NEVADA: IMPLICATIONS FOR DISTRIBUTED DEFORMATION IN THE EASTERN CALIFORNIA SHEAR ZONE-WALKER LANE

A Thesis
Presented to
The Academic Faculty

by

Travis Andrew Foy

In Partial Fulfillment
of the Requirements for the Degree
Master of Science in the
School of Earth and Atmospheric Sciences

Georgia Institute of Technology
May 2011

QUATERNARY FAULTING IN CLAYTON VALLEY, NEVADA: IMPLICATIONS FOR DISTRIBUTED DEFORMATION IN THE EASTERN CALIFORNIA SHEAR ZONE-WALKER LANE

Approved by:

Dr. Kurt Frankel, Advisor
School of Earth and Atmospheric Sciences
Georgia Institute of Technology

Dr. Andrew Newman
School of Earth and Atmospheric Sciences
Georgia Institute of Technology

Dr. Zhigang Peng
School of Earth and Atmospheric Sciences
Georgia Institute of Technology

Date Approved: March 31st, 2011

ACKNOWLEDGEMENTS

First and foremost I would like to thank my advisor, Kurt Frankel for all of his support. He not only helped me learn a great deal more about geology, but his enthusiastic teaching also made work a fun and enjoyable experience. I would also like to thank my other committee members, Andrew Newman and Zhigang Peng for useful comments and suggestions that helped improve the manuscript. I am also greatly indebted to Zach Lifton and Chris Johnson for their help with mapping efforts and, most importantly, with digging pits for soil sampling. Tina Marstellar provided essential aid with cosmogenic nuclide sample preparation in the lab, and Jeff Hoeft was also very helpful in preparation for field work. I would also like to thank Cristina Weber for her constant support throughout grad school. Finally I would like to thank my parents, Joe and Sharon Foy, for their continued support and encouragement. This work was supported financially by NSF and the Geological Society of America's Grants-in-Aid program.

TABLE OF CONTENTS

LIST OF TABLES

LIST OF FIGURES

SUMMARY

The eastern California shear zone (ECSZ) and Walker Lane belt represent an important inland component of the Pacific-North America plate boundary. Current geodetic data indicate accumulation of transtensional shear at a rate of ~9.2 ± 0.3 mm/yr across the region, more than double the total geologic rate ($\leq$ 3.5 mm/yr) for faults in the northern ECSZ over the late Pleistocene [*Bennett et al*., 2003, *Kirby et al*., 2006, *Lee et al*., 2009, *Frankel et al*., 2007]. Unraveling the strain puzzle of the Walker Lane is therefore essential to understanding both how deformation is distributed through the lithosphere along this transtensional part of the Pacific-North America plate boundary and how the plate boundary is evolving through time. The observed mismatch between geodetic and geologic slip rates in the central Walker Lane is characteristic of other active tectonic settings, including the nearby Mojave segment of the ECSZ [*Oskin et al*., 2008] and the Altyn Tagh fault in China [*Cowgill*, 2007]. In each case, lack of fault slip data spanning multiple temporal and spatial scales hinders interpretation of fault interactions and their implications for lithospheric dynamics. The discrepancy between geodetic and geologic slip rates in the northern ECSZ-Walker Lane transition indicates that if strain rates have remained constant since the late Pleistocene [e.g. *Frankel et al.,* in press], then the "missing" strain is distributed on structures other than the two major dextral faults at this latitude (Death Valley-Fish Lake Valley fault and White Mountains fault). Otherwise the region could presently be experiencing a strain transient similar to that of the nearby Mojave section of the ECSZ [e.g., Oskin et al., 2008], or the rate of strain accumulation could actually be increasing over the late Pleistocene [e.g. *Reheis and*

Sawyer, 1997; *Hoeft and Frankel*, 2010]. The Silver Peak-Lone Mountain extensional complex (SPLM), to which the Clayton Valley faults belong, is the prime candidate to account for the "missing" strain. The down-to-the-northwest orientation of the SPLM faults makes them the most kinematically suitable structures to accommodate the regional pattern of NW-SE dextral shear.

We use differential GPS to measure fault offsets and terrestrial cosmogenic nuclide (TCN) geochronology to date offset landforms. Using these tools, we measure extension rates that are time-invariant, ranging from 0.1 ± 0.1 to 0.3 ± 0.1 mm/yr for fault dips of 30° and 60°. These rates are not high enough to account for the discrepancy between geologic and geodetic data in the ECSZ-Walker Lane transition zone. Based on geologic mapping and previously published geophysical data [*Davis*, 1981; *Zampirro*, 2005], deformation through Clayton Valley appears to be very widely-distributed. The diffuse nature of deformation leads to geologic slip rates that are underestimated due to the effects of off-fault deformation and unrecognized fault strands. Our results from Clayton Valley suggest that the discrepancy between geodetic and geologic strain rates at the latitude of the northern ECSZ is a result of long-term geologic rates that are underestimated. If the true geologic rates could be calculated, they would likely be significantly higher and therefore in closer agreement with geodetic data, as is the case everywhere else in the ECSZ north of the Garlock fault [*Frankel et al.*, 2007a, in press; *Kirby et al.*, 2008; *Lee et al.*, 2009a].

CHAPTER 1

INTRODUCTION

One of the major unresolved issues in modern tectonics is the relative temporal and spatial constancy of strain accumulation and release rates along active plate boundaries. This field of research has grown considerably with recent technological advances, such as Global Positioning Systems (GPS), and improved dating techniques, such as terrestrial cosmogenic nuclide (TCN) geochronology, that allow for a previously unprecedented level of accuracy and precision in measuring strain rates and dating deformed geomorphic features [e.g., *Dixon et al.,* 2000; *Gosse and Phillips,* 2001; *Bennett et al.,* 2003]. Combining these tools allows for accurate determination of strain rates over a wide range of timescales, which in turn provides the data necessary to address the relative temporal and spatial constancy of strain rates along active plate boundaries.

Along most plate boundaries strain rates appear to be relatively constant through time [e.g., *Sieh and Jahns,* 1984; *Wernicke et al.,* 2000; *Argus and* Gordon, 2001; Sella *et al.*, 2002; *Bennett et al.,* 2003; *Frankel et al.,* 2007a; *Kozaci et al.,* 2007; *Cowgill et al.,* 2009; *Lee et al.,* 2009a]. There are, however, numerous recent studies that show evidence of deviations from this steady-state behavior along individual fault systems [e.g., *Rockwell et al.,* 2000; *Peltzer et al.,* 2001; *Lee et al.,* 2001a, 2001b, 2009a, 2009b; *Friedrich et al.,* 2003, 2004; *Oskin and Iriondo*, 2004; *Niemi et al.,* 2004; *Weldon et al.,* 2004; *Dolan et al.,* 2007; *Chevalier et al.,* 2005; *Kylander-Clark et al.,* 2005; *Walker et al.,* 2005; *Kirby et al.,* 2006; *Cowgill,* 2007; *Le et al.,* 2007; *Frankel et al.,* 2007a, 2007b;

Oskin et al., 2007, 2008; *Andrew and Walker*, 2009; *Hoeft and Frankel*, 2010]. It remains unclear if temporal variations in strain rate are common along active margins or if they are localized features that mark regions of structural complexity [*Dixon et al.,* 2003; *Friedrich et al.,* 2003; *Bennett et al.,* 2004; *Dolan et al.,* 2007; *Wernicke et al.,* 2008]. The Pacific-North America plate boundary in the western United States offers an ideal setting in which to investigate plate boundary dynamics as this tectonically active region is covered with a dense GPS network and is characterized by an arid environment that preserves excellent exposure of deformed geomorphic features.

Transform motion along the Pacific-North America boundary is accommodated primarily along the right-lateral San Andreas fault system with most residual motion taken up on structures of the eastern California shear zone (ECSZ) and Walker Lane belt in eastern California and western Nevada [Figure 1; *Burchfiel*, 1979; *Dokka*, 1983; *Stewart*, 1988; *Dokka and Travis*, 1990; *Humphreys and Weldon*, 1994; *Reheis and Dixon*, 1996; *Reheis and Sawyer*, 1997; *Hearn and Humphreys*, 1998; *Thatcher et al.*, 1999; *Dixon et al.*, 2000, 2003; *Flesch et al.*, 2000; *McClusky et al.*, 2001 *Miller et al.*, 2001; *Oldow et al.*, 2001; *Bennett et al.*, 2003; *Faulds et al.*, 2005; *Wesnousky*, 2005a, 2005b; *Kirby et al.*, 2006; *Hammond and Thatcher*, 2007; *Frankel et al.*, 2007a, 2007b, 2008, in press; *Oskin et al.*, 2008; *Kreemer et al.*, 2009; *Lee et al.*, 2009a; *Ganev et al.*, 2010; *Liu et al.*, 2010]. This inland portion of the plate boundary consists of a complex arrangement of strike-slip and normal faults that accommodate dextral transtensional shear at a rate of ~9.3 ± 0.2 mm/yr, or about 25% of the total Pacific-North America plate boundary motion [Figure 1**,** *Bennett et al.*, 2003]. As such, the ECSZ and Walker Lane represent an important, evolving component of the plate boundary that is essential to

understanding the kinematics and dynamics of plate boundary deformation in western North America.

Some portions of the Pacific-North America plate boundary appear to display relatively constant strain rates over late Pleistocene to recent timescales [e.g., *Wernicke et al.*, 2000; *Argus and Gordon*, 2001; *Bennett et al.*, 2003; *Frankel et al.*, 2007, in press, *Lee et al.*, 2009a], while other areas exhibit apparent variations in rates of strain storage and release over the same time interval. One such area is in the Mojave Desert where the long-term slip rate over the Quaternary is $\leq 6.2 \pm 1.9$ mm/yr, in contrast to the geodetic measurements of 12 ± 2 mm/yr [*Oskin et al.*, 2008]. This discrepancy suggests a pronounced strain transient through the Mojave section of the ECSZ [*Oskin and Iriondo*, 2004; *Oskin et al.*, 2008].

Similarly, a discrepancy between geodetic and geologic data is observed in the northern ECSZ at ~37.5° N latitude (Figures 1 and 2). The two main faults accommodating plate boundary motion at this latitude are the White Mountains fault zone and the Death Valley-Fish Lake Valley fault zone. Summing the late Pleistocene to recent slip rates for these faults yields a total rate of ≤ 3.5 mm/yr [*Kirby et al.*, 2006; *Frankel et al.*, 2007b], which is less than half of the current region-wide geodetic rate of $\sim 9.3 \pm 0.2$ mm/yr [*Bennett et al.*, 2003; *Frankel et al.*, 2007b]. The most likely structures to account for the "missing" strain are the faults of the Silver Peak-Lone Mountain (SPLM) extensional complex (Figure 2) due to their down-to-the-northwest orientation [e.g., *Oldow*, 2003; *Wesnousky*, 2005a; *Hoeft and Frankel*, 2010]. The extensional complex connects regions of dominantly NW-trending dextral shear to the north and south and has likely played an important role in transferring strain through the ECSZ-Walker Lane since at least the Miocene [*Stewart*, 1988; *Oldow*, 1992; *Oldow et al.*, 1994, 2008; *Petronis et al.*, 2002, 2007, 2009].

As such, the Clayton Valley fault zone and the SPLM extensional complex as a whole represent an important part of this evolving portion of the plate boundary. In order to better understand the dynamics of plate boundary deformation at this latitude, herein, we investigate the late Quaternary history of the Clayton Valley fault zone using differential GPS fault scarp surveys to measure offsets and TCN geochronology to date offset landforms. Combining these tools, we discern extension rates over multiple late Pleistocene to recent timescales with the goal of understanding the role that distributed extensional faulting plays in accommodating strain along this important segment of the Pacific-North America plate boundary. The faults of the extensional complex are the most kinematically suitable structures to account for the geodetic-geologic rate discrepancy at this latitude. Therefore, the recent evolution of the extensional complex has important implications for the dynamics of plate boundary deformation through this portion of the ECSZ and Walker Lane.

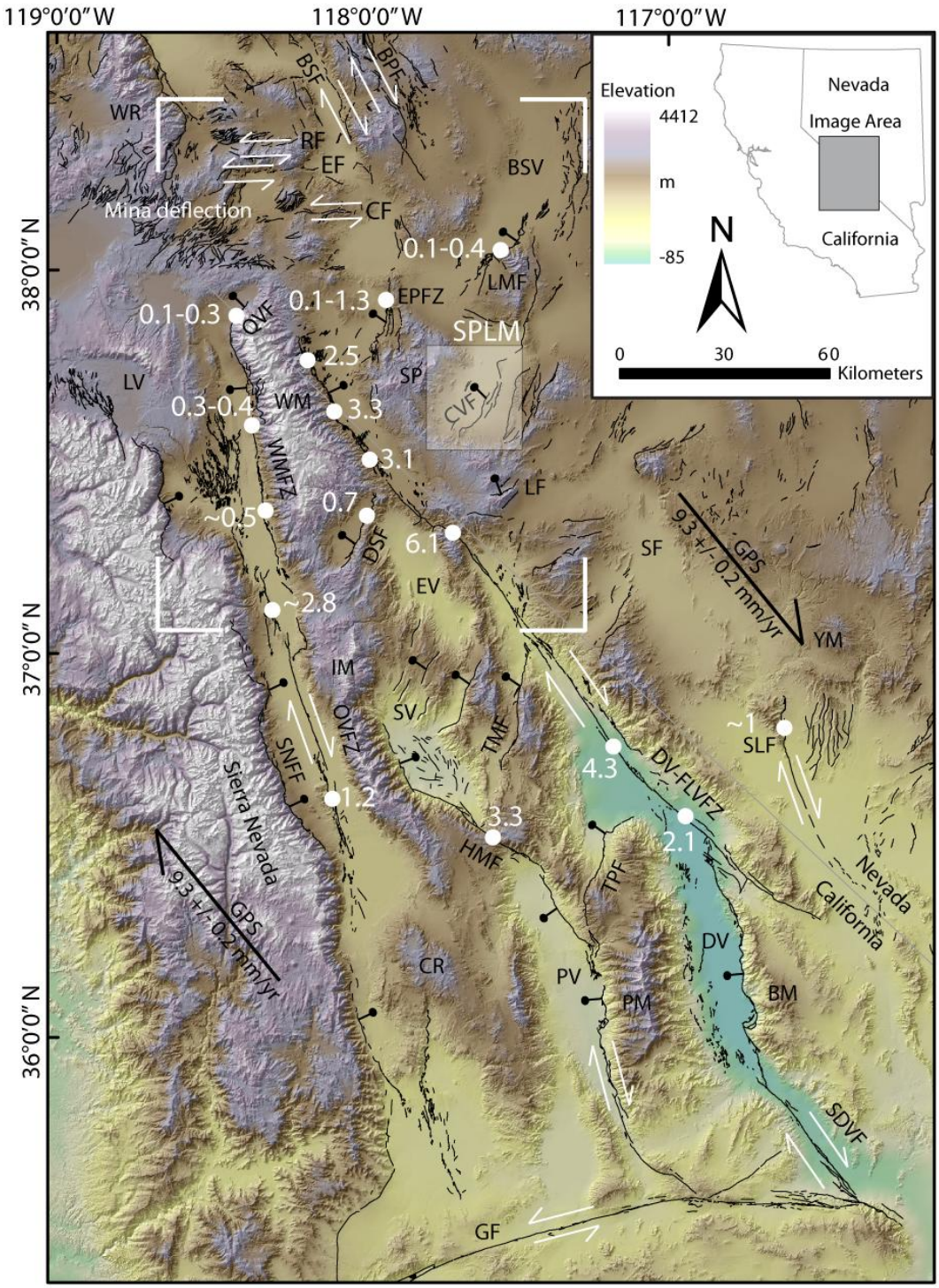

Figure 1. Regional map of the eastern California shear zone and Quaternary faults. Faults are from the U.S. Geological Survey (USGS) Quaternary fault and fold database. White corners indicate location of Figure 2. Shaded box marks Clayton Valley. Late Pleistocene fault slip rates are shown in white and are in mm/yr [Reheis and Sawyer, 1997; Lee et al., 2001b, 2009b; Oswald and Wesnousky, 2002; Kirby et al., 2006, 2008; Guest et al., 2007; Frankel et al., 2007a, 2007b, in press; Hoeft and Frankel, 2010]. GPS derived plate

motion is from Bennett et al. [2003]. Tick marks are on the hanging wall of normal faults and arrows indicate the direction of motion along strike-slip faults. BM: Black Mountains, BSF: Benton Springs fault, BPF: Bettles Well-Petrified Springs fault, BSV: Big Smoky Valley, CR: Coso Range, DSF: Deep Springs fault, DV-FLVFZ: Death Valley-Lake Valley fault zone, EF: Excelsior Mountains fault, EPFZ: Emigrant Peak fault zone, EV: Eureka Valley, GF: Garlock fault, HMF: Hunter Mountain-Saline Valley fault, IM: Inyo Mountains, LF: Lida fault zone, LV: Long Valley Caldera, OVFZ: Owens Valley fault zone, PM: Panamint Mountains, PV: Panamint Valley, QVF: Queen Valley fault, RF: Rattlesnake Flat fault, SDVF: Southern Death Valley fault, SF: Sarcobotus Flat, SL: Stateline fault, SNFF: Sierra Nevada frontal fault, SP: Silver Peak Range, SPLM: Silver Peak-Lone Mountain extensional complex, SV: Saline Valley, TMF: Tin Mountain fault, TPF: Towne Pass fault, WMFZ: White Mountains fault zone, YM: Yucca Mountain.

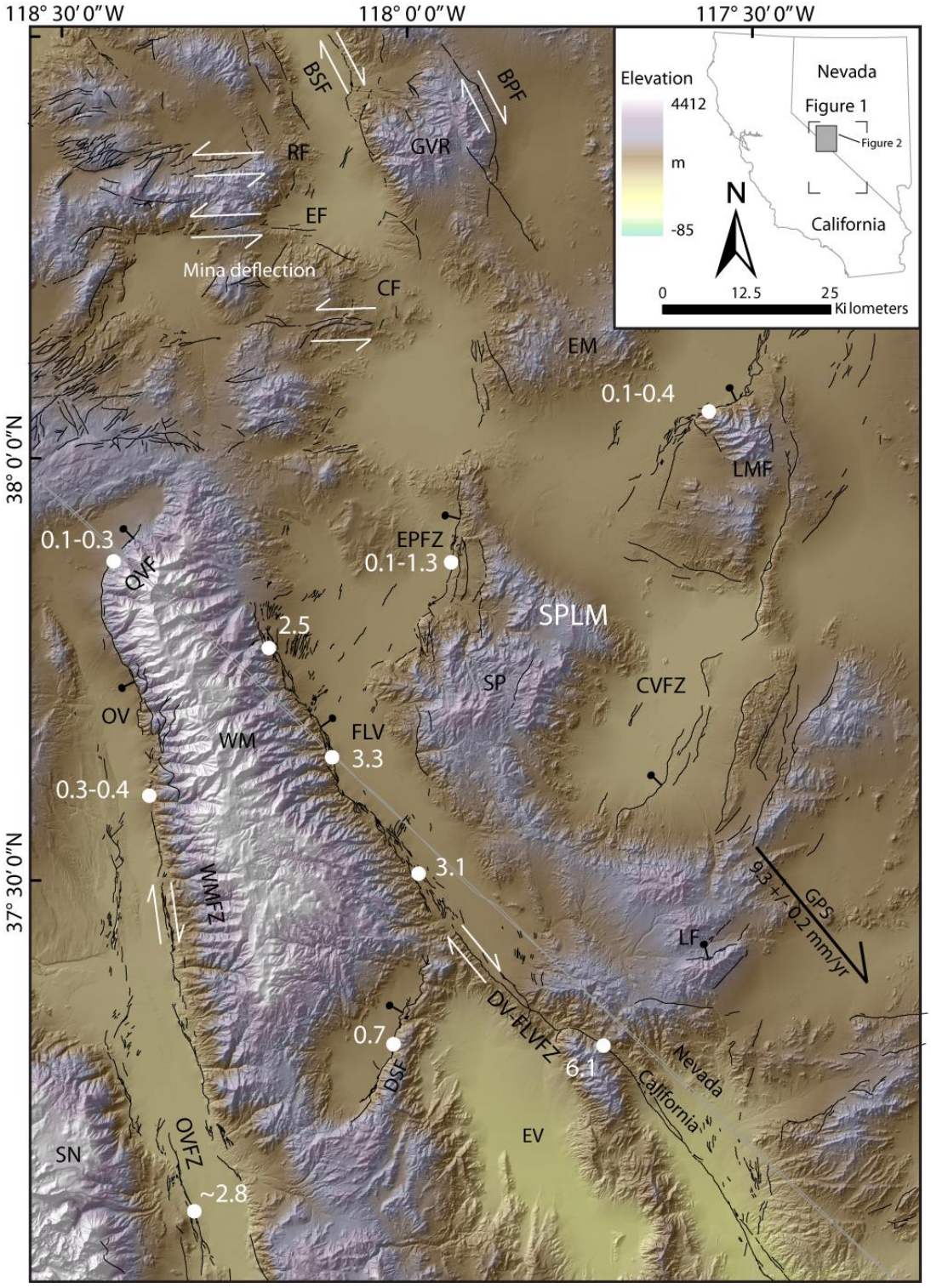

Figure 2: Close-up view of the strain transfer zone between the northern ECSZ and Walker Lane. Faults are from the USGS Quaternary fault and fold database. At the northern end of the White Mountains strain is pulled out of Owens Valley and Fish Lake Valley by the Queen Valley normal fault and the normal faults of the Silver Peak-Lone

Mountain extensional complex. These normal faults ultimately transfer strain northeastward onto the Benton Springs and Bettles Well-Petrified Springs right-lateral faults of the Walker Lane. Inset shows the location of Figure 2 with respect to Figure 1. Late Pleistocene slip rates are shown in white [Reheis and Sawyer, 1997; Kirby et al., 2006, 2008; Frankel et al., 2007a, 2007b, in press; Lee et al., 2001b, 2009b; Hoeft and Frankel, 2010]. GPS vector is from Bennett et al., [2003]. Slip rates agree with the geodetic velocity just south of the White Mountains but quickly decrease towards the northern White Mountains until they are less than half of the geodetic velocity. BSF: Benton Springs fault, BPF: Bettles Well-Petrified Springs fault, CF: Coaldale fault, CVFZ: Clayton Valley fault zone, DV-FLVFZ: Death Valley-Fish Lake Valley fault zone, EF: Excelsior Mountains fault, EM: Excelsior Mountains, EPFZ: Emigrant Peak fault zone, FLV: Fish Lake Valley, GVR: Gabbs Valley Range, LF: Lida fault, OV: Owens Valley, OVFZ: Owens Valley fault zone, QVF: Queen Valley fault, RF: Rattlesnake Flat fault, SN: Sierra Nevada, SPLM: Silver Peak-Lone Mountain extensional complex, WM: White Mountains, WMFZ: White Mountains fault zone.

CHAPTER 2

STUDY AREA

Eastern California Shear Zone- Walker Lane

The ECSZ and Walker Lane represent a diffuse plate boundary zone accommodating dextral shear between the extending Basin and Range province to the east and the rigid Sierra Nevada block to the west [*Locke et al.*, 1940; *Stewart*, 1988; *Hearn and Humphreys*, 1998; *Dixon et al.*, 2000; *Oldow*, 2003; *Faulds et al.*, 2005; *Wesnousky*, 2005; *Liu et al.*, 2010]. While the overall character of deformation (NW-SE dextral shear) displayed by the ECSZ-Walker Lane is the same as that of the San Andreas system, the manner in which that deformation is distributed through the lithosphere differs greatly between the two systems. The ECSZ-Walker Lane is characterized by a very broad, discontinuous zone of deformation. The San Andreas on the other hand exhibits a more simple deformation pattern whereby strain is predominantly taken up along a single through-going structure with minor subsidiary faults branching off of it [*Faulds et al.*, 2005; *Wesnousky*, 2005b]. No such through-going structure exists in the ECSZ-Walker Lane where the dominant NW-trending structural grain is episodically interrupted by regions of east-west sinistral faulting and down-to-the-northwest normal faulting, often coupled with discernible clockwise vertical-axis block rotations [*Nur et al.*, 1986; *Scotti et al.*, 1991; *Cashman and Fontaine*, 2000; *Petronis et al.*, 2002, 2007, 2009; *Wesnousky*, 2005a, 2005b].

Brief History

The complex structural architecture observed today in the ECSZ and Walker Lane reflects both the region's multiphase tectonic history and the youthfulness of the fault system. In addition to plate boundary deformation, the physiography of the ECSZ-Walker Lane has also been influenced by Basin and Range extension. Roughly east-west directed extension of the Basin and Range province began in the mid Miocene (~15 Ma) and continues today [*Burchfiel,* 1979; *Wernicke et al.,* 1988; *Atwater and Stock,* 1988; *Wernicke and Snow,* 1998; *Stockli et al.*, 2003; *Lee et al.,* 2009a]. As the plate boundary continued to evolve following inception of San Andreas fault system and northward migration of the Mendocino triple junction, some of the transform motion began to be taken up by faults at the Sierra Nevada-western Basin and Range transition, resulting in development of the ECSZ-Walker Lane as it exists today [*Burchfiel,* 1979; *Glazner and Bartley,* 1984; *Stewart,* 1988; *Glazner et al.,* 2002; *Stockli et al.*, 2003; *Lee et al.,* 2009a]. Therefore, the array of dip-slip and strike-slip faults that define the ECSZ-Walker Lane has been shaped by driving forces related to both the evolution of the Pacific-North America plate boundary and the more recent interaction of plate boundary kinematics with Basin and Range extension, the nature of which is still not completely understood.

The structural complexity of the ECSZ-Walker Lane compared to the San Andreas also reflects the relative youthfulness of the system [*Faulds et al.,* 2005; *Wesnousky,* 1990, 2005b]. Laboratory experiments and field studies show that strike-slip fault systems are generally characterized by several distinct faults early in their development that ultimately consolidate into a singular through-going structure as the system matures [e.g., *Wilcox et al.,* 1973; *Wesnousky,* 1988; *An and Sammis,* 1996]. Following this line of reasoning, *Faulds et al.,* [2005] propose that the ECSZ-Walker

Lane may represent a continental scale transform system analogous to the San Andreas that is in the early stages of development. The northward migration of the Medocino triple junction may ultimately result in the faults of the ECSZ-Walker Lane becoming a more kinematically suitable configuration for the plate boundary than the San Andreas [e.g., *Glazner and Bartley,* 1984; *Faulds et al.*, 2005; *Wesnousky,* 2005b; *Frankel et al.,* in press].

Fault Kinematics

The southern end of the ECSZ extends northward from the Big Bend in the San Andreas fault through the Mojave Desert where it is comprised of a series of discontinuous, NW-trending, sub-parallel fault strands that show evidence of late Cenozoic right-lateral displacement [*Dokka,* 1983; *Dokka and Travis,* 1990; *Rockwell et al.*, 2000; *Peltzer et al.*, 2001; *Oskin and Iriondo,* 2004]. The Mojave appears to be characterized by a recent episode of clustered seismicity over the last ~1000 years, including two large earthquakes in the 1990s (M_w 7.3 Landers and M_w 7.1 Hector Mine) [*Sieh et al.,* 1993; *Wald and Heaton,* 1994; *Rockwell et al.,* 2000; *Freed and Burgmann,* 2004; *Dolan et al.,* 2007].

North of the Garlock fault, the northern ECSZ is characterized by NW-SE dextral slip along four main fault systems- the Owens Valley, Hunter Mountain-Saline Valley, Death Valley-Fish Lake Valley, and Stateline fault systems (Figure 1). Strain is transferred on and off of these major fault systems by a series of down-to-the-northwest normal faults, including the Deep Springs, Eureka Valley, Towne Pass, and Emigrant Peak faults [*Wright and Troxel,* 1970; *Reheis and Dixon,* 1996; *Lee et al.,* 2001a; *Frankel et al.,* in press]. The distinct strain transient observed in the Mojave does not appear to continue north of the Garlock fault as late Pleistocene to recent slip rates along these four

fault systems sum to ~9-10 mm/yr at ~37° N, which is in good agreement with the geodetically determined rate of ~9.3 ± 0.2 mm/yr [*Bennett et al.,* 2003; *Frankel et al.,* 2007a; *Lee et al.,* 2009a]. This portion of the ECSZ is characterized by a complex history of faulting. While thermochronologic data indicate that the current transtensional stress regime initiated at ~3 Ma, there is also evidence of large magnitude (> 65 km) right lateral displacement across Owens Valley that likely records much older deformation [*Stewart,* 1988; *Stockli et al.,* 2003; *Glazner et al.,* 2005; *Kylander-Clark et al.,* 2005; *Lee et al.,* 2009a].

Further north, the belt of deformation narrows towards the northern White Mountains where dextral shear is taken up on two principal structures: the White Mountains and northern Death Valley-Fish Lake Valley fault zones. At the northern end of the White Mountains, geologic rates again disagree with the geodetic data. The same region-wide geodetic rate of ~9.3 mm/yr still applies [*Bennett et al.,* 2003], but the late Pleistocene slip rates for the White Mountains and northern Death Valley- Fish Lake Valley fault zones are only 0.3-0.4 mm/yr and 2.5-3.1 mm/yr respectively [*Kirby et al.,* 2006; *Frankel et al.,*2007b]. Therefore, only ~1/3 of the GPS-based geodetic velocity can be attributed to these structures.

North of the White Mountains, the locus of deformation steps to the east and the fault geometry changes abruptly from the predominant NW-SE regional trend to roughly E-W. This region is known as the Mina deflection, a zone of left-lateral strike-slip and down-to-the-northwest normal faulting that connects the ECSZ to the south with the Walker Lane to the north [Figure 2; *Nielsen,* 1965; *Stewart,* 1988; *Oldow* 1993; *Oldow et al.,* 1994, 2001; *Wesnousky,* 2005b; *Lee et al.,* 2009b; *Tincher and Stockli,* 2009]; the change in geometry is attributed to pre-Cenozoic structure [*Oldow et al.,* 1994]. The Mina deflection acts to transfer strain between the two sub-parallel fault systems via left-lateral strike-slip faulting and clockwise vertical-axis block rotation [*Cashman and Fountaine,* 2000; *Petronis et al.,* 2002, 2007, 2009; *Stockli et al.,* 2003; *Faulds et al.,*

2005; *Wesnousky,* 2005a]. From the northern ECSZ, strain is funneled into the Mina deflection from Owens Valley and Fish Lake Valley by the Queen Valley fault as well as the SPLM faults [*Oldow et al.,* 1994, 2001, 2008; *Reheis and Sawyer,* 1997; *Petronis et al.,* 2002, 2007, 2009; *Oldow,* 2003; *Stockli et al.,* 2003; *Lee et al.,* 2009b; *Ganev et al.,* 2010; *Hoeft and Frankel,* 2010].

The SPLM lies in this transition zone between the ECSZ and Walker Lane where long-term geologic slip rates do not agree with the geodetic velocity (Figure 2). The extensional complex is thought to have played an important role in transferring strain between the misaligned ECSZ and Walker Lane early in its history and recent work suggests that it still does so today [*Oldow et al.,* 1994, 2008; *Reheis and Sawyer,* 1997; *Oldow,* 2003; *Hoeft and Frankel,* 2010].

Silver Peak-Lone Mountain Extensional Complex

The Silver Peak-Lone Mountain extensional complex is a zone of distributed faulting with several well-expressed normal faults including the Clayton Valley, Emigrant Peak, Lida, and Lone Mountain faults. During the mid-late Miocene, strike-slip displacement in the northern ECSZ was focused on the northern Death Valley-Fish Lake Valley fault system [*Stewart,* 1988; *Oldow et al.,* 2008] and was transferred northward onto en-echelon faults of the central Walker Lane via displacement on a northwest-dipping detachment fault beneath the extensional complex [*Oldow et al.,* 1994, 2008]. Motion on the detachment was accompanied by 20-30° of clockwise vertical-axis block rotation and the growth of turtleback structures [*Oldow et al.,* 2008, *Petronis et al.,* 2002, 2007, 2009]. In the late Pliocene (~3 Ma), progressive growth of the turtleback structures ultimately locked the detachment [*Oldow,* 2003; *Oldow et al.,* 2008, 2009]. *Stockli et al.,* [2003] also document that at the same time, the Queen Valley fault began undergoing rapid exhumation associated with the opening of the Queen Valley pull-apart basin. Similar rapid exhumation is recorded by low-temperature thermochronologic data from

uplifted footwall rocks throughout the western Mina deflection [*Tincher and Stockli,* 2009]. A renewed period of uplift and exhumation is also recorded along the eastern Inyo Mountains fault zone at ~3 Ma that is interpreted to coincide with initiation of the right-lateral Hunter Mountain fault [*Lee et al.,* 2009a]. The onset of rapid exhumation north of the White Mountains coupled with the apparent locking of the detachment beneath the SPLM at ~3 Ma is interpreted to signal the opening of a new pathway for strain transfer through the Mina deflection.

Although the main locus of strain transfer apparently shifted north in the late Pliocene, the faults of the SPLM are still active today, as reflected by their pronounced surficial expression cutting through Quaternary alluvium. Furthermore, recent work by *Hoeft and Frankel* [2010] suggests that the extension rates along the Lone Mountain fault may have been increasing since ~92 ka, implying that the extensional complex still plays an active role in accommodating strain transfer between the misaligned structures of the northern ECSZ and Walker Lane. Therefore, we determine late Pleistocene extension rates for the Clayton Valley fault to further investigate the role of the SPLM in accommodating late Quaternary regional strain transfer.

CHAPTER 3

GEOLOGIC MAPPING

Previous mapping efforts in Clayton Valley predominantly dealt with the lithium brine deposits located near the town of Silver Peak and were thus concentrated toward the northern end of the valley [e.g., *Albers and Stewart,* 1972; *Wilson,* 1975; *Bisdorf and Smith,* 1979; *Davis and Vine,* 1979; *Davis,* 1981; *Zampirro,* 2005]. The evaporating ponds located at Silver Peak represent one of the most economically important sources of lithium in the U.S. [*Davis and Vine,* 1979]. With the exception of *Davis* [1979, 1981], little effort has been made to differentiate Quaternary units. Therefore, in order to make accurate interpretations of the late Quaternary faulting history in Clayton Valley, we made a detailed (1:10,000) geologic map of Quaternary alluvial deposits and the associated faults [Figure 3; Figure 4; Figure 5; Figure 6; *Foy et al.,* in review].

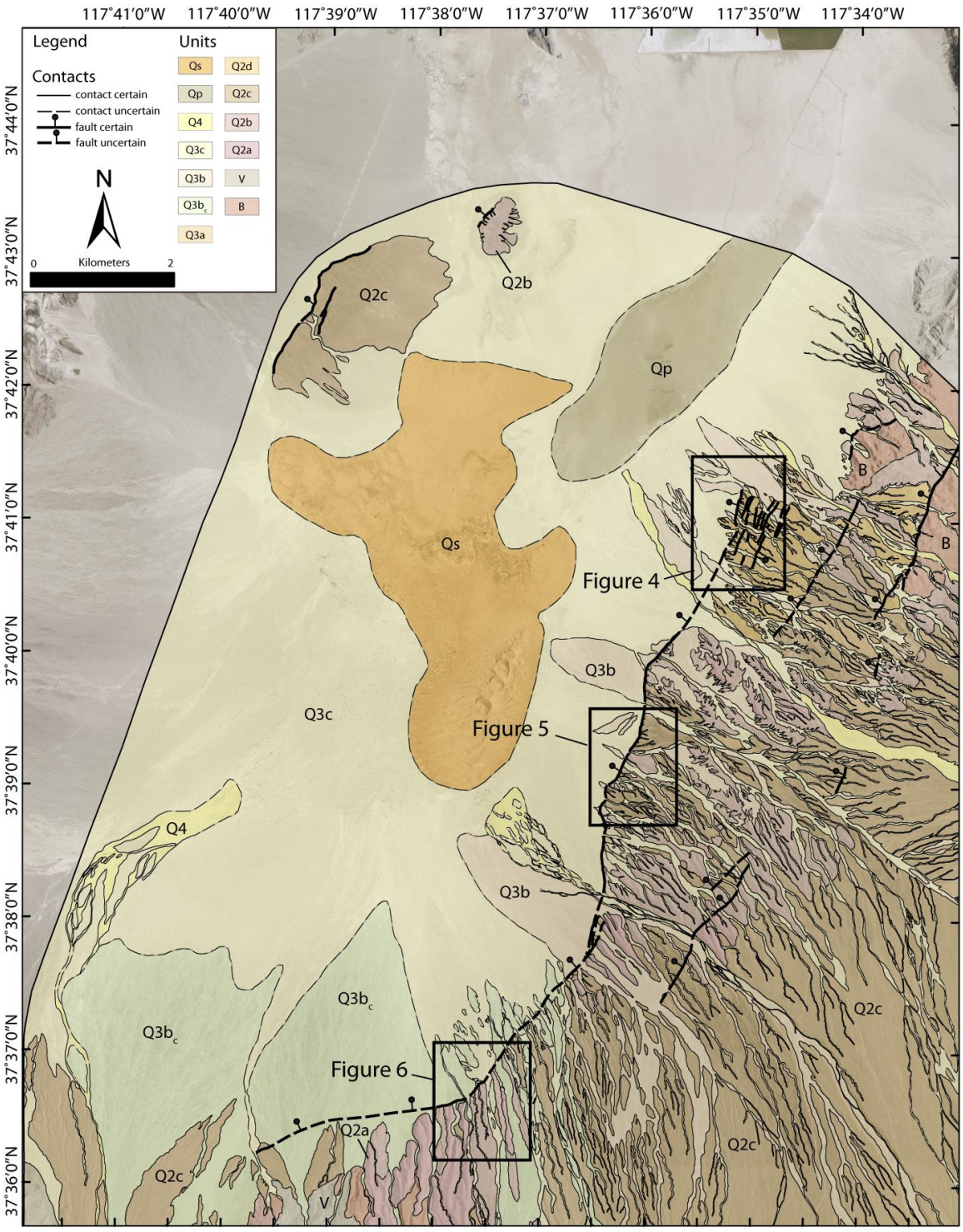

Figure 3. Surficial geologic map of southeastern Clayton Valley, Nevada. Ball is on the downthrown side of normal faults. Rectangles show locations of Figures 4-6. See Table 1 for detailed unit descriptions

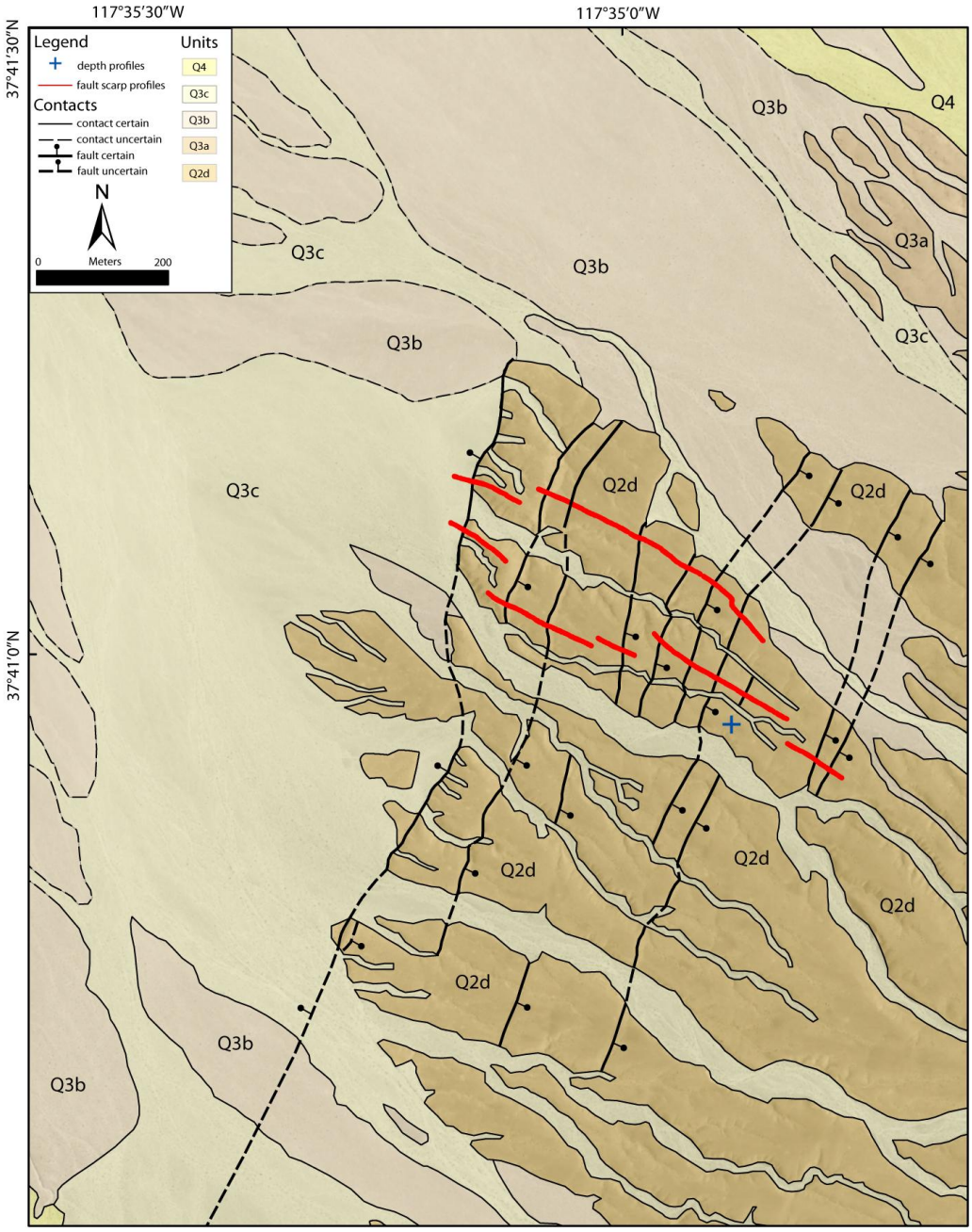

Figure 4. Close-up map view showing heavily faulted Q2d deposits. See Figure 3 for location. Depth profile sampling location is denoted by the blue cross near the center of the image. Ball is on the downthrown side of normal faults. Q2d deposits are cut by the main down-to-the-northwest fault as well as a series of distributed antithetic scarps. Red lines denote GPS fault scarp surveys. All scarp profiles are provided in Appendix B. Total measured vertical displacement is 17.8 ± 1.2 m. See Table 4 for associated horizontal displacements and extension rates for varying fault dips.

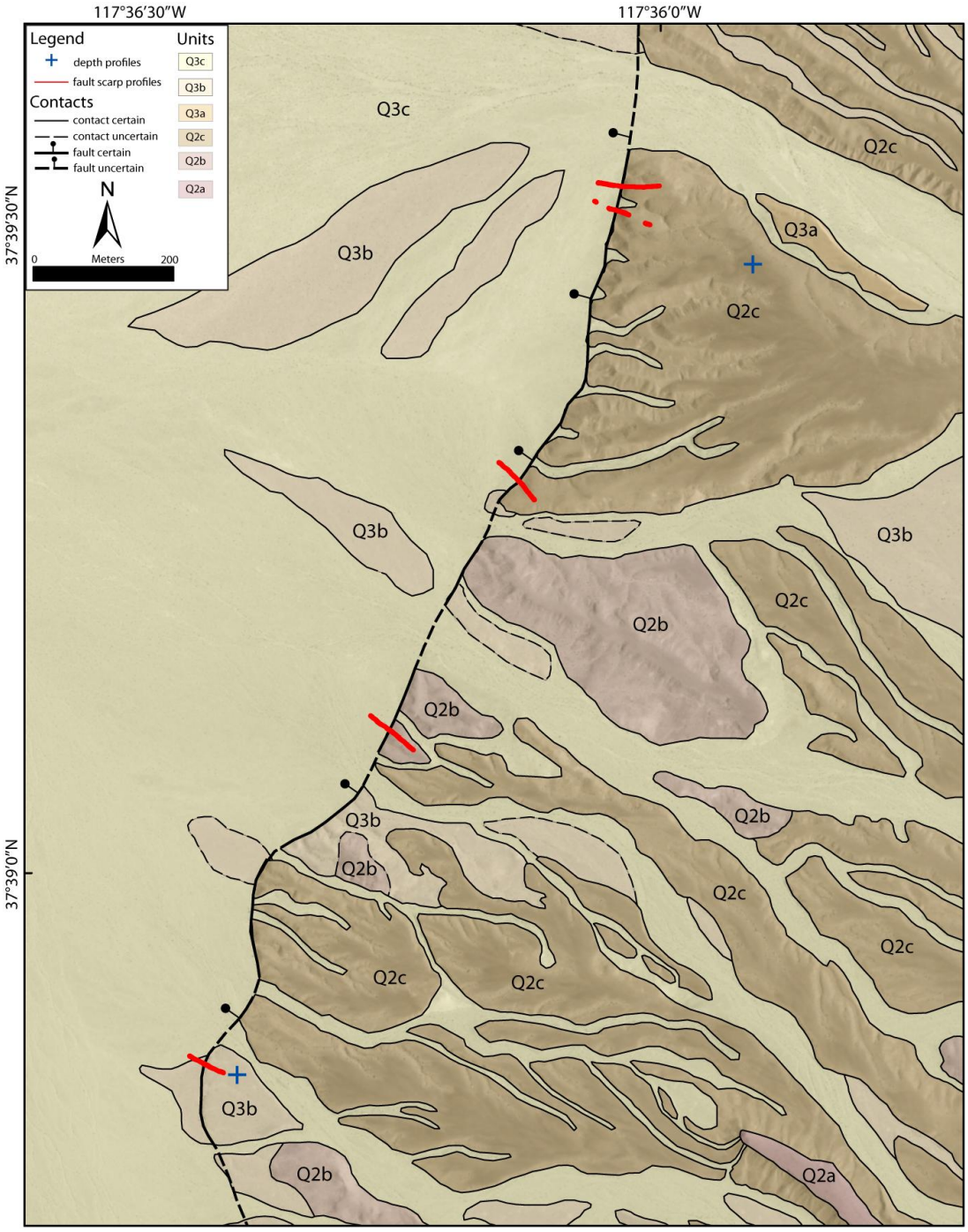

Figure 5. Close-up map view showing Q3b and Q2c depth profile sampling locations. See Figure 3 for map area location. Sampling locations denoted by blue crosses. Ball is on the downthrown side of normal faults. Red lines denote GPS fault scarp surveys. Total measured vertical displacements for Q3b and Q2c are 3.2 ± 0.3 and 13.6 ± 0.5 m respectively. See Table 4 for associated horizontal displacements and extension rates for different fault dips. Scarp profiles are provided in Appendix B.

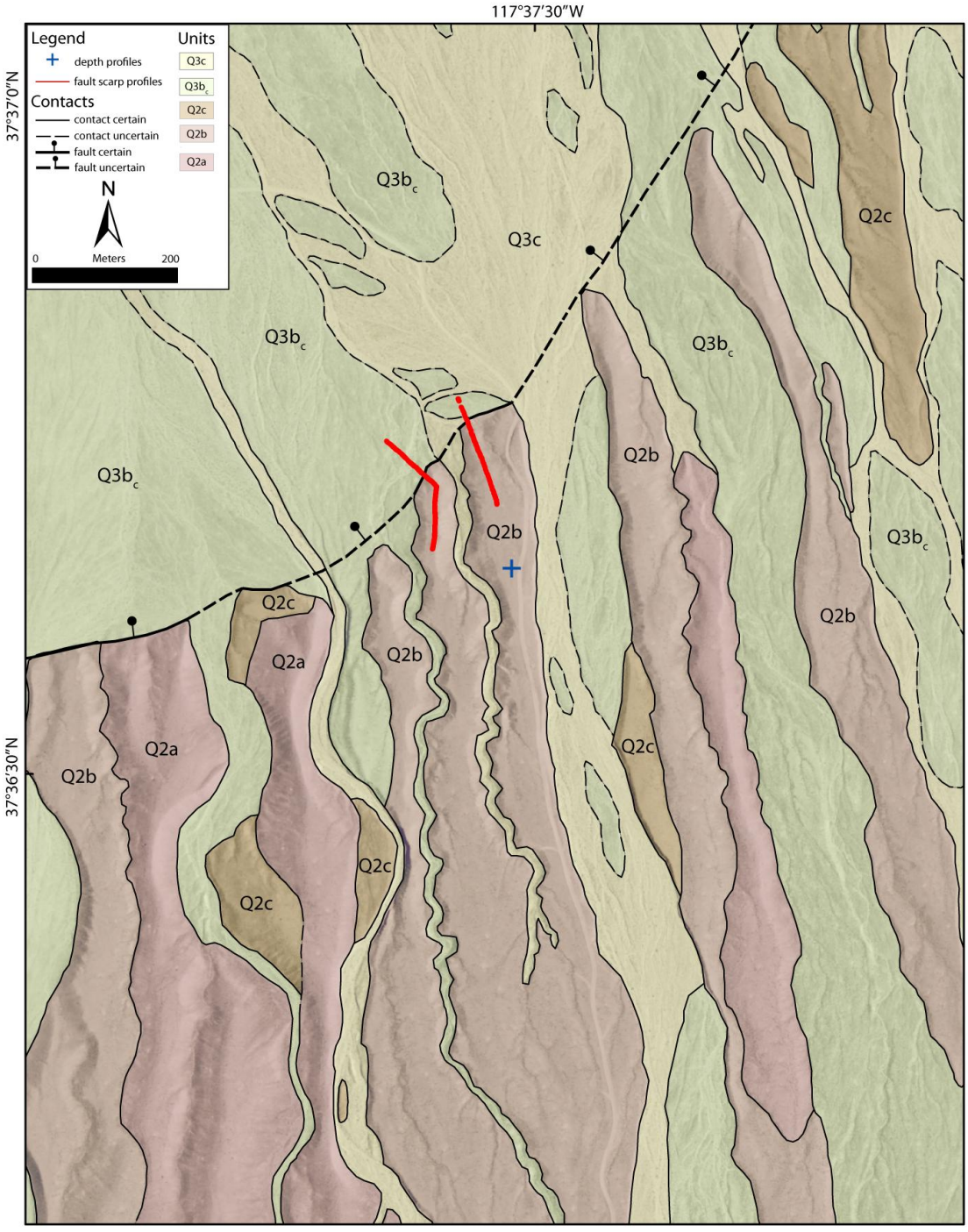

Figure 6. Close-up map view showing Q2b depth profile sample location. See Figure 3 for location of map area. Ball is on the downthrown side of normal faults. Sampling site is denoted by the blue cross and GPS fault scarp surveys are denoted by red lines. Total displacement measured across Q2b is 14.0 ± 0.5 m. See Table 4 for associated horizontal displacements and extension rates for different fault dips. See Appendix B for scarp profiles.

Mapping efforts were focused in the southeastern portion of Clayton Valley where the surface trace of the fault is best expressed in the late Quaternary stratigraphy. Mapping was conducted using 1-m-resolution color orthorectified aerial photographs from the U.S. Department of Agriculture as a base map and aided by aerial stereophotographs provided by the Bureau of Land Management. Alluvial fans were differentiated on the basis of well-established criteria such as height above the active channel, development of desert varnish and pavement, degree of rubification, soil development, degree of fan dissection, and bar and swale surface morphology [e.g., *Bull*, 1991; *Ritter*, 1993; *Frankel and Dolan*, 2007]. Eight alluvial fan units were mapped and are consistent with the western North American alluvial stratigraphic framework established by *Bull*, [1991]. From oldest to youngest, the fan units are as follows: Q2a, Q2b, Q2c, Q2d, Q3a, Q3b, Q3c, and Q4. Surfaces of Q3b age are further subdivided into two separate map units due to the fact that the southern portion of the map area contains extensive Q3b deposits with crypto-biotic soil (Figure 1 and Figure 6). For detailed unit descriptions, please see Table 1. In addition, undifferentiated bedrock and volcanic ash units were also mapped through portions of the valley, some of which also appear to have been deformed by earlier Cenozoic faults. However, bedrock deformation is beyond the focus of this study and herein we focus on deformed alluvial landforms.

The main down-to-the-northwest fault strand is extremely well-expressed through the alluvium and stands out in clear juxtaposition with the surrounding landscape. The primary fault strand has a sinuous surface trace, varying in strike throughout the valley from ~N30°E to ~N75°E. There is evidence of widely distributed normal faulting throughout the basin, with anomalous uplifted and SE-tilted fan surfaces exposed in the middle of the valley floor. The clearest evidence for distributed deformation is in unit Q2d, which is broken up by a series of closely-spaced antithetic scarps as well as the main down-to-the-northwest scarp (Figure 4). Data from well-logs from the Foote Mineral Company and seismic reflection profiles also highlight the fact that faulting is

distributed throughout the valley floor and has effectively broken the basin up into many different structural blocks, although there is little to no evidence of these faults cutting surficial features [*Davis,* 1981; *Zampirro,* 2005; *Foy et al.*, in review]. In the southeastern portion of the valley, where the fault is well-expressed in the alluvium, we measure vertical offsets with differential GPS. Offsets were measured through four different fan units- Q2b, Q2c, Q2d, and Q3b- in order to assess the faulting history over multiple timescales.

Table 1: Characteristics of Alluvial Fan Units in Clayton Valley, Nevada.

Unit	Height above active channel (m)	Varnish	Pavement development	Rubification	Soil characteristics	Degree of fan dissection	Bar & swale morphology
Q4	0	None	None	None	None	None	Strong, amplitude ~1 m
Q3c	~0.5	Negligible	Negligible	Weak, light red-pink	Immature, < 5 cm thick A horizon	None	Strong, amplitude ~1 m
Q3b	~1-1.5	Incipient	Incipient	Moderate, light red	Immature, ~ 5 cm thick A horizon, strong pedogenic carbonate development	None	Strong, amplitude ≤ 0.5 m
Q3a	1.5-2.5	Moderate	Well-developed	Strong orange-red	Immature, ~5-10 cm thick A horizon	None	Subdued, amplitude < 0.5 m
Q2d	2-4	Heavily varnished	Mature	Very strong dark orange-red	Well-developed, ~10-15 cm thick A horizon, very silty	Slightly dissected	Subdued, amplitude < 20 cm
Q2c	2-4	Heavily varnished	Very mature, completely interlocking	Very strong dark orange-red	Well-developed, ~10-15 cm thick A horizon, strong pedogenic carbonate development	Slightly dissected	Very subdued, amplitude < 10 cm
Q2b	3-9	Heavily varnished	Mature, but starting to decay	Strong orange-red	Well-developed, ~10-20 cm thick A horizon, bouldery with carbonate coating underneath clasts	Moderately dissected	Negligible
Q2a	5-10	Still distinct, but decaying	Decaying	Strong orange-red	Well-developed, ~10-20 cm thick A horizon	Strongly dissected	Negligible

CHAPTER 4

SCARP PROFILES

Differential GPS surveys were collected at 1 Hz. intervals using Trimble GeoXH GPS units in order to accurately determine fault offsets. Post-processing differential correction results in decimeter accuracy. Vertical displacements were measured using the Scarp Dater software of *Hilley and Arrowsmith* [2003], and those scarps representing the maximum offset across each surface were used to calculate extension rates. In all, a total of 32 scarp profiles were collected (please see Appendix B). In some cases surface roughness makes it difficult to measure vertical displacement from the scarp profiles accurately if, for instance, a channel is incised across the base of the scarp. For this reason, smoothing windows were applied to the profiles as necessary. This was done by averaging out elevations over a one to five meter horizontal distance to create a smoother surface profile and allow for a more accurate determination of vertical displacement.

Uncertainties in displacement measurements are a combination of the decimeter accuracy of the GPS measurements and uncertainty related to surface roughness. The youngest fan surveyed is unit Q3b which has a maximum vertical displacement of 3.2 ± 0.3 m. Q2d surfaces are cut by both the main down-to-the-northwest fault and a series of down-to-the-southeast antithetic faults (Figure 4). Scarp profiles were taken through the Q2d unit across ten individual fault scarps with resolvable displacement, including nine antithetic scarps. The combined vertical displacement sums to 17.8 ± 1.2 m and a maximum single scarp of 6.4 ± 0.3 m. Profiles collected across the Q2c unit yield a total vertical offset of 13.6 ± 0.5 m, with a maximum single scarp height of 9.2 ± 0.3 m. The oldest unit on which fault offsets were measured is Q2b. Q2b surfaces occur throughout the study area but are concentrated near the southern end of the valley, where the largest individual scarps are present. Scarps surveyed across the Q2b unit have a total measured displacement of 14.0 ± 0.5 m and a maximum scarp height of 11.6 ± 0.3 m.

CHAPTER 5

TERRESTRIAL COSMOGENIC NUCLIDE GEOCHRONOLOGY

We used ^{10}Be TCN geochronology to date the offset fan surfaces [e.g., *Gosse and Phillips,* 2001]. TCN geochronology is particularly advantageous when the features of interest lack appreciable amounts of organic material for radiocarbon dating or when the timescale of interest exceeds the limits of radiocarbon (~40 ka), both of which apply for alluvial fans in Clayton Valley. Excellent surface exposures in the arid desert environment of Clayton Valley combined with prolonged surface stability provide the ideal setting in which to apply the TCN method [e.g., *Bierman et al.,* 1995; *Hancock et al.,* 1999; *Kirby et al.,* 2006; *Frankel et al.,* 2007a, 2007b, in press; *Le et al.,* 2007; *Oskin et al.,* 2007, 2008; *Armstrong et al.,* 2010; *Hoeft and Frankel,* 2010; *Owen et al.,* 2011].

The concentration of a cosmogenic nuclide in a sample is a function of exposure time, as well as the half-life of the nuclide of interest. Beryllium-10 and other in situ produced cosmogenic nuclides (e.g. ^{3}He, ^{14}C, ^{21}Ne, ^{26}Al, ^{36}Cl) can be used to date depositional surfaces assuming that the production rates are reasonably well-known and careful sampling procedures are followed to limit complicating factors such as the influence of erosion/aggradation and inheritance [e.g., *Lal et al.,* 1991; *Anderson et al.,* 1996; *Gosse and Phillips,* 2001].

Various scaling factors have been proposed to address the potential for production rates to vary with time [e.g., *Lal et al.,* 1991; *Stone,* 2000; *Dunai,* 2001; *Gosse and Phillips,* 2001; *Desilets and Zreda,* 2003; *Pigati and Lifton,* 2004; *Lifton et al.,* 2005; *Desilets et al.,* 2006; *Staiger et al.,* 2007; *Balco et al.,* 2008]. However, no consensus has been reached on how to best model time-variable production rates. For this reason, we

assume a time-invariant ^{10}Be production rate when calculating surface exposure ages for the displaced fan units.

Sample Collection

TCN samples can be collected using either surface clasts or a depth profile. For our purposes, a depth profile was more appropriate due to the fact that the fans of interest are far from the source area, which greatly increases the potential for inheritance, and large clasts were generally not present on the fan surfaces. TCN production decreases exponentially with depth beneath Earth's surface and become negligible by ~2-3 m in alluvium [*Anderson et al.,* 1996; *Hancock et al.,* 1999]. If significant TCN concentrations are present at depth, this reflects an inherited TCN component acquired prior to final deposition [*Anderson et al.,* 1996]. Therefore, by using a depth profile instead of surface samples, the amount of inheritance can be quantified, allowing for a more accurate age measurement.

Along those lines, soil pits were dug in stable parts of the displaced fan surfaces, away from the eroded channel edges (Figure 7). Sample locations are shown in Figures 4, 5, and 6. Samples were collected from five to six different depths within each pit and were extracted at closer spacing near the surface where TCN production is highest. For Q2b, Q2c, and Q2d pits, ~ 1200-1500 grams of soil was collected from depths of 25 cm, 50 cm, 75 cm, 125 cm, and 200 cm (Table 2). A comparable amount of material was extracted from the Q3b pit from depths of 25, 50, 75, 100, 150, and 200 cm (Table 2). For each sample depth, the thickness of the sampled horizon was restricted to $\leq$ 10 cm. Each pit was characterized by massive, debris-flow dominated stratigraphy.

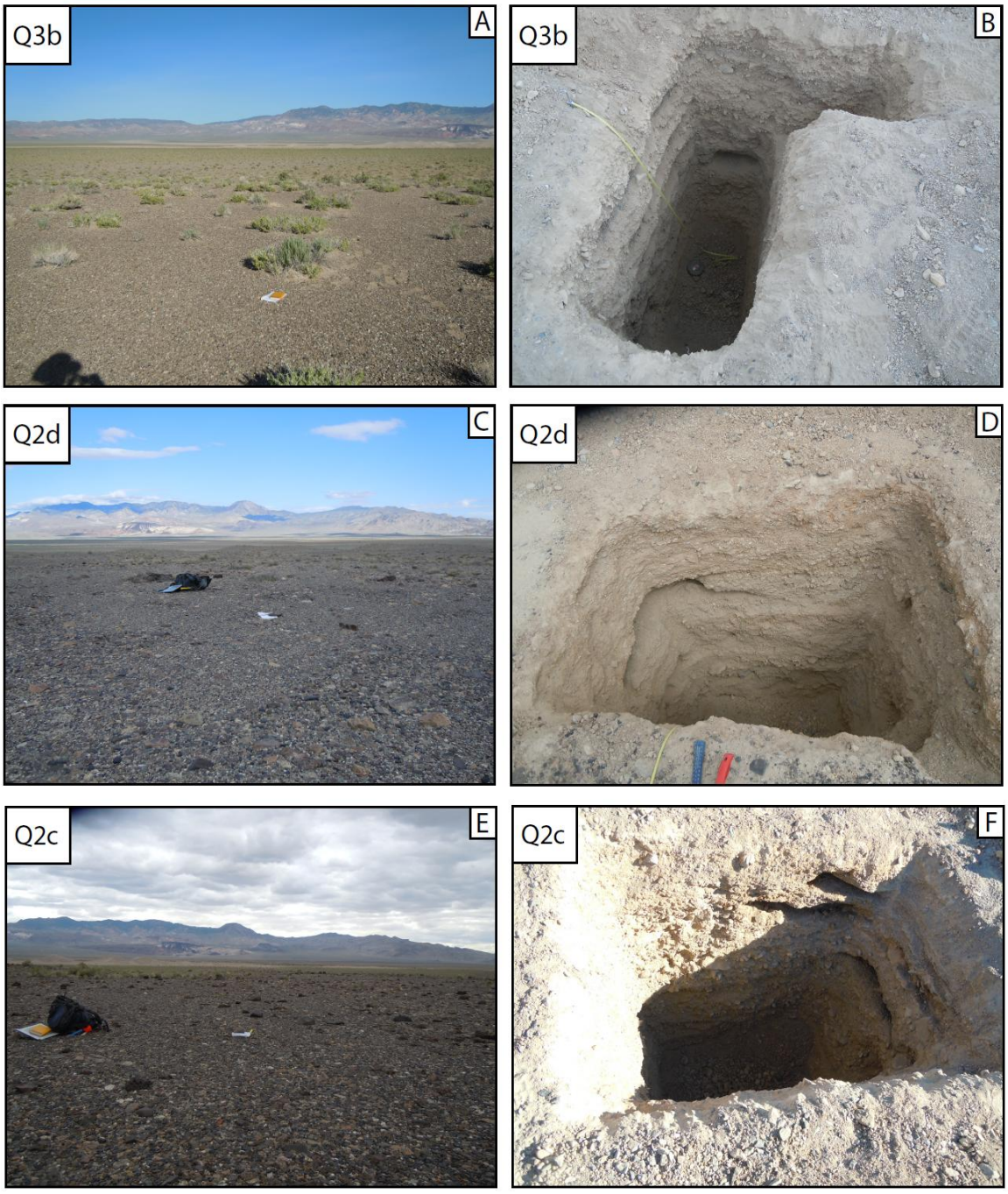
Q3b
A
Q3b
B
Q2d
C
Q2d
D
Q2c
E
Q2c
F

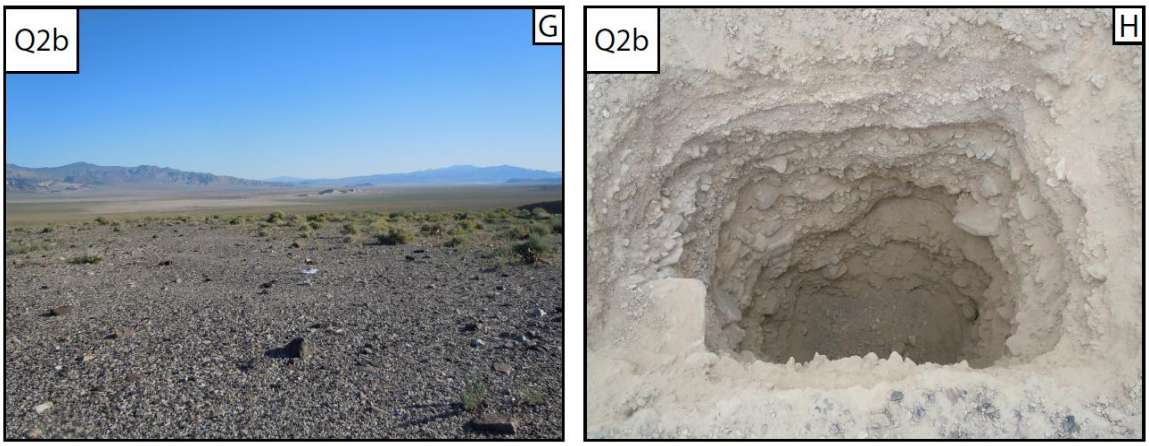

Figure 7. Terrestrial cosmogenic nuclide depth profile sampling sites. A, C, E, and G show the sampling locations before digging. B, D, F, and H show the finished pits. Each pit is 2 m deep and ~2 m x 1 m across. See Table 1 for alluvial fan unit descriptions.

Table 2: ^{10}Be Cosmogenic Nuclide Depth Profile Analytical Results

Sample	Latitude (°N)	Longitude (°W)	Elevation (m)	Depth (cm)	Shielding Factor[a]	Quartz (g)	Be Carrier (mg)	^{10}Be/^{9}Be (E-13)[b,c]	^{10}Be Concentration (10^6 atoms g^{-1} SiO_2)[c, d, e]
Q3b	37.64746	-117.60675	1347	-	-	-	-	-	-
CV060810-1				195-205	1	46.00	0.4260	11.60 ± 0.30	0.71 ± 0.02
CV060810-3				105-95	1	44.10	0.3880	13.80 ± 0.30	0.80 ±0.02
CV060810-4				70-80	1	40.10	0.4270	11.5 ± 0.30	0.81 ± 0.02
CV060810-5				55-45	1	40.80	0.4180	11.00 ± 0.30	0.74 ± 0.02
CV060810-6				25-35	1	35.20	0.4250	8.60 ± 0.30	0.68 ± 0.03
Q2d	37.68248	-117.58141	1351	-	-	-	-	-	-
CV061210-1				190-200	1	50.51	0.4127	14.51 ± 0.37	0.78 ± 0.02
CV061210-2				120-130	1	41.69	0.4150	15.44 ± 0.43	1.01 ± 0.03
CV061210-3				70-80	1	50.26	0.4161	19.25 ± 0.47	1.05 ± 0.03
CV061210-4				50-60	1	41.53	0.4188	17.30 ± 0.50	1.15 ± 0.04
CV061210-5				20-30	1	30.10	0.4170	14.83 ± 0.36	1.35 ± 0.04
Q2c	37.65787	-117.59847	1356	-	-	-	-	-	-
CV061310-1				190-200	1	70.77	0.5150	7.10 ± 0.50	0.34 ± 0.02
CV061310-2				120-130	1	40.19	0.4150	6.34 ± 0.20	0.44 ± 0.01
CV061310-3				75-85	1	30.70	0.3902	8.14 ± 0.19	0.69 ± 0.02
CV061310-4				40-50	1	20.10	0.3840	6.34 ± 0.22	0.81 ± 0.03
CV061310-5				22-32	1	20.10	0.3985	8.07 ± 0.20	1.06 ± 0.03
Q2b	37.61092	-117.62524	1452	-	-	-	-	-	-
CV061110-1				190-200	1	60.72	0.4261	19.0 ± 0.13	0.89 ± 0.06
CV061110-2				120-130	1	59.99	0.4265	18.37 ± 0.65	0.87 ± 0.03
CV061110-3				70-80	1	40.02	0.4261	16.14 ± 0.36	1.15 ± 0.03
CV061110-4				45-55	1	31.34	0.4254	14.48 ± 0.36	1.31 ± 0.04
CV061110-5				25-35	1	30.32	0.4192	16.85 ± 0.33	1.55 ± 0.03

[a] No geometric correction for topography was necessary (horizon < 20° in all directions).
[b] Isotope ratios were normalized to ^{10}Be standards prepared by *Nishiizumi et al.* [2007] with a value of 2.85 x 10^{12} and using a ^{10}Be half-life of 1.36 x 10^{6} years.
[c] Uncertainties are reported at the 1σ confidence level.
[d] A mean blank value of 90406 ± 37685 atoms was used to correct for background for Q2c and Q2b. A value of 548736 ± 78545 atoms was used for Q2d.
[e] Propagated uncertainties include error in the blank, carrier mass (1 %), and counting statistics.

Sample Preparation

Samples were prepared at the Georgia Tech TCN geochronology laboratory and analyzed by accelerator mass spectrometry (AMS) at Purdue Rare Isotope Measurement Laboratory (PRIME Lab). The primary mineral used for ^{10}Be analysis is quartz (SiO_2) owing to the fact that the two principal target elements for ^{10}Be production are O and Si. The use of quartz is also advantageous due to its stoichiometric simplicity and strong resistance to weathering. Each sample was sieved to retain only the 250-710 μm grain size for TCN analysis. After sieving, quartz was isolated by standard techniques [e.g. *Kohl and Nishiizumi,* 1992]. Following quartz purification, Be was extracted by ion exchange chromatography, precipitated out as $Be(OH)_2$, and oxidized to BeO. The BeO was then thoroughly mixed with niobium and packed into stainless steel cathodes for AMS analysis.

Exposure Age Modeling

Measured ^{10}Be/^{9}Be ratios were converted into ^{10}Be concentrations, and exposure ages were modeled following the Monte Carlo routine of *Hidy et al.* [2010]. The *Hidy et al.* [2010] model specifically incorporates geological constraints from the study area and explicitly propagates error from all relevant internal sources. The approach is based on the fact that the shape of a given depth-profile curve is characteristic of a specific exposure age, erosion/aggradation history, inheritance, vertical mixing, and bulk density

variation for a given sampling site. Therefore, the exposure age, inheritance, and erosion history can be quantified given site specific information, or at least reasonable assumptions, regarding density, shielding, and site production rate [*Hidy et al.*, 2010]. For each model run, density, inheritance, and erosion were allowed to vary within a prescribed range defined by reasonable estimates based on the depositional environment. Density was allowed to vary between 1.8 and 2.4 g/cm^3. The range of inheritance was defined by a maximum equal to the ^{10}Be concentration of the deepest sample modeled and a minimum equal to half of the maximum. Erosion was also allowed to vary between -1 and 1 cm/ka with negative values representing aggradation on the fan surface [e.g., *Reheis et al.*, 1995; *Reheis*, 2006]. Maximum aggradation/erosion was allowed to vary from -50 to 50 cm. For each sampled fan unit, the model parameters were allowed to vary in this manner for 100,000 simulations in order to determine a best-fit profile, inheritance, and associated uncertainties. Uncertainties are reported at the 2σ confidence level. A full description of TCN sample characteristics and analytical results is provided in Table 2. See Table 3 and Figure 8 for best-fit solutions.\

Table 3: Exposure age modeling best-fit solutions

Fan Unit	Denudation rate (cm ka^{-1})[a]	Inheritance (10^4 atoms g^{-1} SiO_2)[b]	Age (ka)[b, c]
Q2d	-0.13 +0.55/-0.64	71.6 +8.8/-9.4	91 +13/-12
Q2c	-0.45 +0.53/-0.10	21.3 +9.4/-10.6	96 +9/-8
Q2b	-0.07 +1.10/-0.39	77.7 +4.1/-9.2	137 +10/-11

[a] Negative values represent aggradation.
[b] Uncertainties are reported at the 2σ confidence level.
[c] Beryllium-10 model ages were calculated with the TCN Depth Profile Calculator [*Hidy et al.*, 2010] (http://geochronology.earthsciences.dal.ca/downloads-models.html).

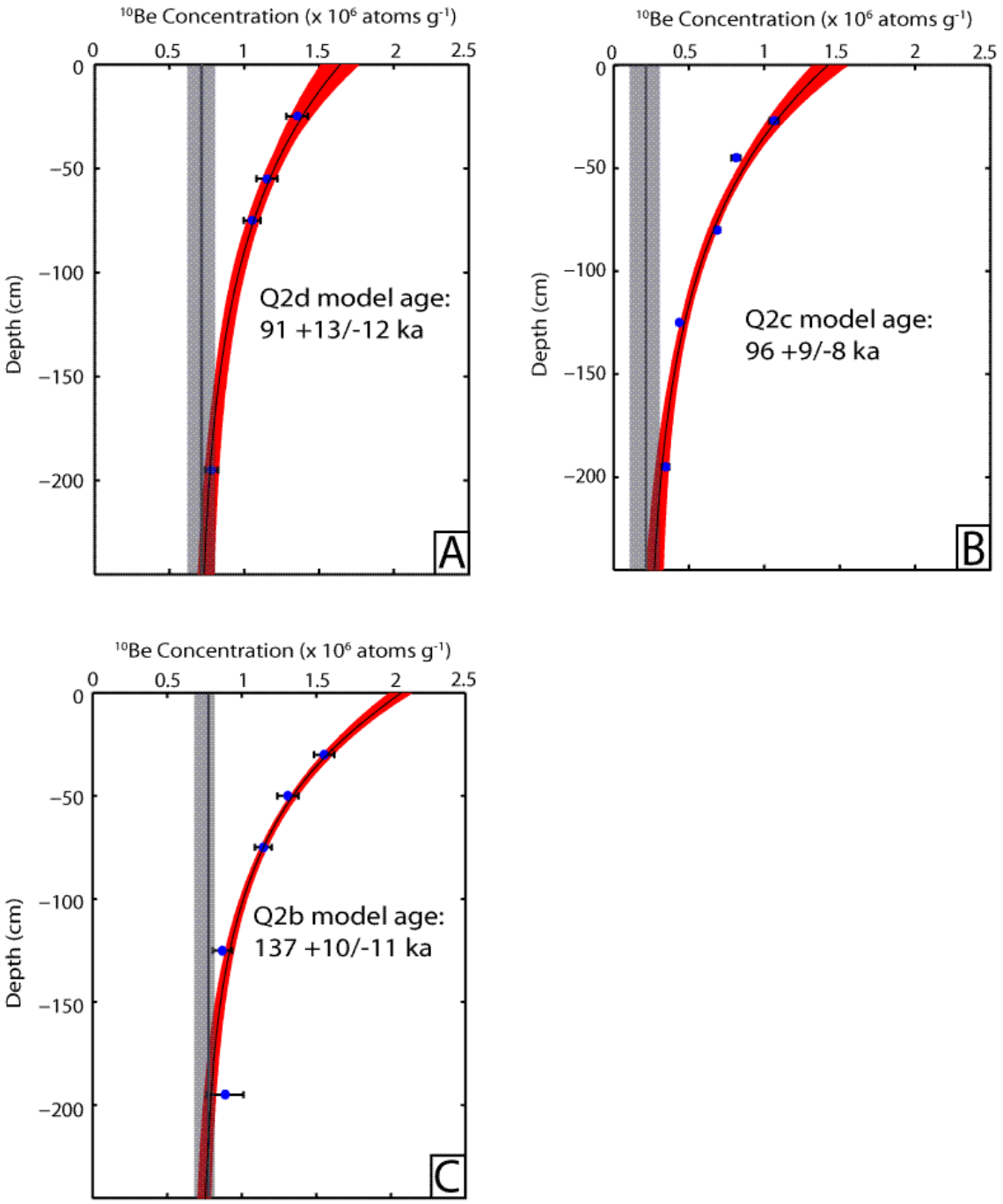

Figure 8. TCN depth profile solutions. Blue dots and associated error bars indicate ^{10}Be concentrations determined by accelerator mass spectrometry at PRIME Lab. Solid black line shows the best-fit solution within the red space that defines the full range of 100,000 Monte Carlo solutions from which the best-fit parameters were determined [e.g. *Hidy et al.*, 2010]. Solid gray line marks the best-fit inheritance value and the gray rectangle marks the full range of allowable inheritance values. Uncertainties are presented at the 2σ confidence level. See Table 3 for a list of best-fit solutions and Figures 4, 5, and 6 for sampling locations. A: Q2d. B: Q2c. C: Q2b.

Q2b Depth Profile

Using the best-fit erosion value of -0.07 cm/ka, the best-fit values for inheritance and age are 77.7 +4.1/-9.2 x 10^4 atoms $^{10}Be/g\ SiO_2$ and 137 +10/-11 ka. The Q2b age given here agrees well with ages from similar surfaces in Fish Lake Valley and Death Valley [*Machette et al.,* 2008; *Ganev et al.,* 2010; *Hoeft and Frankel,* 2010].

Q2c Depth Profile

A chi-squared statistic of 10 was used to model the Q2c depth profile. This yields a best-fit erosion rate of -0.45 cm/ka, and best-fit inheritance and age values of 21.3 +9.4/-10.6 x 10^4 atoms $^{10}Be/g\ SiO_2$ and 96 +9/-8 ka respectively.

Q2d Depth Profile

The 125 cm sample was excluded when modeling the Q2d depth profile because it does not strictly follow the theoretical relationship between ^{10}Be concentration and depth. Using the other four samples, modeling of the Q2d profile yields a best-fit erosion rate of -0.13 cm/ka and a best-fit inheritance value of 71.6 +8.8/-9.4 x 10^4 atoms $^{10}Be/g\ SiO_2$. The best-fit exposure age is 91 +13/-12 ka.

Statistically, units Q2d and Q2c are overlapping in age. Nevertheless, they are separated into different map units on the basis of surface morphology and soil development. Q2c surfaces are planar with completely interlocking desert pavement, well-varnished surface clasts, and negligible bar and swale morphology. Q2d surfaces are characterized by slightly less well-developed desert pavement and locally contain more pronounced bar and swale. There is also significantly greater pedogenic carbonate development in Q2c (Stage III) than in Q2d soil (Stage I). These observations of surface morphology and soil development lead us to the interpretation that there exists a small

time gap between deposition of Q2c and Q2d units. Q2d and Q2c ages are in good agreement with age measurements for similar fan deposits in Fish Lake Valley, Death Valley, and along the northwest Lone Mountain piedmont [*Frankel et al.,* 2007a, 2007b; *Machette et al.,* 2008; *Ganev et al.,* 2010; *Hoeft and Frankel,* 2010]

Q3b Depth Profile

Cosmogenic data from the Q3b profile are equivocal and appear to reflect significant bioturbation in the upper ~0.5 m of soil (Figure 9). As a result, we are unable to model the age directly. Nevertheless, the ages of Q2b (137 +10/-11 ka) and Q2c (96 +9/-8 ka) deposits in Clayton Valley are nearly identical to those determined for correlative Q2b (137 ± 25 ka) and Q2c (92 ± 9 ka) deposits along the nearby Lone Mountain piedmont [*Hoeft and Frankel,* 2010; in review]. Therefore, given the similarities between the surface morphology of Q3b surfaces in Clayton Valley and those at Lone Mountain, we assume that the age of Clayton Valley Q3b surfaces is similar to the 17 ± 1 ka age measured at Lone Mountain [*Hoeft and Frankel,* 2010].

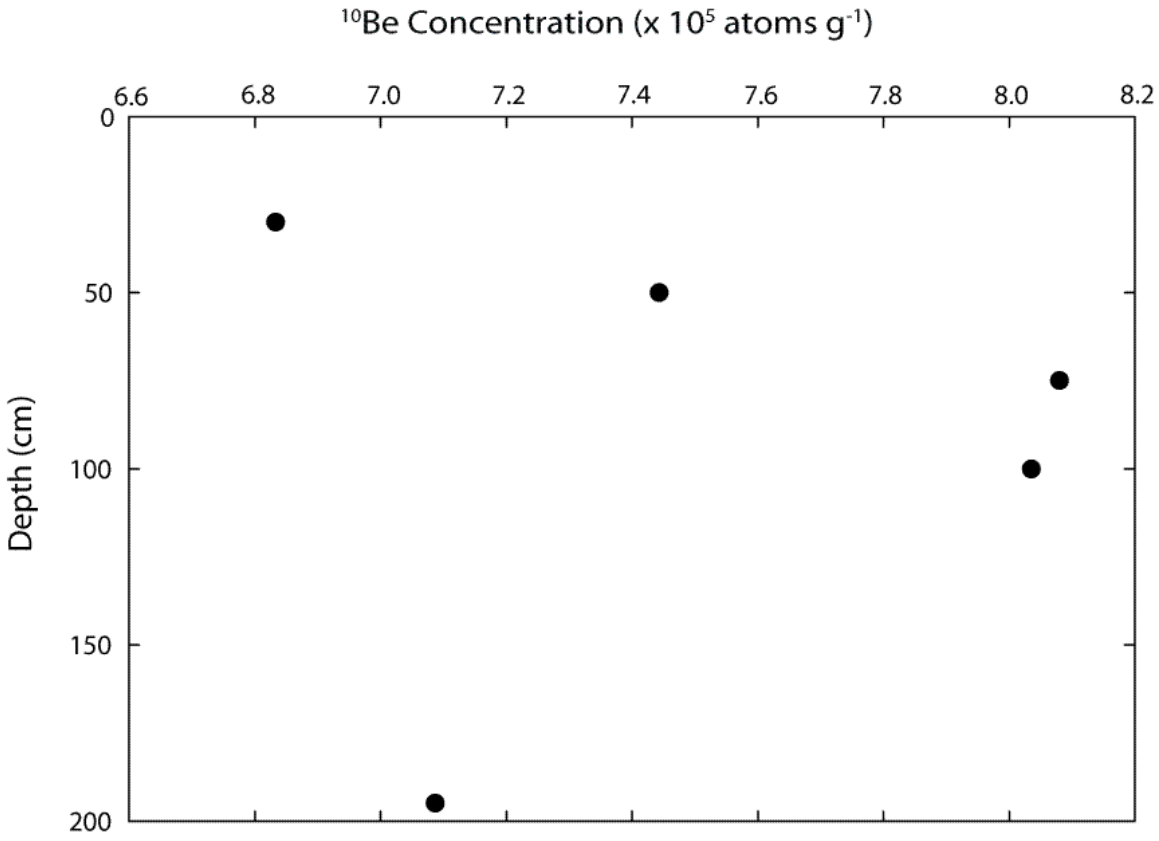

Figure 9. Plot of ^{10}Be concentration versus depth from the Q3b depth profile. Beryllium-10 data from the Q3b pit are equivocal and do not allow for direct exposure age modeling as was conducted for the other sampled deposits. Therefore, we use the age of correlative Q3b deposits determined by ^{10}Be TCN dating along the nearby Lone Mountain piedmont (17 ± 1 ka) to estimate extension rates for offset Q3b deposits in Clayton Valley. See Table 4 for displacements and extension rates for varying fault dips.

CHAPTER 6

EXTENSION RATES

Having measured vertical displacements from the surveyed scarp profiles, we then calculate corresponding horizontal displacements and extension rates. Nowhere is a fault plane exposed in the study area on which to take a direct measurement of dip. Fault dip has important implications for calculating precise extension rates (the lower the dip, the greater the amount of extension) and evidence exists throughout the western U.S. for both high-angle and low-angle normal faulting [e.g., *Wernicke,* 1981; *Wernicke et al.,* 1988; Axen *et al.,* 1999; *Burchfiel et al.,* 1987; *Lee et al.,* 2001a, 2009a, 2009b; *Phillips and Majkowski,* 2011]. Nevertheless, the exact geometry of the fault in Clayton Valley (i.e. shallow, steep, listric) is unknown. Traditional Andersonian fault mechanics predict that normal faults should dip ~ 60° [*Anderson,* 1951]. Accordingly when direct measurement of fault dip is not possible, most studies of normal faults generally assume a 60° dip when calculating extension rates. However, there is abundant evidence of low-angle normal faulting throughout western North America [e.g., *Wernicke,* 1981; *Burchfiel et al.,* 1987; *Yin,* 1989; *Caskey et al.,* 1996; *Axen et al.,* 1999; *Cichanski,* 2000; *Abbott et al.,* 2001; *Anders et al.,* 2001; *Hayman et al.,* 2003; *Kirby et al.,* 2004; *Numelin et al.,* 2007; *Hoeft and Frankel,* 2010; *Phillips and Majkowski,* 2011], as shown by the 40° dip measured along the Lone Mountain fault in the northern segment of the SPLM.

Since no fault planes are exposed on which to measure dip in Clayton Valley, we calculate horizontal displacements for dips of 30° and 60° to provide a range of possible extension values (Table 4 and Figure 10). Extension rates are calculated using the

probabilistic approach of *Zechar and Frankel* [2009], whereby measurements of age and displacement are each treated as a random variable characterized by a probability density function (pdf). Age and displacement probability distributions can each be treated as a Gaussian distribution or as a boxcar function. The slip rate pdf is then computed as the convolution of the age and displacement pdf's (Figure 11). For our purposes, displacements are treated as a Gaussian distribution with symmetric errors. Since modeled age uncertainties are also very nearly symmetric, age measurements are treated as Gaussian distributions as well. Uncertainties are computed at the 1σ confidence level. The rates presented here are minimum values as the implicit assumption of these calculations is that faulting was syndepositional. In reality, the age of offset fan deposits represents an upper bound for the time of faulting.

This method yields an extension rate for unit Q2d between 0.1 ± 0.1 and 0.3 ± 0.1 mm/yr since ~91 ka for fault dips of 30° and 60° respectively (Figure 12). Data from unit Q2c and Q2b yield complimentary extension rates of 0.1 ± 0.1-0.2 ± 0.1 mm/yr for 30° and 60° fault dips since ~96 ka and ~137 ka respectively (Figure 12). As mentioned above, we use the age of correlative offset Q3b surfaces along the nearby Lone Mountain fault zone [*Hoeft and Frankel*, 2010; in review] to estimate extension rates since Q3b deposition. Doing so yields an extension rate of ~0.1-0.3 mm/yr for a range of fault dips from 30° to 60°.

Table 4: Horizontal displacements and extension rates for fault dips of 30° and 60°.

Fan Unit	Vertical displacement (m)	Extension with 30° dip (m)	Extension with 60° dip (m)	Extension rate with 30° dip (mm/yr)	Extension rate with 60° dip (mm/yr)
Q3b	3.2 ± 0.3	5.5 ± 0.3	1.8 ± 0.3	0.3*	0.1*
Q2d	17.8 ± 1.2	30.8 ± 1.2	10.3 ± 1.2	0.3 ± 0.1	0.1 ± 0.1
Q2c	13.6 ± 0.5	23.6 ± 0.5	7.9 ± 0.5	0.2 ± 0.1	0.1 ± 0.1
Q2b	14.0 ± 0.5	24.2 ± 0.5	8.1 ± 0.5	0.2 ± 0.1	0.1 ± 0.1

*Terrestrial cosmogenic nuclide samples collected from Q3b deposits are equivocal and do not allow for direct modeling of exposure age or explicit treatment of uncertainty as with the other units. The extension rate estimates presented for Q3b are based on the age of correlative deposits (17 ± 1 ka) at nearby Lone Mountain [*Hoeft and Frankel*, 2010].

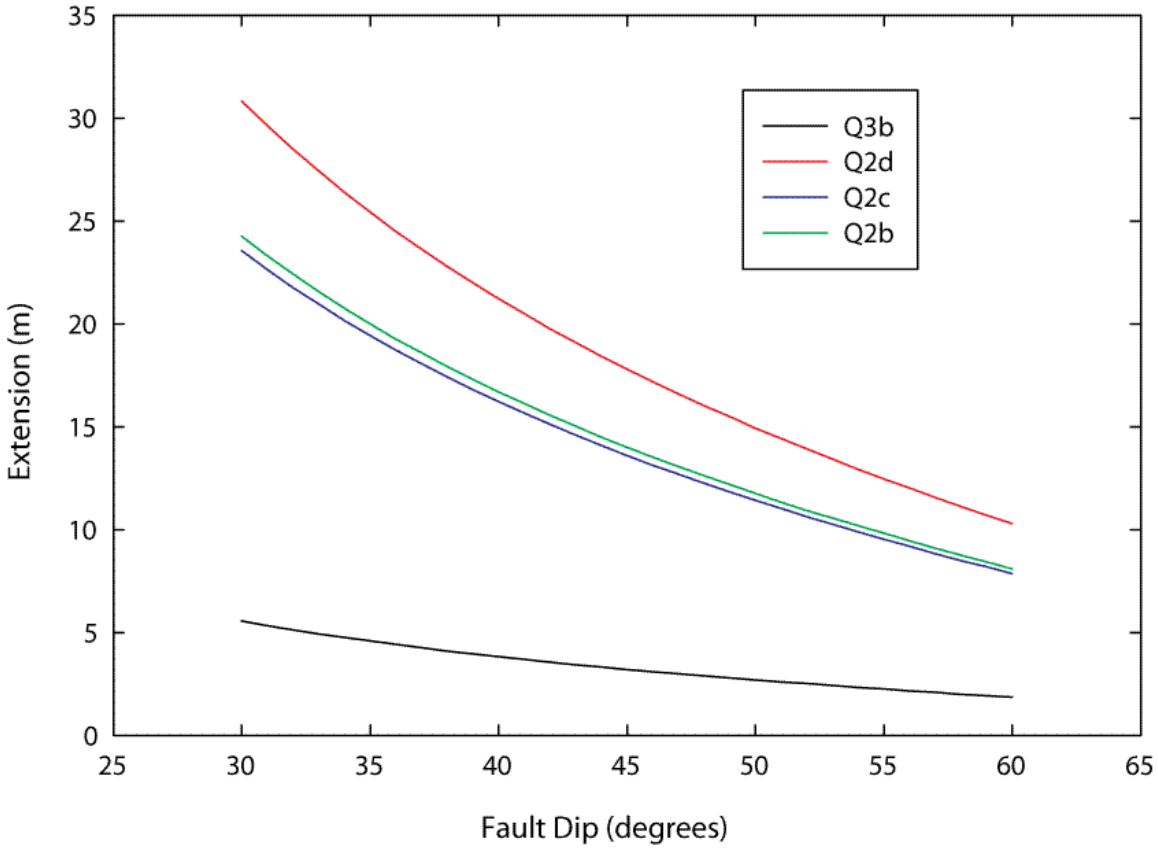

Figure 10. Extension as a function of dip angle. For a given vertical displacement, the amount of horizontal extension accommodated by a normal fault is highly dependent on fault dip. Steeply-dipping faults with accommodate less extension than shallowly-dipping faults for the same vertical displacement. Since there were no fault planes exposed on which to directly measure fault dip, we calculate horizontal displacements and associated extension rates for dips between 30° and 60° (Table 4).

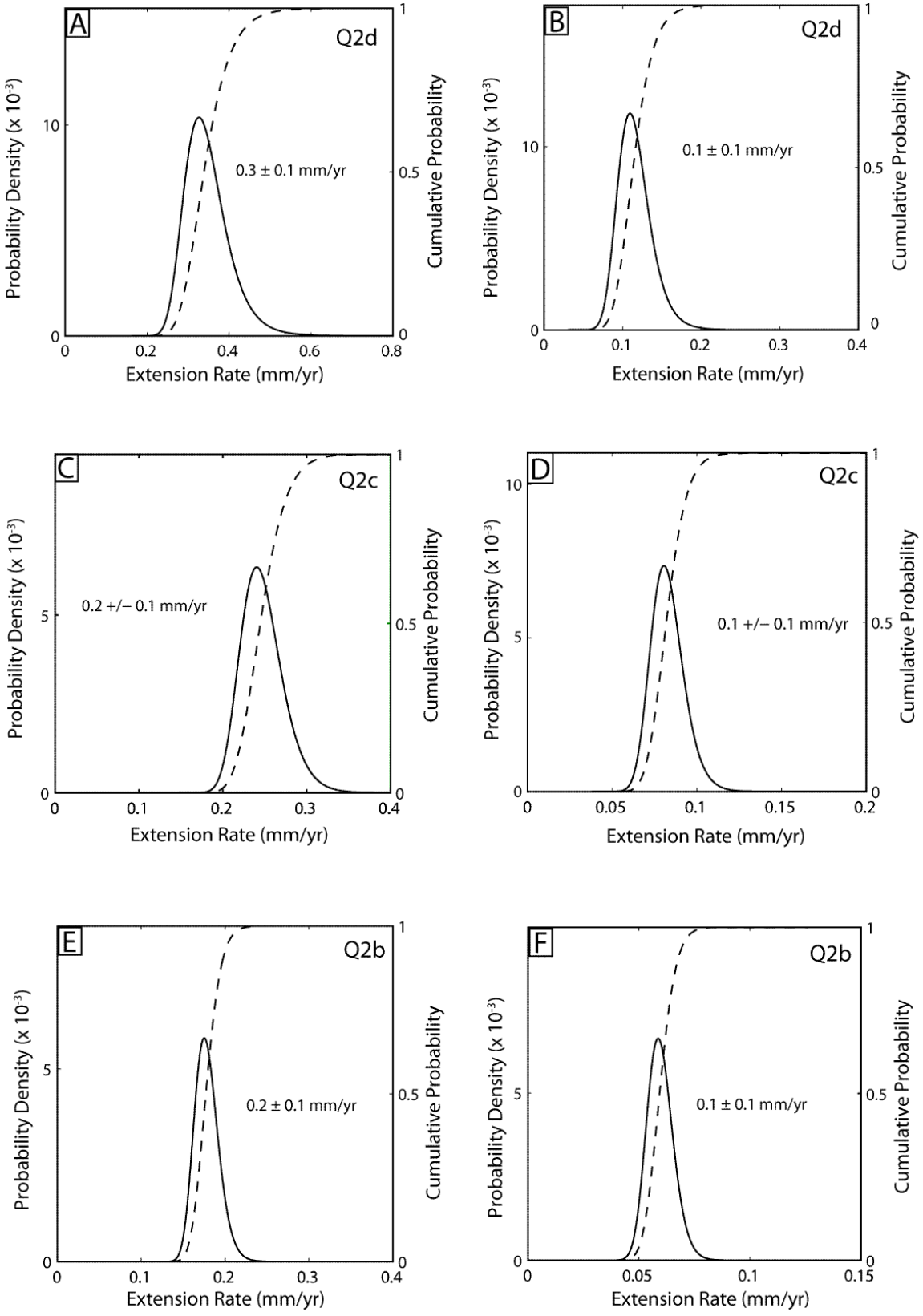
A
Q2d
0.3 ± 0.1 mm/yr
B
Q2d
0.1 ± 0.1 mm/yr
C
Q2c
0.2 +/– 0.1 mm/yr
D
Q2c
0.1 +/– 0.1 mm/yr
E
Q2b
0.2 ± 0.1 mm/yr
F
Q2b
0.1 ± 0.1 mm/yr
Probability Density (x 10-3)
Cumulative Probability
Extension Rate (mm/yr)

Figure 11. Extension rate probability density functions (pdf's) based on total measured offset and modeled TCN age for each displaced fan surface [e.g., *Zechar and Frankel*, 2009]. Uncertainties are presented at the 1σ confidence level. Solid black line represents probability density function produced by the convolution of TCN age and offset measurement pdf's. Dashed line represents the cumulative probability distribution for the same data. A: Extension rate pdf for Q2d with a fault dip of 30º. B: Extension rate pdf for Q2d with a fault dip of 60º. C: Extension rate pdf for Q2c with a fault dip of 30º. D: Extension rate pdf for Q2c with a fault dip of 60º. E: Extension rate pdf for Q2b with a fault dip of 30º. F: Extension rate pdf for Q2b with a fault dip of 60º.

CHAPTER 7

DISCUSSION

Late Pleistocene Slip Rates

The primary question this study aims to address is the temporal constancy of strain rates in the ECSZ-Walker Lane transition zone. If it is reasonable to assume that the rate of strain accumulation across this region has been constant over the late Holocene [e.g., *Frankel et al.,* in press], then the difference between the geodetic rate of 9.3 ± 0.2 mm/yr [*Bennett et al.,* 2003] and the sum of late Pleistocene geologic slip rates (≤ 3.5 mm/yr) for the White Mountains fault zone and northern Death Valley-Fish Lake Valley fault zone [*Kirby et al.,* 2006, *Frankel et al.,* 2007b] should be accounted for on other structures. The SPLM extensional complex contains the most prominent structures east of the Death Valley-Fish Lake Valley fault zone. These normal faults are the most kinematically suitable structures to account for the strain deficit due to their down-to-the-northwest orientation within the regional NW-SE trending zone of dextral shear defined by the ECSZ and Walker Lane (Figure 2). We calculate an extension rate of 0.1 ± 0.1-0.2 ± 0.1 mm/yr since ~137 ka and ~96 ka based on offset Q2b and Q2c deposits, and an extension rate of 0.1 ± 0.1-0.3 ± 0.1 mm/yr since ~91 ka and ~17 ka based on Q2d and Q3b offset. Summing the late Pleistocene Clayton Valley extension rates with the combined White Mountains and northern Death Valley-Fish Lake Valley fault late Pleistocene slip rates (≤ 3.5 mm/yr) yields a total right-lateral shear rate of < 4 mm/yr, which is still significantly lower than the regional geodetic rate of 9.3 ± 0.2 mm/yr [*Bennett et al.,* 2003].

The discrepancy between geodetic and geologic strain rates at the latitude of Clayton Valley is enigmatic as geodetic data and geologic slip rates appear to agree everywhere else in the ECSZ between the Garlock fault and Clayton Valley. Summing late Pleistocene geologic slip rates for the Owens Valley, Hunter Mountain-Saline Valley, Death Valley-Fish Lake Valley, and Stateline fault systems at ~37° N yields a total rate of ~9-10 mm/yr, which agrees with the geodetic velocity to 9.3 ± 0.2 mm/yr [Figure 1; *Bennett et al.,* 2003; *Frankel et al.,* 2007a; *Lee et al.,* 2009a]. Further north, late Pleistocene slip rates for the Owens Valley, Deep Springs, and Death Valley-Fish Lake Valley faults sum to ~9 mm/yr in the direction of the *Bennett et al.* [2003] GPS vector [*Kirby et al.,* 2008; *Frankel et al.,* in press]. Spatial variation in slip rate is well-documented along the Death Valley-Fish Lake Valley fault system [e.g., *Wright and Troxel,* 1970; *Frankel et al.,* 2007b, in press]. Slip rate decreases northward from 6.1 +1.3/-1.0 mm/yr at Cucumongo Canyon in the center of the fault system to 2.5 +0.4/-0.3 mm/yr at Furnace Creek in northern Fish Lake Valley [Figure 2; *Frankel et al.,* 2007b, in press]. *Ganev et al.* [2010] also document a commensurate northward increase in extension rate along the northern extent of the fault. Taken together, these observations agree with the suggestion that dextral shear is pulled off of the northern Death Valley-Fish Lake Valley fault system and transferred onto normal faults of the SPLM extensional complex. Given these observations, the total extension rates of the SPLM faults should account for the northward decrease in right-lateral slip along the Death Valley-Fish Lake Valley fault. The measured extension rates, however, are clearly not high enough to do so.

There are three possible explanations for the mismatch between short-term and long-term strain rates. First, the "missing" strain could be accommodated by structures other than the White Mountains and Death Valley-Fish Lake Valley fault zones, in which case strain rates have remained constant since the late Pleistocene. Conversely, the region could be experiencing a strain transient similar to that of the nearby Mojave Desert or the rate of strain accumulation across this region could be increasing. Based on the data from Clayton Valley, there is little or no evidence of an increase in extension rate that would argue for an increase in strain accumulation since the late Pleistocene as has been suggested for the Emigrant Peak and Lone Mountain faults [e.g., *Reheis and Sawyer*, 1997; *Hoeft and Frankel,* 2010]. We cannot preclude the possibility of a strain transient, especially given the complex fault architecture throughout this region. However, our results indicate that the geodetic-geologic rate discrepancy of the ECSZ-Walker Lane transition can be explained as a result of the effects of distributed deformation.

Distributed Deformation

Plate boundary deformation is generally approximated as one of two end-member models [e.g., *Thatcher,* 2009]. Block models assume that deformation is localized along discrete faults bounding individual microplates [e.g., *Avouac and Tapponnier,* 1993; *Shen et al.,* 2005; *Meade,* 2007; *Thatcher et al..,* 2007; *Loveless and Meade,* 2011], whereas continuum models treat deformation as occurring diffusely throughout the lithosphere [e.g., *Molnar and Tapponnier*, 1975; *Molnar,* 1988; *Thatcher*, 1995; *England and Molnar,* 2005; *Gan et al.,* 2007]. The block model clearly best approximates deformation on the scale of global plate tectonics. On the smaller scale of an actively deforming continental margin, however, the continuum model becomes more appropriate as block

size decreases and the width of microplate bounding fault zones increases [e.g., *Thatcher*, 2009]. Our results from Clayton Valley indicate that the ECSZ-Walker Lane transition may be best approximated by the broadly-distributed, diffuse deformation of a continuum rather than being concentrated on a few major faults. In this case, geologic fault slip rates are likely to be underestimated due to the effects of unrecognized fault strands and/or off-fault deformation. Since geologic rates agree with geodetic data throughout the ECSZ everywhere between Clayton Valley and the Garlock fault, they should agree at the latitude of Clayton Valley if the rate of strain accumulation has remained constant since the late Pleistocene. Taking into account the diffuse nature of deformation observed in Clayton Valley, it is evident that not all of the deformation is being recorded in the surficial geology.

Seismic and well-log data published from investigations of the subsurface lithium-brine aquifers located near the town of Silver Peak [*Davis,* 1981; *Zampirro,* 2005] also point to deformation that is very diffuse throughout Clayton Valley. The geophysical data reveal a synclinal basin structure that is several thousand feet deep, thickening towards the south-southeast [*Davis*, 1981; *Zampirro,* 2005]. A series of high-angle intrabasin normal faults are also revealed in the seismic data, many of which are not expressed at the surface [*Zampirro,* 2005]. Although these faults certainly contribute to the total slip budget for Clayton Valley, they are not recorded in the surficial geology and hence displacement attributed to them is missing from the geologic record.

Missing strain is also reflected in the fact that offset measured across Q2b deposits (~137 ka) is less than the offset measured across younger Q2d deposits (~91 ka). The older Q2b deposits in the southern portion of the map area should have experienced

at least the same displacement as younger Q2d deposits further north, if not more. While it is possible that this pattern of displacement could be attributed to along-strike variations in slip as the highly-faulted Q2d deposits are located further north than the older Q2b deposits (Figure 3), the geophysical data discussed above support the conclusion of diffuse deformation. The fact that older deposits have experienced greater displacement is also evident from the observation that the maximum scarp height increases with age between the four surveyed fan units (Figure 12). It is also important to note that in many cases the hanging wall of the faulted deposits is not preserved but is instead buried by younger alluvial deposits (Figure 4, Figure 5, and Figure 6). Furthermore, the deformation expressed in Q2d deposits occurs over a relatively wide zone with at least 10 different mapped fault scarps contributing to the total measured deformation. Where this distributed faulting is exposed at the surface in unit Q2d (Figure 4), a significantly greater amount of deformation is observed than in nearby Q2c deposits that are the same age within error. The seismic and well-log data combined with map relationships discussed above strongly argue for deformation that is of a very diffuse, distributed nature in Clayton Valley as opposed to being localized along a few discrete structures. This further underscores the fact that geologically-determined slip rates are minimum values and the true rates could potentially be significantly higher, which would in turn bring them into closer agreement with the geodetic data.

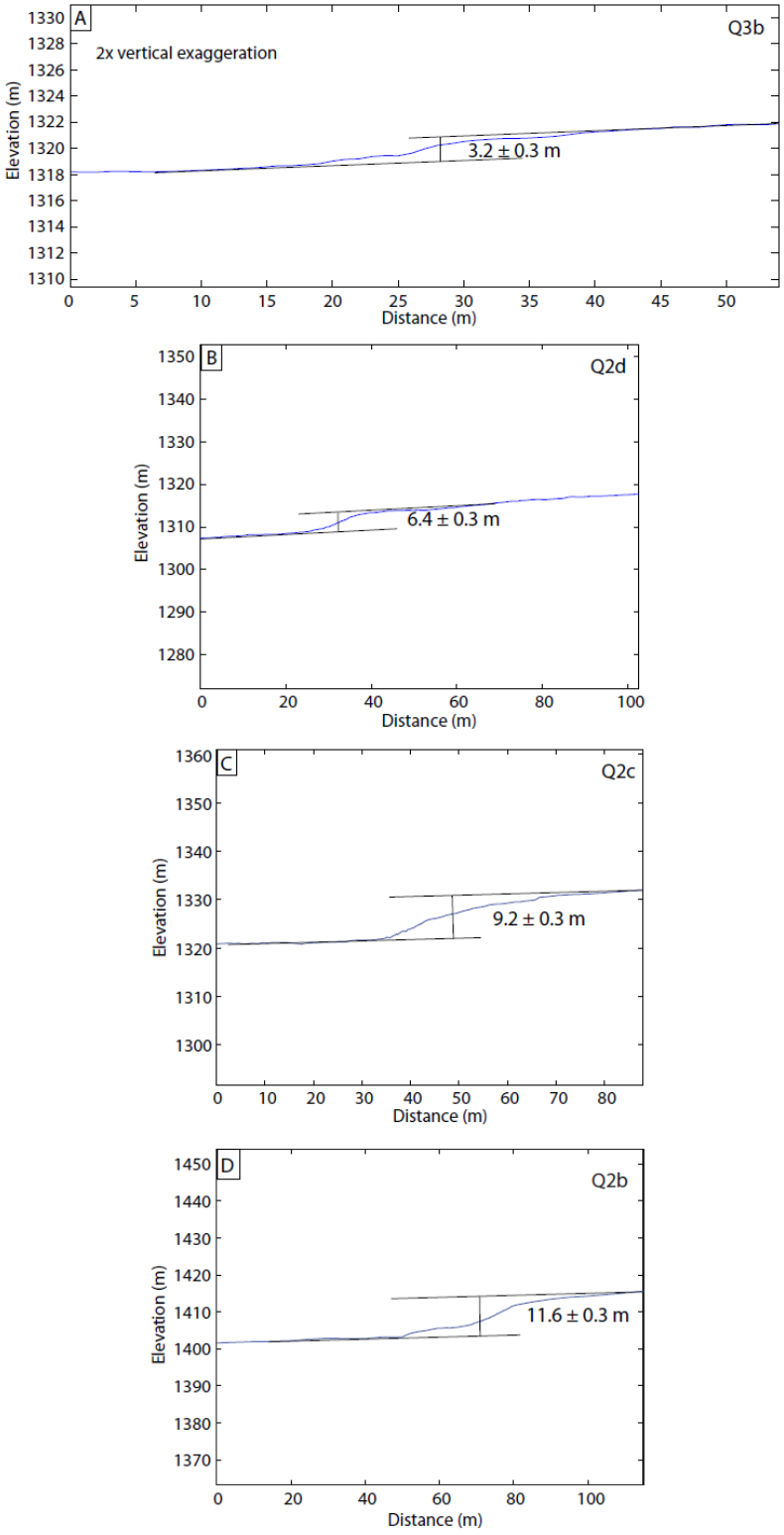

Figure 12. Profiles showing the maximum scarp height across each surveyed unit. Maximum scarp height increases with age, supporting the argument that a potentially significant amount of strain is missing from the geologic record. A: Q3b. B: Q2d. C: Q2c. D: Q2b.

As discussed earlier, the disorganized nature of the ECSZ-Walker Lane partly reflects the youth of the shear zone relative to the San Andreas system [*Faulds et al.,* 2005; *Wesnousky,* 2005b]. Based on field studies of strike-slip fault systems in California, *Wesnousky* [1990, 2005b] suggests that fault trace complexity varies inversely with cumulative offset and that the greater complexity and disorganization of the ECSZ-Walker Lane is largely due to the fact that it has taken up considerably less total slip than the San Andreas. Over the last 30 Ma, the San Andreas fault system has grown in response to northward migration of the Mendocino triple junction [*Atwater and Stock,* 1998]. It has been hypothesized that as the Mendocino triple junction continues to migrate northward the faults of the ECSZ-Walker Lane may offer a more kinematically suitable orientation for the Pacific-North America plate boundary than the San Andreas fault [e. g., *Glazner and Bartley,* 1984; *Faulds et al.,* 2005; *Wesnousky,* 2005b; *Frankel et al.,* in press]. If this interpretation is accurate, the plate boundary would eventually move inland to the area presently defined by the ECSZ and Walker Lane. The continued growth of the shear zone would likely lead to the development of a more continuous, through-going fault trace analogous to the San Andreas.

The distributed nature of deformation at the northern terminus of the ECSZ is analogous to the eastern terminus of the left-lateral Garlock fault in southern California. The structural character of deformation along the eastern Garlock is markedly different from the central and western segments of the fault which appear to be characterized by slip that is relatively localized on the main trace of the fault and does not appear to be accompanied by large magnitude block rotations [*Guest et al.,* 2003; *McGill et al.,* 2009]. Displacements of 48-64 km have been attributed to the central and western portions of

the fault, and measured slip approaches zero towards its eastern end [*Davis and Burchfiel,* 1973]. Some of this deformation may be taken up by clockwise vertical-axis block rotations in the northeastern Mojave [*Guest et al.,* 2003]. This lack of resolvable slip along the eastern Garlock is analogous to the anomalously low geologic slip rates at the northern end of the ECSZ; in both cases deformation appears to be missing from the geologic record. As such, the Garlock fault provides another example of a fault zone with a broadly similar deformation pattern to that observed at the northern termination of the ECSZ. With both the Garlock and the northern ECSZ, it is clear that a higher degree of complexity exists at the end of the fault system where slip is transferred off of the main fault trace and onto other structures; specifically, these strain transfer zones appear to be characterized by more diffuse deformation.

Strain Transfer

Strain transfer between the misaligned structures of the ECSZ and Walker Lane occurs primarily by left-lateral strike-slip faulting within the Mina deflection and down-to-the-northwest normal faulting in the Silver Peak-Lone Mountain extensional complex, both of which are accompanied by clockwise vertical-axis block rotations [*Oldow et al.,* 1994; *Reheis and Sawyer,* 1997; *Petronis et al.,* 2002, 2007, 2009; *Frankel et al.,* 2007b; *Lee et al.,* 2009a; *Ganev et al.,* 2010; *Hoeft and Frankel,* 2010]. The Queen Valley fault at the northern end of the White Mountains acts to transfer strain from Owens Valley into the Mina deflection. Similarly, the faults of the Silver Peak-Lone Mountain extensional complex pull strain off of the northern Death Valley-Fish Lake Valley fault [*Lee et al.,* 2009a; *Ganev et al.,* 2010]. The Mina deflection and Silver Peak-Lone Mountain extensional complex ultimately transfer strain from Owens Valley and Fish Lake Valley

through a right-step northeastward onto the en-echelon right-lateral Benton Springs and Bettles Well-Petrified Springs faults of the Walker Lane (Figure 2 and Figure 13). The extension rates presented here provide a more complete picture of regional dynamics and show that the Clayton Valley fault zone plays an important role in accommodating strain transfer between the ECSZ and Walker Lane.

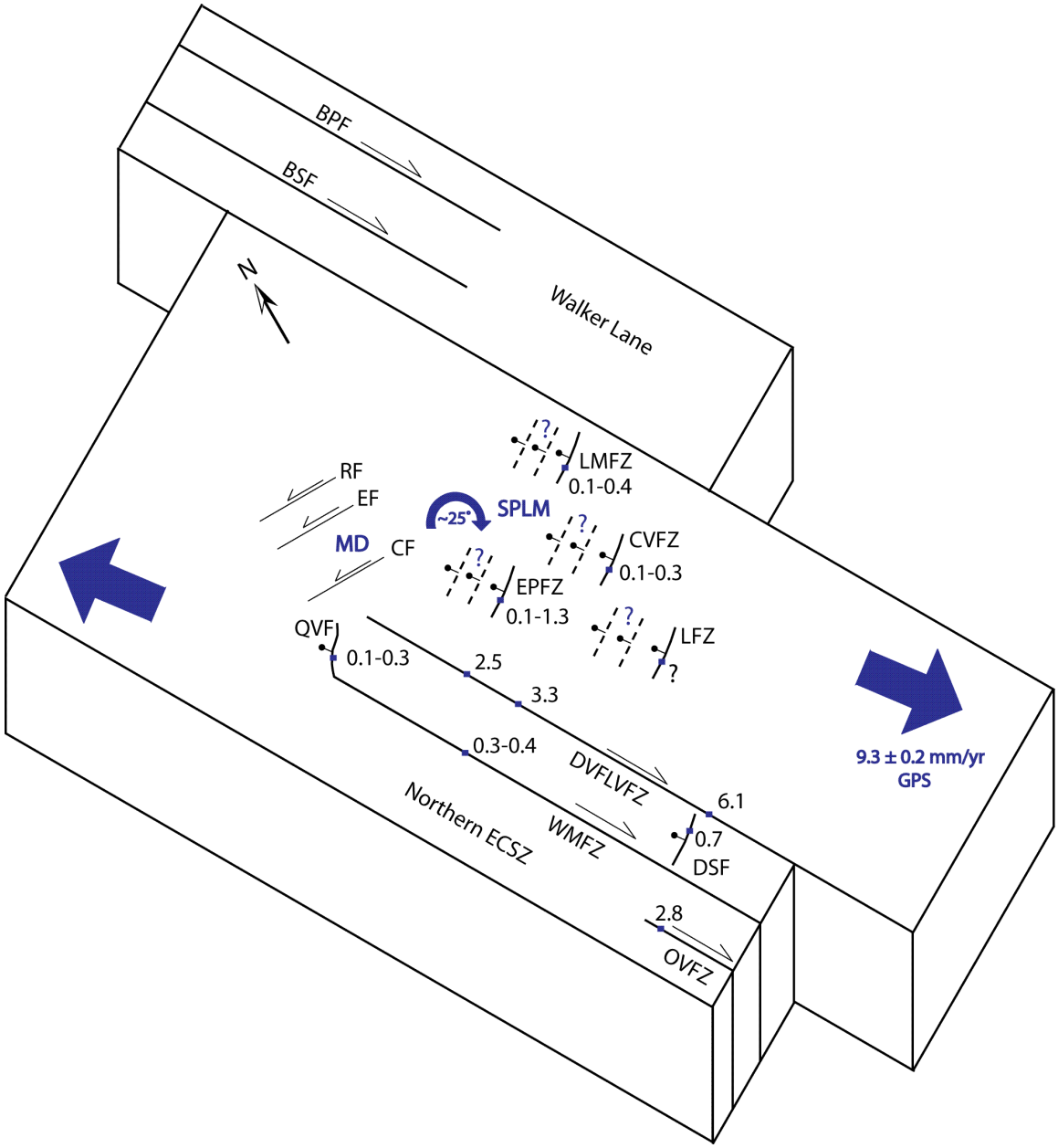

Figure 13. Block diagram illustrating diffuse deformation through the eastern California shear zone (ECSZ)-Walker Lane transition. GPS vector is from *Bennett et al.,* [2003]. Late Pleistocene fault slip rates are in mm/yr [*Reheis and Sawyer,* 1997; *Frankel et al.,* 2007a, 2007b, in press; *Kirby et al.,* 2008; *Lee et al.,* 2001b, 2009b; *Hoeft and Frankel,* 2010; this study]. At the northern termination of the ECSZ, deformation is pulled off of the White Mountains and Death Valley-Fish Lake Valley faults and transferred through a right step northeastward to the en echelon faults of the Walker Lane. Strain transfer is accommodated via left-lateral strike-slip faulting, down-to-the-northwest normal faulting, and clockwise vertical-axis block rotations. Throughout the ECSZ, geologic fault slip rates agree with the GPS rate everywhere between the Garlock fault and the northern White Mountains where geologic rates suddenly decrease to less than half of the GPS rate. Our results from Clayton Valley indicate that this discrepancy is the result of distributed deformation that causes geologic rates to be underestimated. Dashed-in lines represent hypothetical subsurface normal faults such as those revealed in the seismic data in Clayton Valley [*Zampirro,* 2005]. BPF: Bettles Well-Petrified Springs fault, BSF: Benton Springs fault, CF: Coaldale fault, CVFZ, Clayton Valley fault zone, DSF: Deep Springs fault, DVFLVFZ: Death Valley-Fish Lake Valley fault zone, EM: Excelsior Mountains fault, EPFZ: Emigrant Peak fault zone, LFZ: Lida fault zone, LMFZ: Lone Mountain fault zone, MD: Mina deflection, OVFZ: Owens Valley fault zone, QVF: Queen Valley fault, RF: Rattlesnake Flat fault, SPLM: Silver Peak-Lone Mountain extensional complex, WMFZ: White Mountains fault zone.

Seismic Hazard

The distributed faulting described above in Clayton Valley also has important implications for seismic hazard analysis as it highlights the fact that often times the geologic record underestimates the total amount of deformation experienced by a given region. This makes it very difficult to accurately assess not only fault slip rates but also the associated seismic hazard. This is especially important for heavily populated areas, such as the Los Angeles basin, that are known to lie in a region with abundant blind thrust faults [e.g., *Leon et al.,* 2007, 2009].

CHAPTER 8

CONCLUSIONS

Using geomorphic mapping along with TCN geochronology of offset surfaces and GPS surveys of fault displacements, we calculate the first geologic extension rates for the Clayton Valley fault. Eight separate alluvial fan deposits are mapped through southeastern Clayton Valley: Q2a, Q2b, Q2c, Q2d, Q3a, Q3b, Q3c, and Q4. Modeled TCN data yield ages for Q2b, Q2c, and Q2d deposits of 137 +10/-11 ka, 96 +9/-8 ka, and 91 +13/-12 ka respectively. TCN data are equivocal for the sampled Q3b surface, so we assume an age of 17 ± 1 ka based on correlative Q3b deposits at nearby Lone Mountain. Combining these ages with measured displacements yields an extension rate of 0.1 ±0.1-0.2 ± 0.1 mm/yr since ~96 ka and ~137 ka for Q2c and Q2b deposits for fault dips of 30° to 60°. Q2d data yield an extension rate between 0.1 ± 0.1-0.3 ± 0.1 mm/yr since ~91 ka for fault dips of 30° to 60°. Similarly, the estimated Q3b extension rate using the age from Lone Mountain is between 0.1 to 0.3 mm/yr since ~17 ka.

Based on mapping efforts and previously published seismic and well-log data, faulting appears to be diffuse and widely-distributed throughout Clayton Valley. The distributed deformation is best expressed in Q2d deposits that are offset by the main down-to-the-northwest fault as well as a series of antithetics. The total measured displacement across Q2d (17.8 ± 1.2 m) is greater than that of both Q2c deposits that are the same age within error (13.6 ± 0.5 m) and older Q2b deposits (14.0 ± 0.5 m). Even though the total displacement does not increase with age as would be expected, the maximum individual scarp height does increase with age. This indicates that not all of the

deformation is being captured in the geologic record. Seismic data corroborate this assertion by revealing several intrabasin faults that are not expressed at the surface.

The distributed deformation of Clayton Valley has important implications for understanding the dynamics of plate boundary deformation in the vicinity of the ECSZ-Walker Lane transition. Measured late Pleistocene slip rates across the ECSZ at the latitude of the central Death Valley-Fish Lake Valley fault sum to ~9 mm/yr, which is in good agreement with geodetic data. Moving northward along strike, however, geologic slip rates appear to rapidly decrease, resulting in a pronounced discrepancy between late Pleistocene geologic rates and decadal geodetic rates. If deformation is widely-distributed throughout this region as indicated by the diffuse fault network in Clayton Valley, this could help explain the apparent discrepancy. The effects of off-fault deformation and unrecognized fault strands can lead to significantly underestimated geologic slip rates. If it were possible to capture all of the deformation across Clayton Valley, the extension rates would likely be significantly higher, thereby bringing long-term geologic slip rates into closer agreement with short-term geodetic measurements in the northern ECSZ. Our results do not suggest an increase in strain accumulation across the northern ECSZ as has been proposed for the Emigrant Peak and Lone Mountain faults [e.g. *Reheis and Sawyer,* 1997; *Hoeft and Frankel,* 2010]. Instead, the pattern of deformation in Clayton Valley suggests that the mismatch between geodetic data and geologic slip rates in the ECSZ-Walker Lane transition zone can be explained as a consequence of distributed deformation.

APPENDIX A

GEOLOGIC MAP OF CLAYTON VALLEY, NEVADA

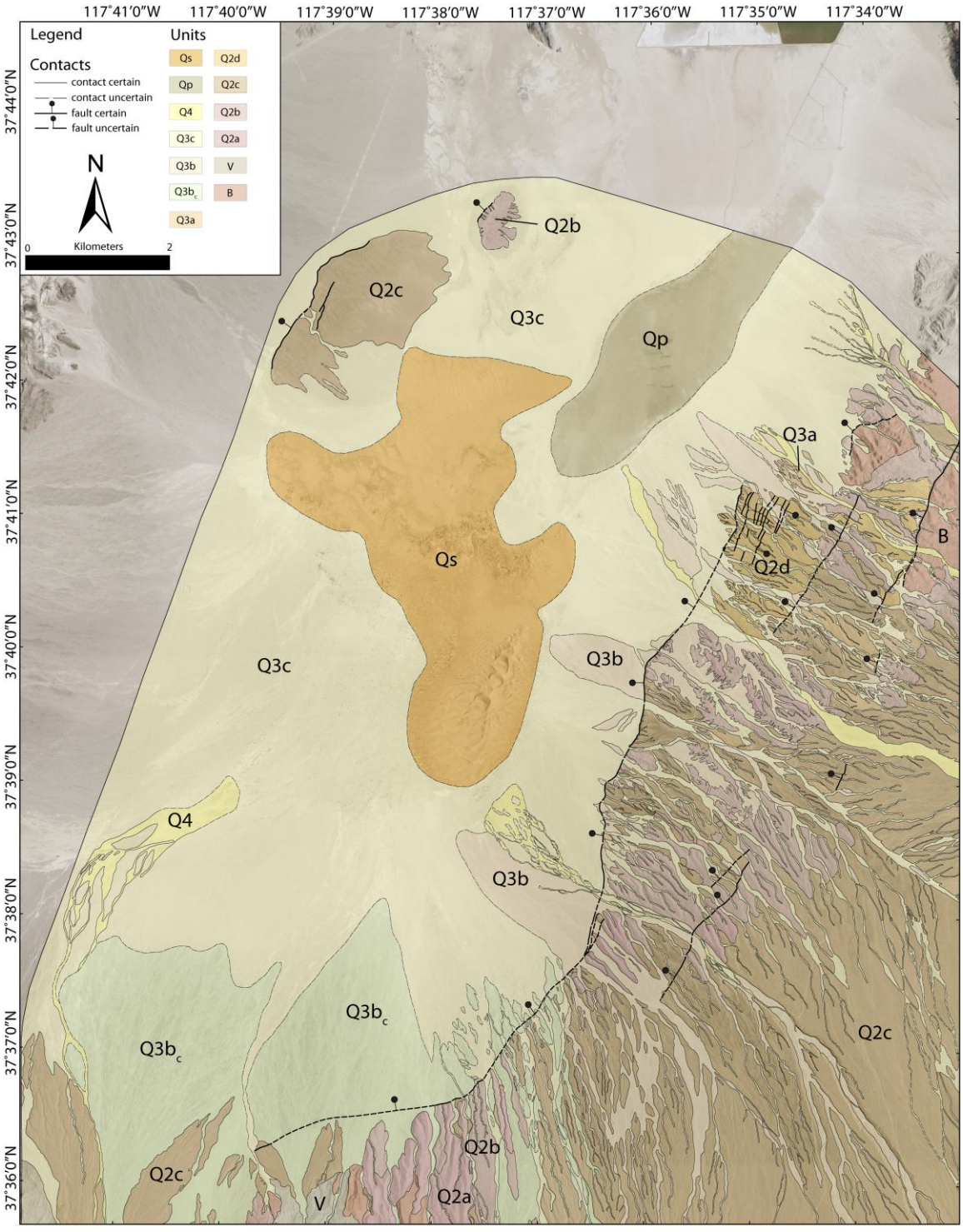

Legend

Quaternary Units

Qs: Unconsolidated eolian deposits of tan-yellow sand and silt. Eolian deposits include large sand dunes near the center of the valley and the surrounding area that is covered by a thick flat-lying layer of sand.

Qp: Playa deposits consisting of gray-brown sand, silt, and clay. The playa is vegetated and is the remnant of an earlier late Quaternary pluvial lake in Clayton Valley.

Q4: Unit Q4 includes the active and most recently abandoned stream channels. Deposits consist of poorly-sorted sub-angular pebble and cobble gravels mixed with silt and sand. Clasts lack varnish or rubification with no desert pavement development. Q4 surfaces are characterized by strong depositional morphology with gravelly bars and sandy swales and a lack of soil development. Amplitude of bar and swale morphology is ~1 m.

Q3c: Q3c surfaces preserve strong bar and swale morphology similar to Q4 but stand stratigraphically higher (~0.5-1 m above the active channel). Q3c surfaces are very silty and contain sparse vegetation.

Q3b: Q3b surfaces stand ~1-2 m above the active channel. Bar and swale morphology is more subdued relative to Q3c and Q4. Q3b is also distinguished by an immature soil development (< 5 cm thick A horizon) and locally immature varnish and desert pavement development. Q3b soils are characterized by Stage II pedogenic carbonate development.

Q3a: Q3a surfaces stand ~1.5-2.5 m above the active channel, are well-sorted, and display a strong desert pavement. Surface clasts are strongly-varnished and have a strong orange-red rubification underneath. A subdued bar and swale morphology is still

preserved (< 0.5 m). A relatively well-developed soil is present beneath Q3a surfaces with a ~5-10 cm thick A horizon.

Q2d: Q2d surfaces occur ~2-4 m above the active channel and have mature desert pavement with strong varnish and rubification. Locally, however, surfaces have a less strongly-interlocking pavement with higher preservation of depositional bar and swale morphology. Soils are very silty and display Stage I pedogenic carbonate. Cosmogenic ^{10}Be exposure age: 91 +13/-12 ka

Q2c: Q2c surfaces typically occur ~2-4 m above the active channel and display the classic, flat desert pavement surface. Surface clasts are heavily varnished, well-sorted, and display dark orange-red rubification on their undersides. Surface clasts are tightly-packed and completely interlocking. Original bar and swale morphology is very subdued to nonexistent and surfaces are essentially flat and planar. Soils are well-developed with a ~10-15 cm thick A horizon and Stage III pedogenic carbonate development. Cosmogenic ^{10}Be exposure age: 96 +9/-8 ka.

Q2b: Q2b surfaces are stratigraphically and topographically higher than younger deposits (~3-9 m above the active channel) and are best characterized by their strongly dissected nature and the fact that they are beginning to round off and diffuse into the surrounding landscape. Strong varnish and rubification can still be found on surface clasts but desert pavement is beginning to wear away and clasts are no longer as strongly interlocking as with Q2c. Surface clasts are strongly weathered and little or no depositional morphology is preserved. Q2b surfaces also contain a well-developed, bouldery soil with ~10-20 cm thick A horizon and Stage III pedogenic carbonate development. Q2b surfaces are concentrated in the southern portion of Clayton Valley

and are more highly vegetated than surfaces further north. Cosmogenic ^{10}Be exposure age: 137 +10/-11 ka

Q2a: Q2a deposits are the oldest alluvial units described in this portion of Clayton Valley and stand highest above the active channel (~6-10+ m). Q2a surfaces are generally sharp crests with little or no depositional morphology preserved. A mature soil is formed beneath the surface consisting of a ~10-20 cm thick A horizon. Surfaces have a similar morphology to Q2b but are even more strongly weathered and dissected. Surface clasts are moderately to heavily varnished and strongly rubified.

Bedrock/Volcanic Units

B: Bedrock- undifferentiated white-tan sedimentary rocks of unknown age consisting of sandstone, shale, marl, conglomerate, and breccia.

V: Volcanics- white volcanic ash deposits of unknown age.

APPENDIX B

GPS FAULT SCARP PROFILES

Q3b Profiles:

0605G

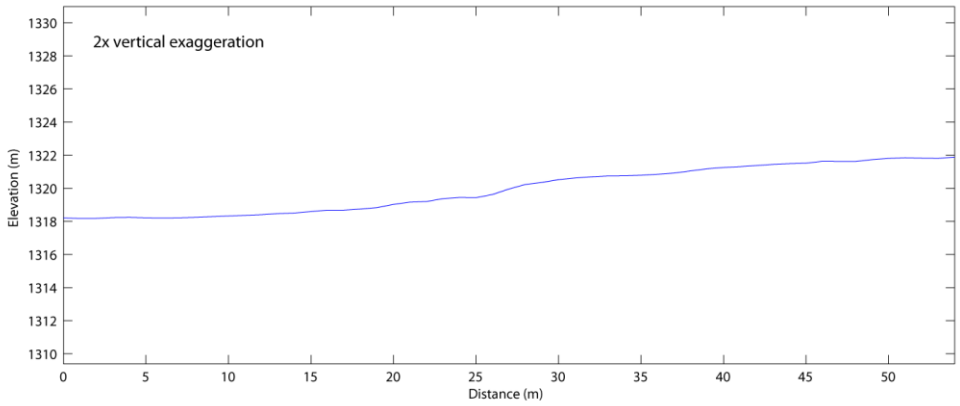

0605H

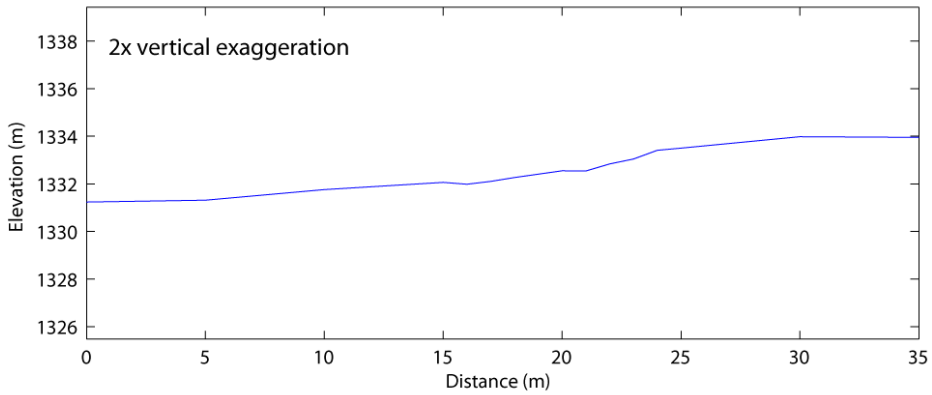

0605I

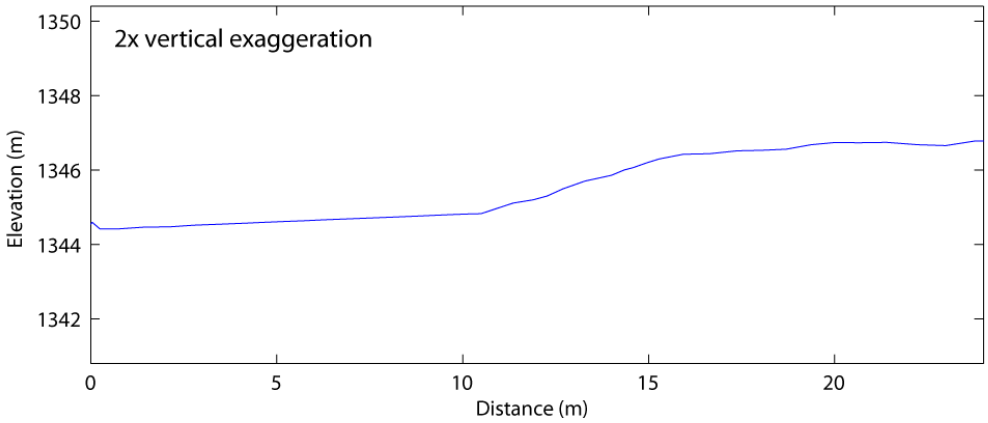

Q2d Profiles:

0604A

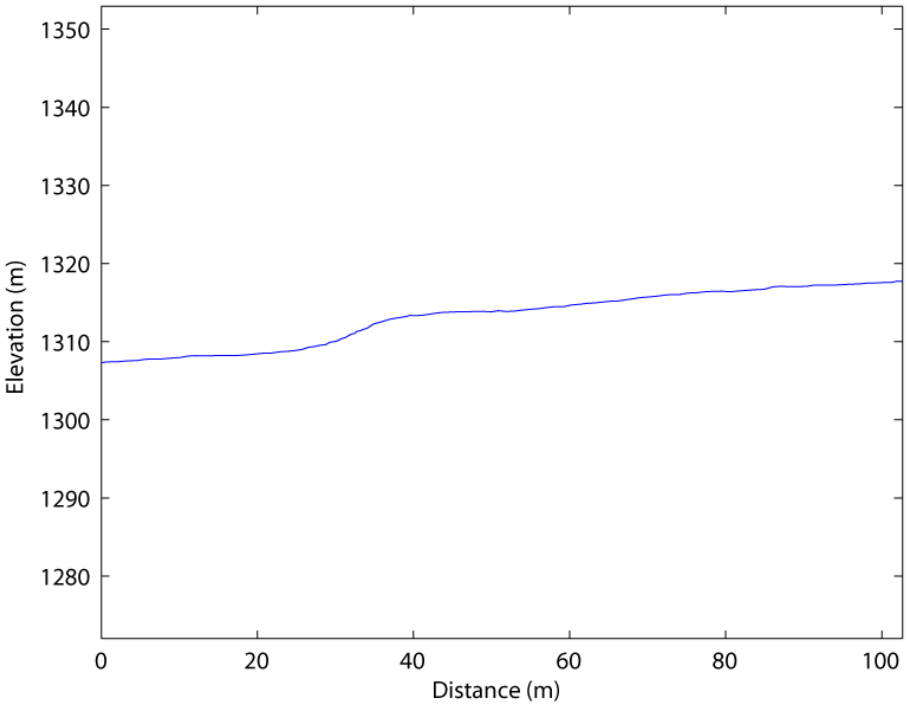

0604B-1

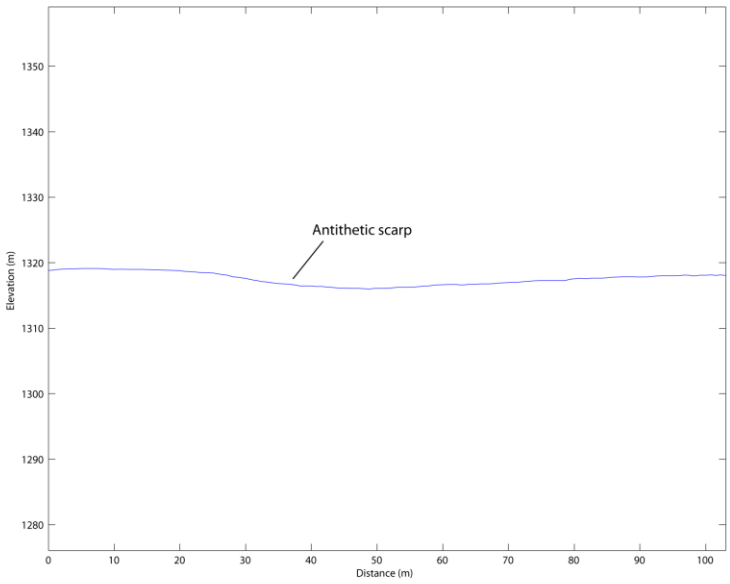

0604B-2

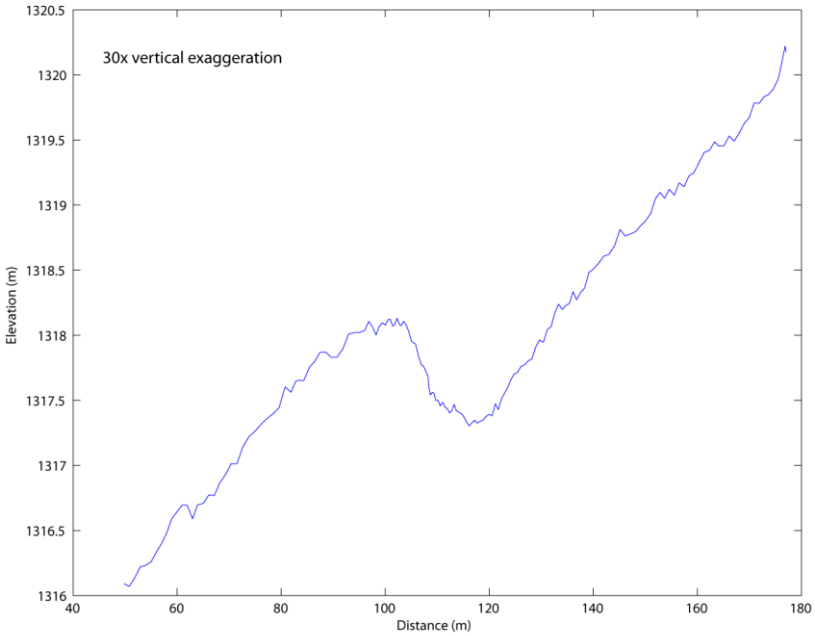

0604C

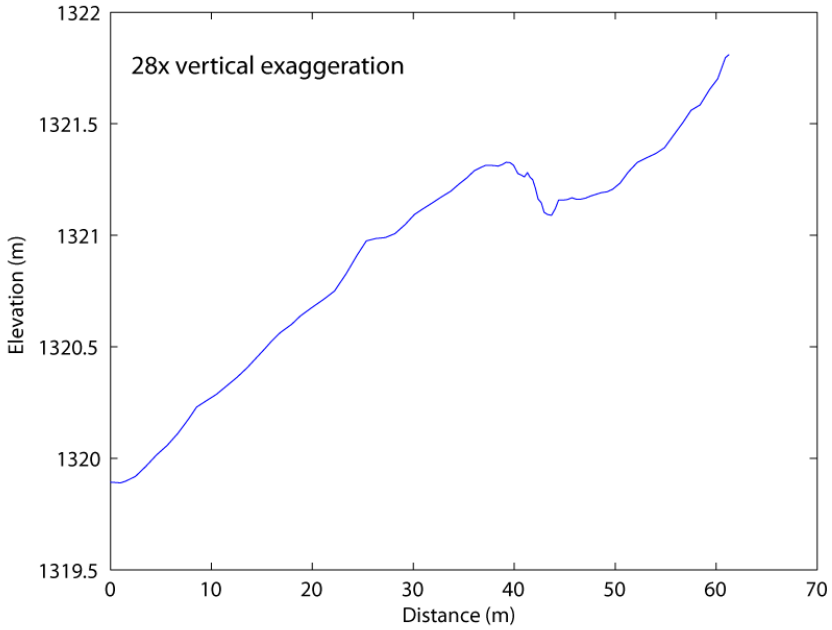

0604D-1

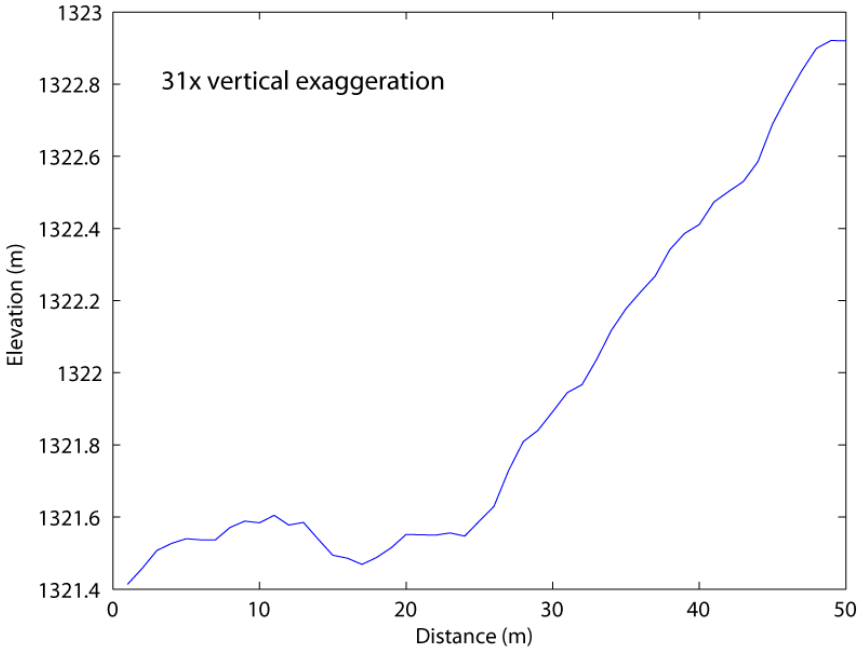

0604D-2

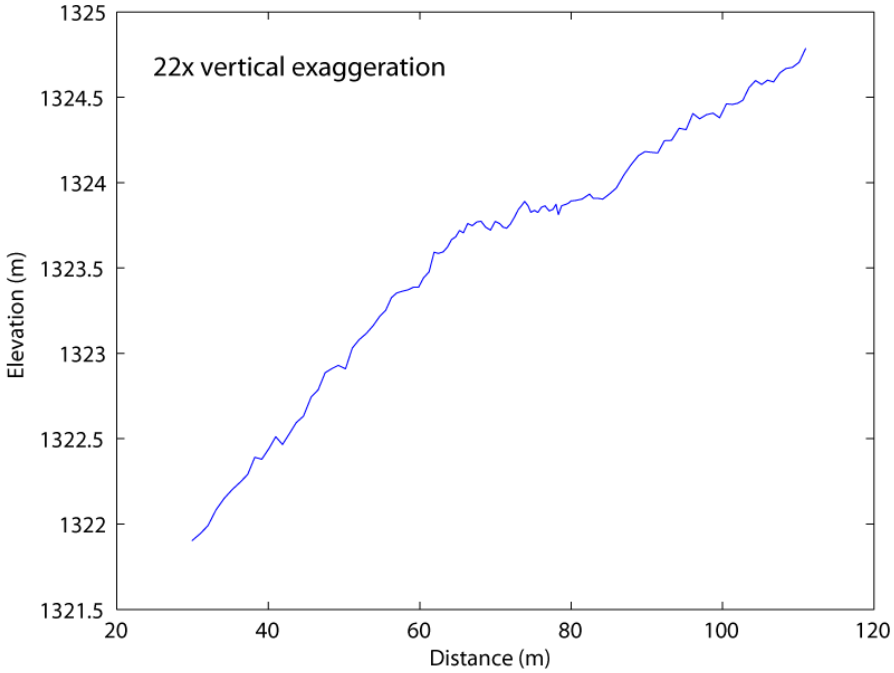

0604D-3

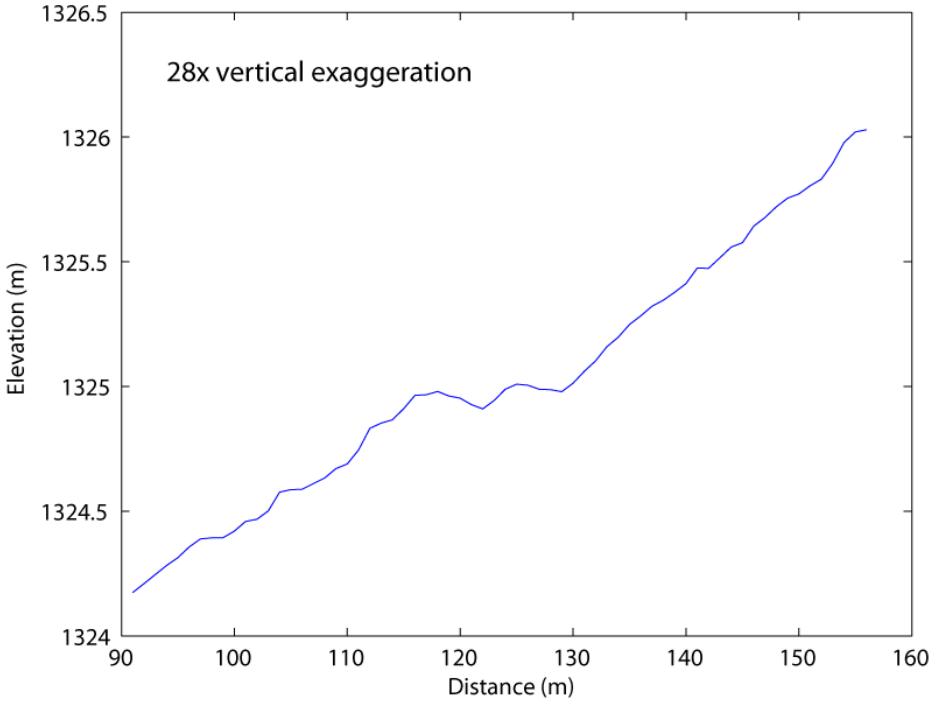

0604D-4

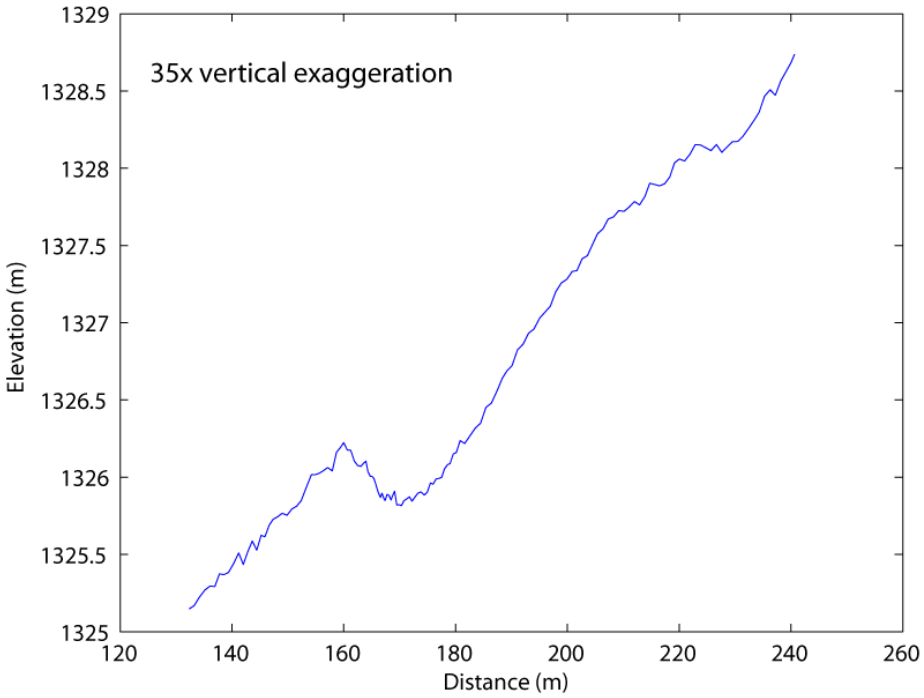

0604E

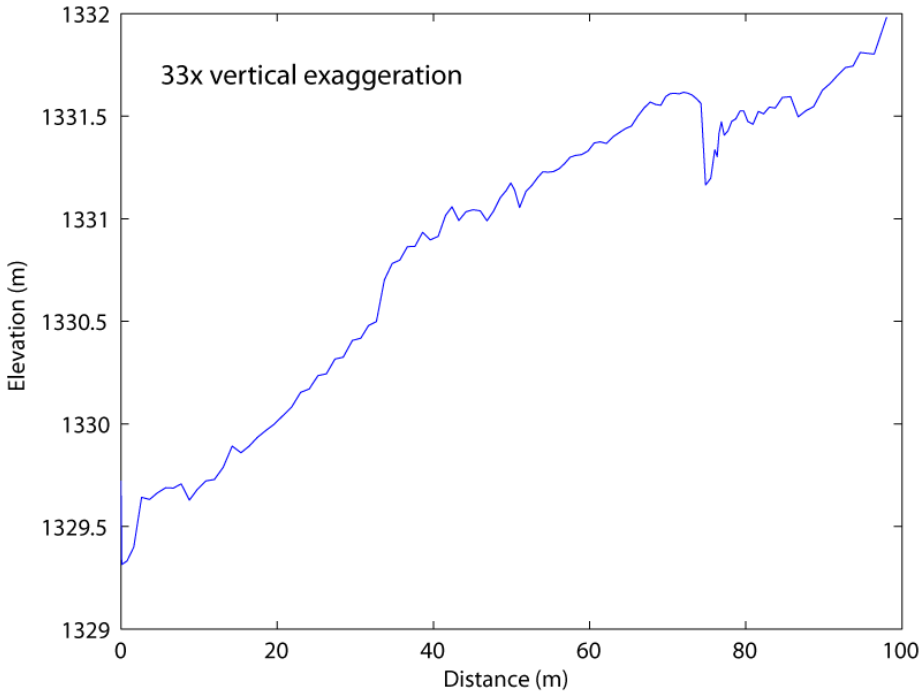

0604F

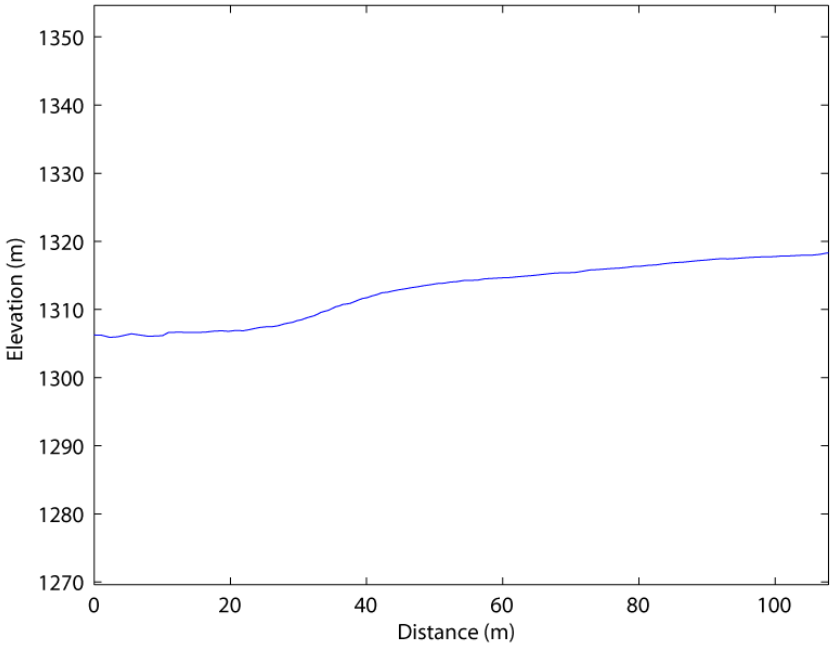
1350
1340
1330
1320
1310
1300
1290
1280
1270
Elevation (m)
0
20
40
60
80
100
Distance (m)

0604G

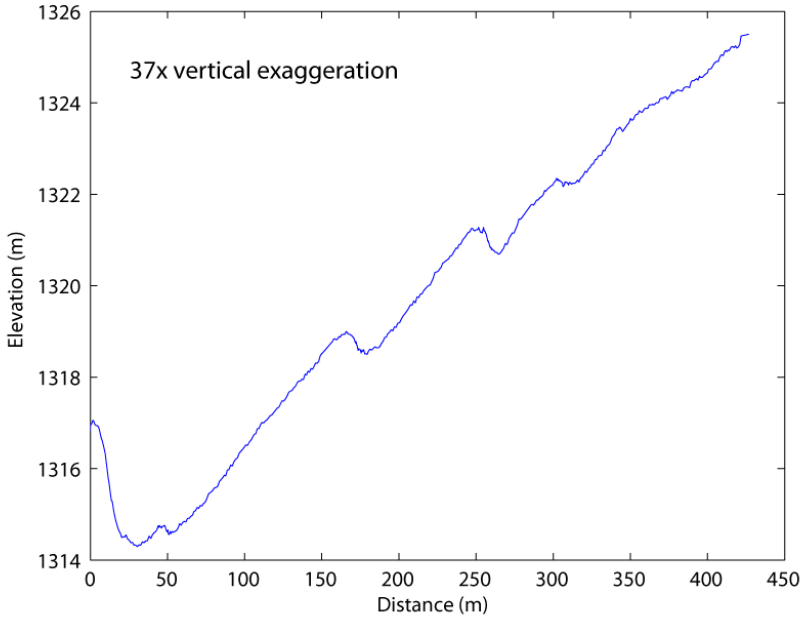
37x vertical exaggeration
1326
1324
1322
1320
1318
1316
1314
Elevation (m)
0
50
100
150
200
250
300
350
400
450
Distance (m)

Q2c Profiles:

0605B

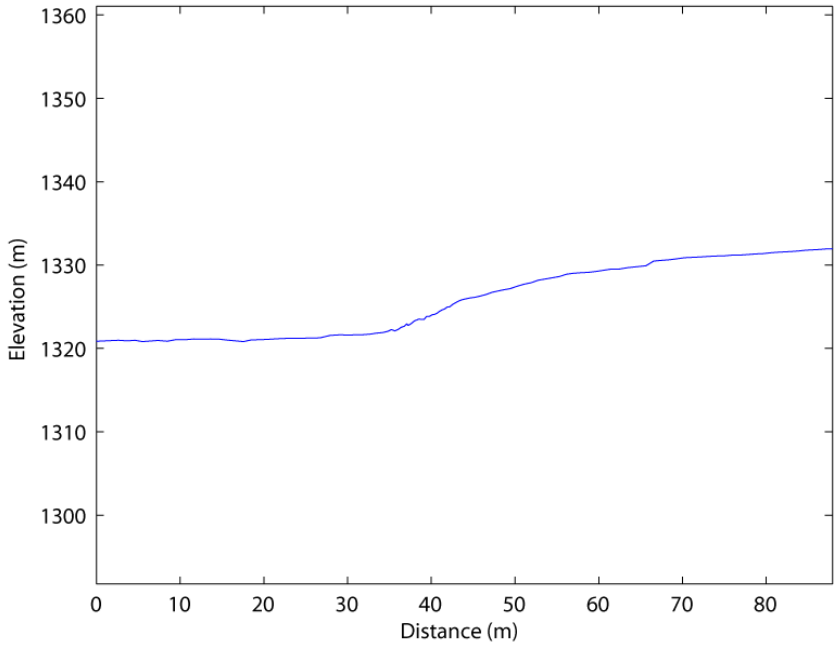

0605D

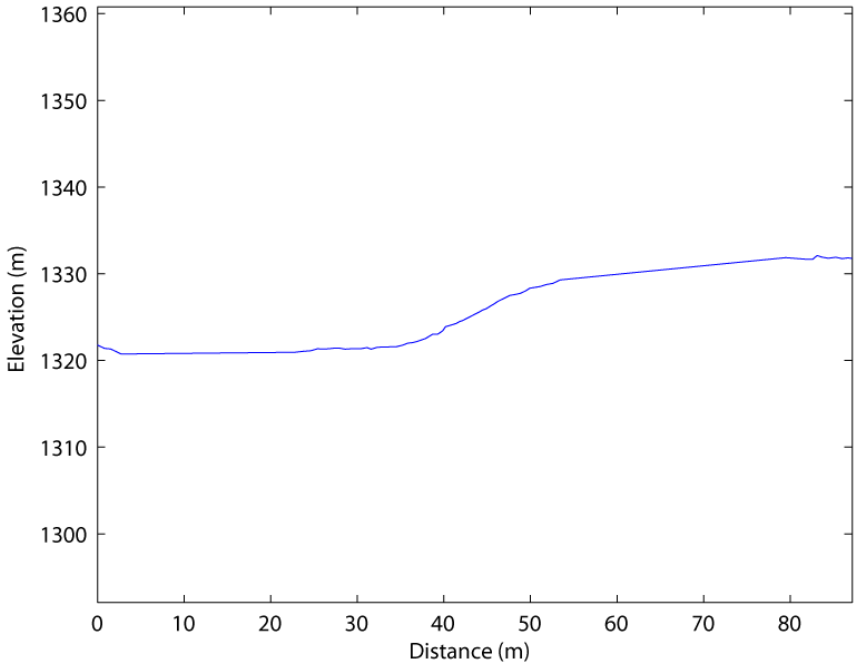

0605E

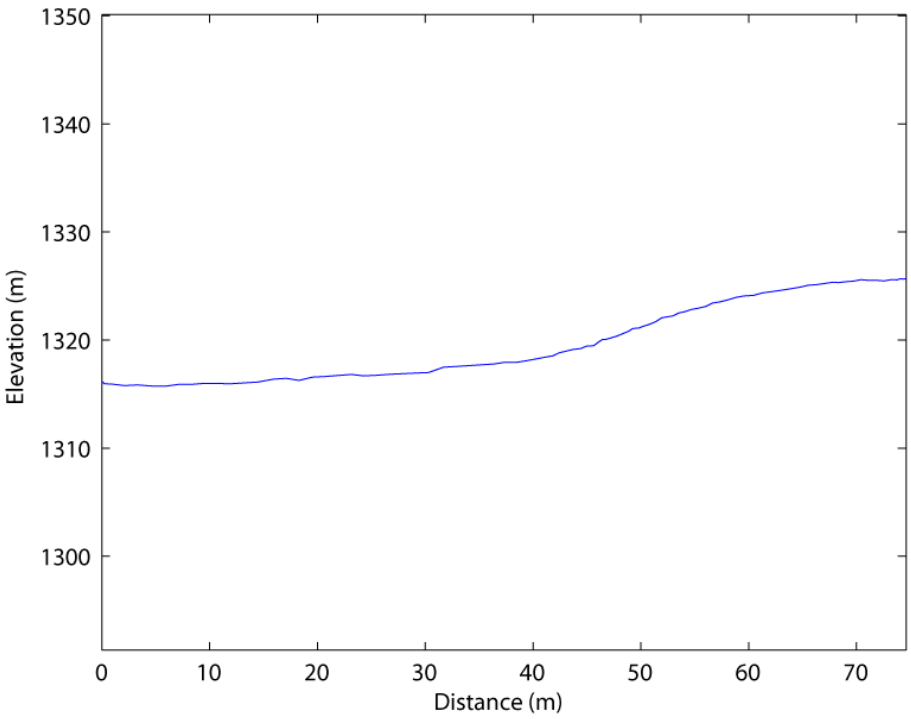

0605J-1

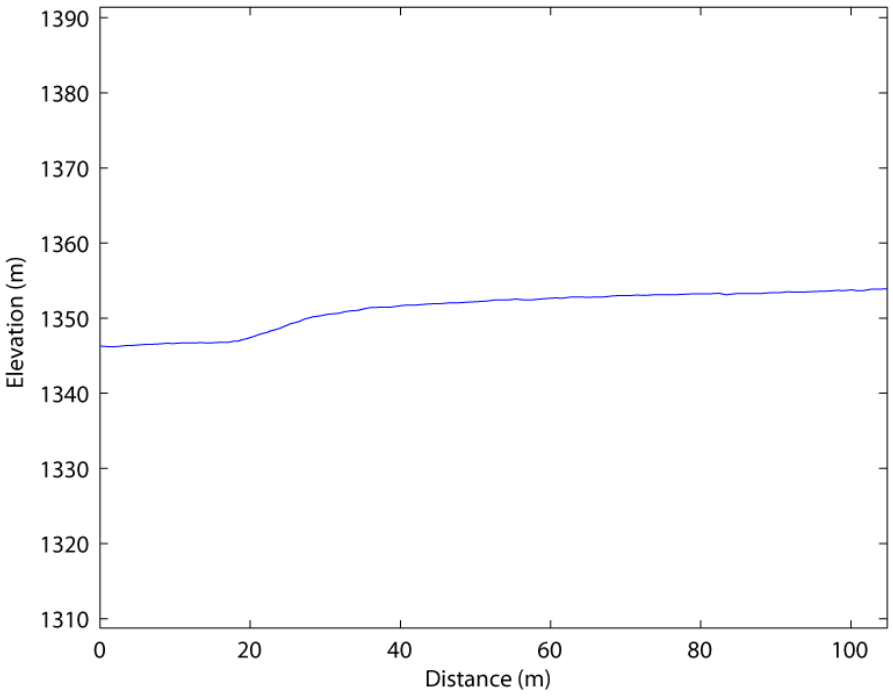

0605K

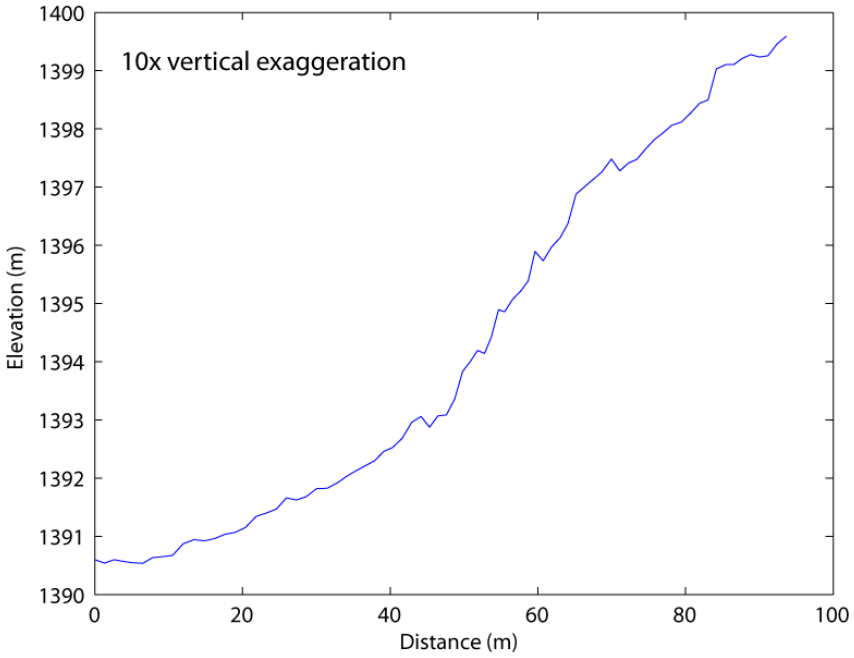
10x vertical exaggeration
Elevation (m)
Distance (m)
1400
1399
1398
1397
1396
1395
1394
1393
1392
1391
1390
0
20
40
60
80
100

0607A

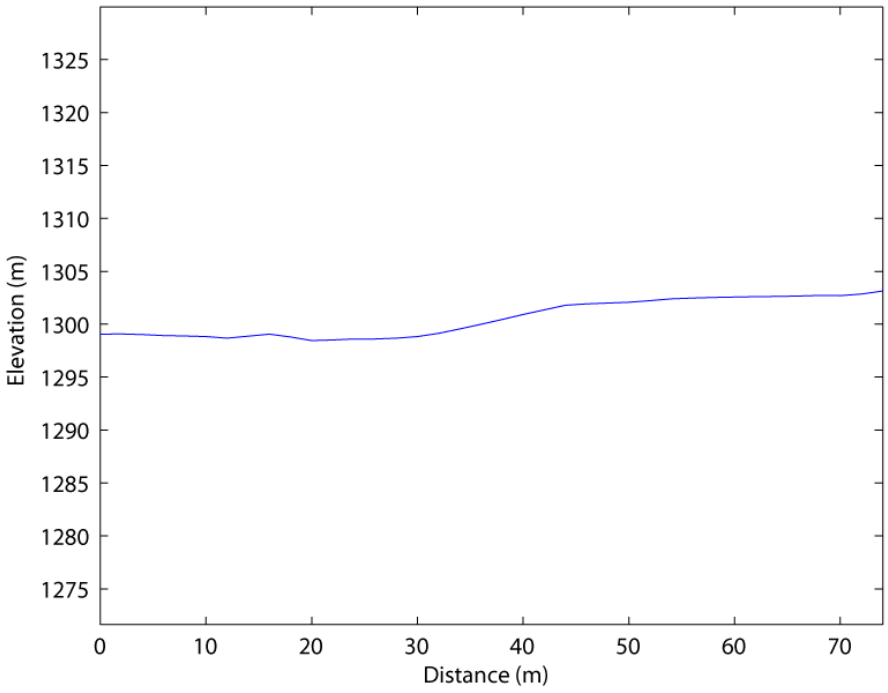
Elevation (m)
Distance (m)
1325
1320
1315
1310
1305
1300
1295
1290
1285
1280
1275
0
10
20
30
40
50
60
70

0607B

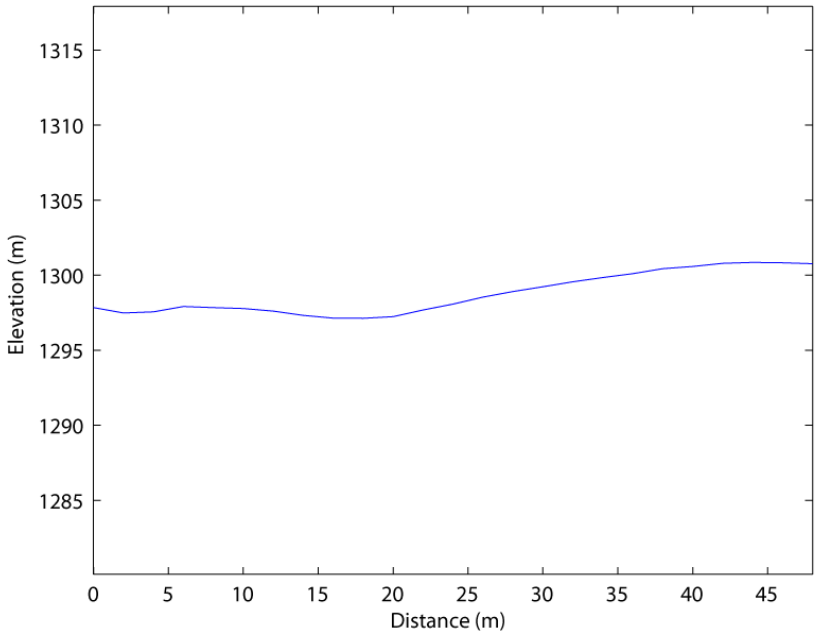
1315
1310
1305
1300
1295
1290
1285
Elevation (m)
0
5
10
15
20
25
30
35
40
45
Distance (m)

0607C

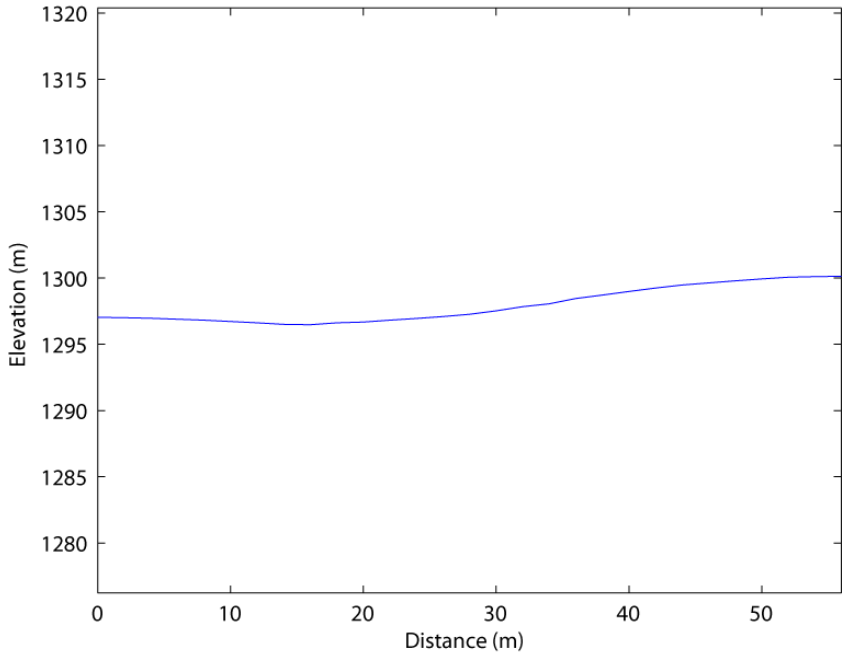
1320
1315
1310
1305
1300
1295
1290
1285
1280
Elevation (m)
0
10
20
30
40
50
Distance (m)

Q2b Profiles:

0602A-1

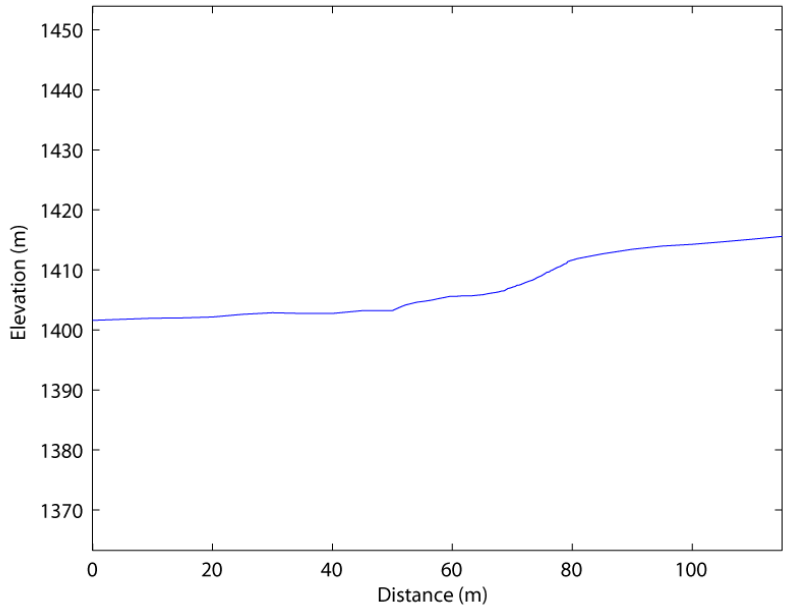

0602A-2

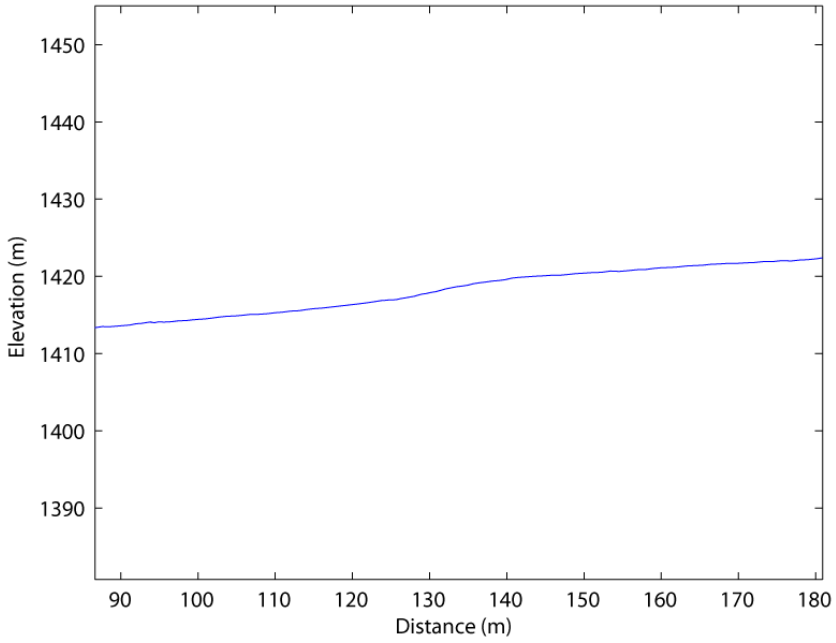

0605A

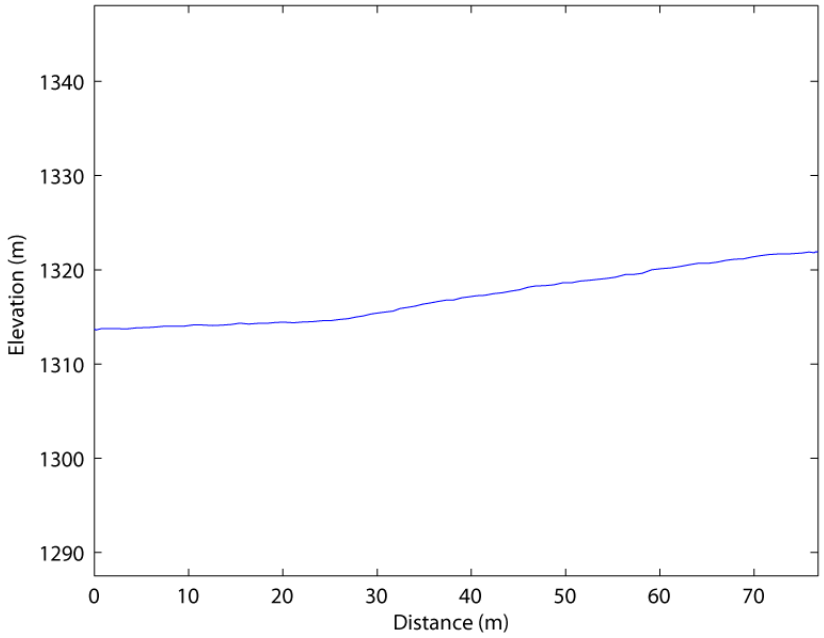
1340
1330
1320
1310
1300
1290
Elevation (m)
0
10
20
30
40
50
60
70
Distance (m)

0605F

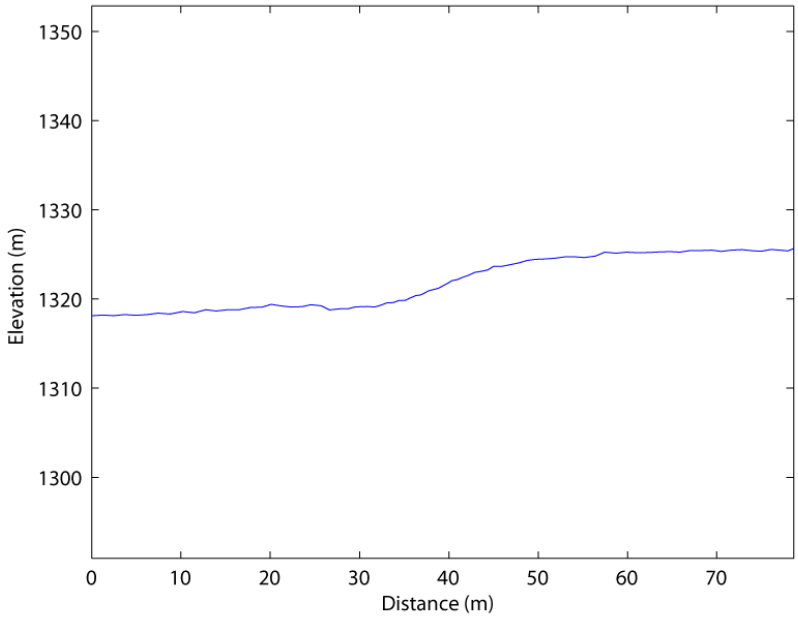
1350
1340
1330
1320
1310
1300
Elevation (m)
0
10
20
30
40
50
60
70
Distance (m)

0605J-2

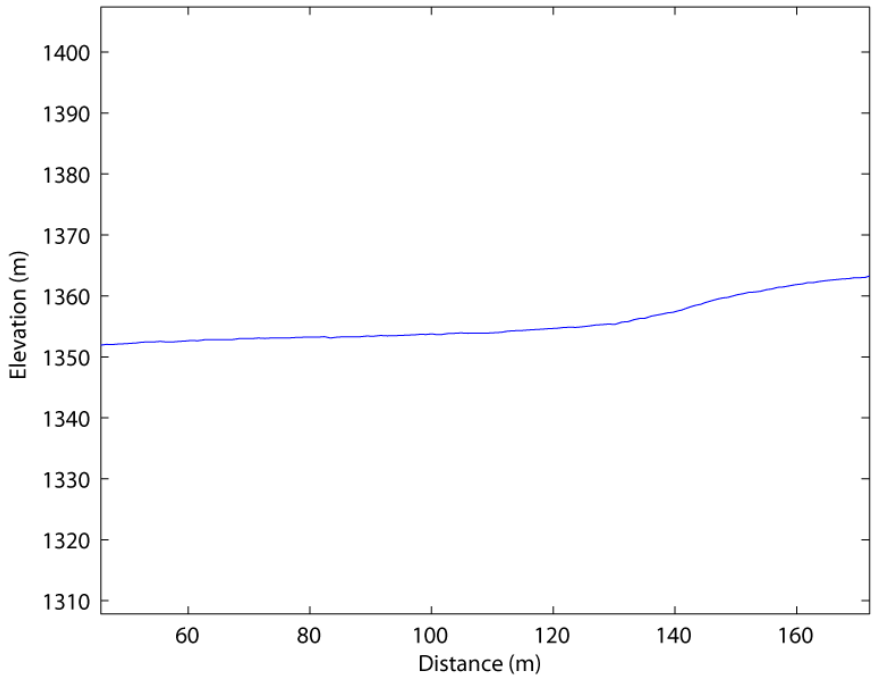

0607D

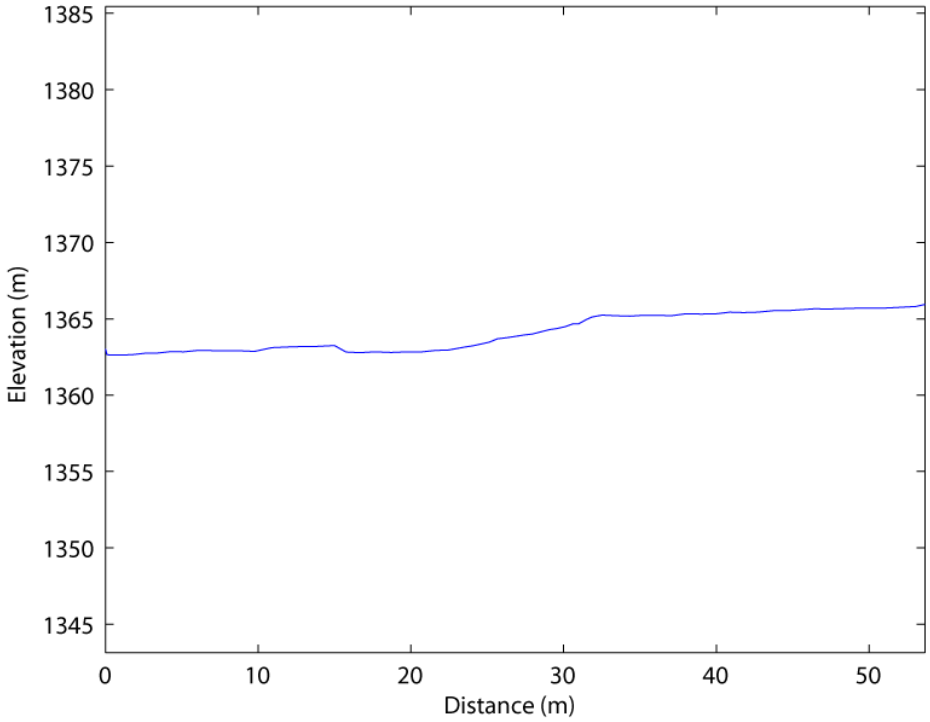

0611A-1

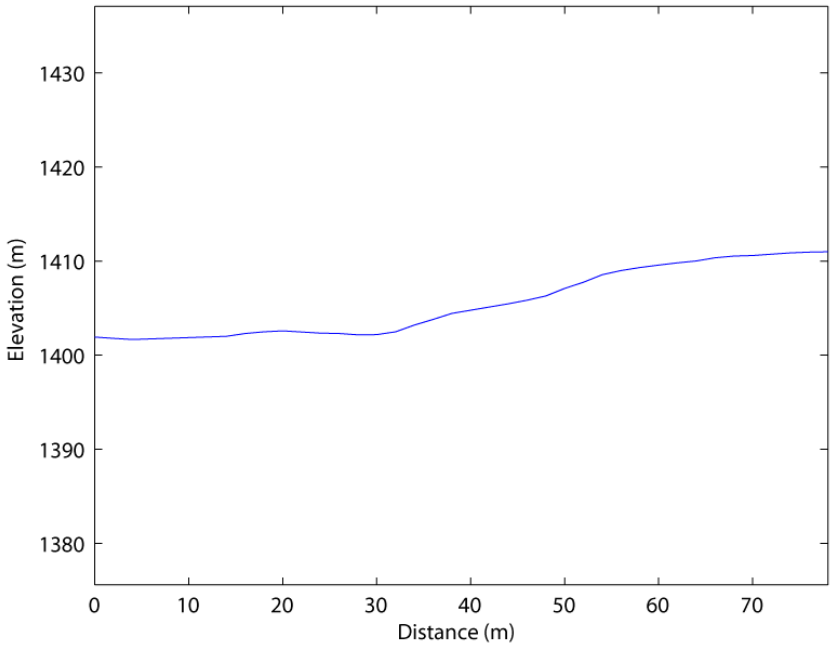

0611A-2

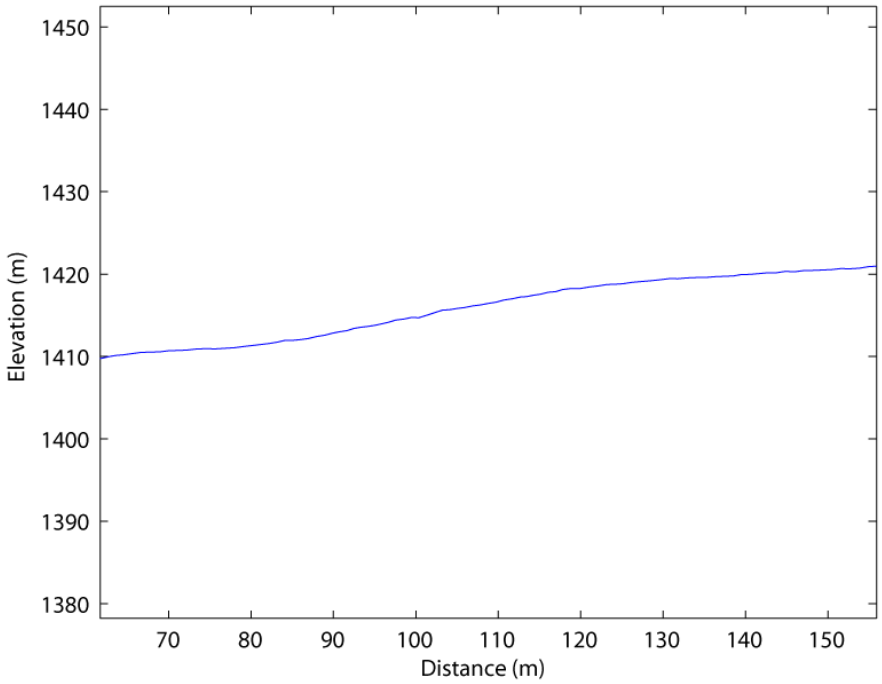

0614A

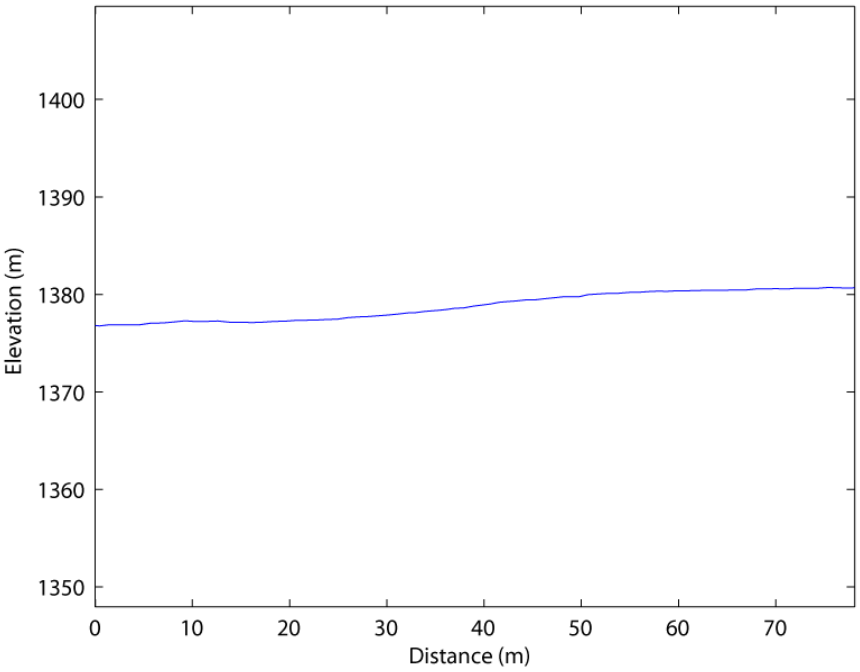
1400
1390
1380
1370
1360
1350
Elevation (m)
0
10
20
30
40
50
60
70
Distance (m)

0614B

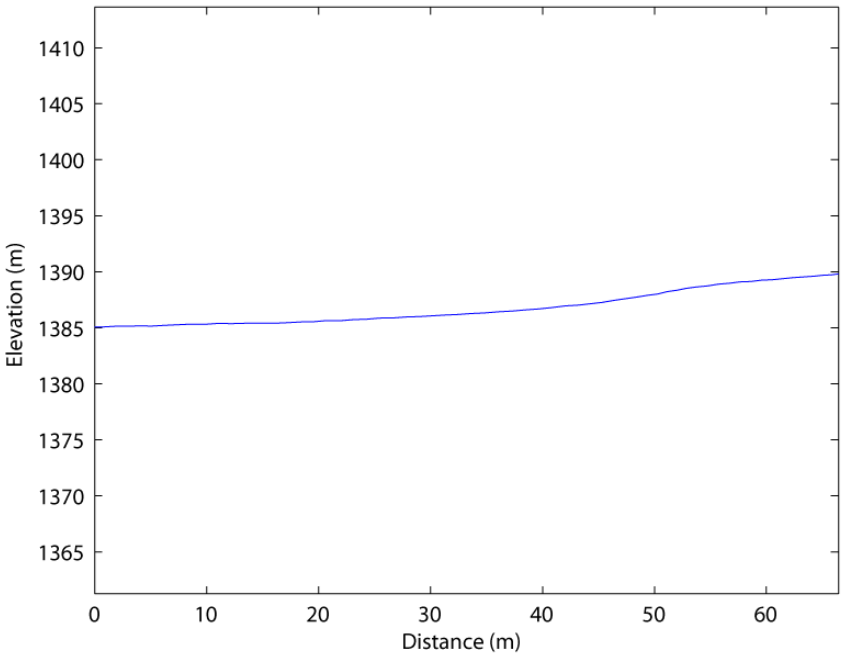
1410
1405
1400
1395
1390
1385
1380
1375
1370
1365
Elevation (m)
0
10
20
30
40
50
60
Distance (m)

Profile Number	Latitude/Longitude of Starting Point	Latitude/Longitude of Endpoint	Map Unit	Scarp Height(s) (m)
0602A-1	37.612505º N/ 117.627251º W	37.611773º N/ 117.626485º W	Q2b	11.6 ± 0.3
0602A-2	37.611942º N/ 117.626464º W	37.611166º N/ 117.62652º W	Q2b	2.4 ± 0.2
0604A	37.685173º N/ 117.586206º W	37.684651º N/ 117.585259º W	Q2d	6.0 ± 0.3
0604B-1	37.684214º N/ 117.585553º W	37.683769º N/ 117.584536º W	Q2d	5.0 ± 0.2
0604B-2	37.683998º N/ 117.585065º W	37.683499º N/ 117.583771º W	Q2d	2.0 ± 0.1
0604C	37.683600º N/ 117.583656º W	37.683370º N/ 117.583027º W	Q2d	0.6 ± 0.1
0604D-1	37.683670º N/ 117.582693º W	37.683384º N/ 117.582281º W	Q2d	1.1 ± 0.1
0604D-2	37.683481º N/ 117.582452º W	37.683090º N/ 117.581678º W	Q2d	0.8 ± 0.1
0604D-3	37.683175º N/ 117.581872º W	37.682891º N/ 117.581239º W	Q2d	0.4 ± 0.1
0604D-4	37.682996º N/ 117.581468º W	37.682510º N/ 117.580406º W	Q2d	1.0 ± 0.1
0604E	37.682170º N/ 117.580388º W	37.681705º N/ 117.579445º W	Q2d	0.5 ± 0.1
0604F	37.685807º N/ 117.586148º W	37.685453º N/ 117.585023º W	Q2d	6.4 ± 0.3
0604G	37.685642º N/ 117.584702º W	37.683577º N/ 117.580819º W	Q2d	10.2 ± 0.7
0605A	37.667547º N/ 117.597604º W	37.667016º N/ 117.597057º W	Q2b	5.4 ± 0.2
0605B	37.658908º N/ 117.600970º W	37.658868º N/ 117.599986º W	Q2c	9.2 ± 0.3
0605D	37.658670º N/ 117.601028º W	37.658372º N/ 117.600127º W	Q2c	9.2 ± 0.3
0605E	37.655308º N/ 117.602547º W	37.654827º N/ 117.601970º W	Q2c	7.4 ± 0.4

0605F	37.652045º N/ 117.604593º W	37.651606º N/ 117.603900º W	Q2b	5.4 ± 0.3
0605G	37.647660º N/ 117.607480º W	37.647449º N/ 117.606932º W	Q3b	3.2 ± 0.3
0605H	37.641075º N/ 117.607191º W	37.640998º N/ 117.606810º W	Q3b	2.2 ± 0.5
0605I	37.633909º N/ 117.607906º W	37.633816º N/ 117.607659º W	Q3b	1.8 ± 0.5
0605J-1	37.633921º N/ 117.607594º W	37.633166º N/ 117.606887º W	Q2c	4.8 ± 0.3
0605J-2	37.633596º N/ 117.607281º W	37.632698º N/ 117.606422º W	Q2b	7.0 ± 0.3
0605K	37.628141º N/ 117.594320º W	37.627426º N/ 117.593766º W	Q2c	4.4 ± 0.2
0607A	37.713952º N/ 117.652489º W	37.713760º N/ 117.651940º W	Q2c	?*
0607B	37.712116º N/ 117.650120º W	37.711860º N/ 117.649682º W	Q2c	?*
0607C	37.711771º N/ 117.650426º W	37.711504º N/ 117.649883º W	Q2c	?*
0607D	37.679486º N/ 117.571543º W	37.679261º N/ 117.571009º W	Q2b	2.2 ± 0.4
0611A-1	37.613035º N/ 117.626134º W	37.612384º N/ 117.625810º W	Q2b	7.2 ± 0.3
0611A-2	37.612521º N/ 117.625878º W	37.611726º N/ 117.625515º W	Q2b	5.8 ± 0.2
0614A	37.641880º N/ 117.584388º W	37.641320º N/ 117.583856º W	Q2b	2.8 ± 0.4
0614B	37.638444º N/ 117.585611º W	37.637973º N/ 117.585148º W	Q2b	3.4 ± 0.2

*Offsets for profiles 0607A, 0607B, and 0607C cannot be accurately determined due to a high degree of scarp modification by incised channels and a dirt road at the base of the scarps.

REFERENCES

Abbott, R. E., J. N. Louie, S. J. Caskey, and S. Pullammanappallil (2001), Geophysical confirmation of low-angle normal slip on the historically active Dixie Valley fault, Nevada, *Journal of Geophysical Research, 106*, 4169-4181.

Albers, J. P., and J. H. Stewart (1972), Geology and mineral deposits of Esmeralda County, Nevada, *Nevada Bureau of Mines and Geology Bulletin, 78*, 80 p.

An, L. J., and C. G. Sammis (1996), Development of strike-slip faults: Shear experiments in granular materials and clay using a new technique, *Journal of Structural Geology, 18*, 1061-1078.

Anders, M. H., N. Christie-Blick, S. Wills, and S. C. Krueger (2001), Rock deformation studies in the Mineral Mountains and Sevier Desert of west-central Utah: Implications for upper crustal low-angle normal faulting, *Geological Society of America Bulletin, 113*, 895-907, doi: 10.1130/0016-7606(2001)113<0895:RDSITM>2.0.CO;2.

Anderson, E. M. (1951), The dynamics of faulting and dyke formation, with application to Britain, Oliver and Boyd, Edinburgh, Scotland, 206 p.

Anderson, R. S., J. L. Repka, and G. S. Dick (1996), Explicit treatment of inheritance in dating depositional surfaces using in situ ^{10}Be and ^{26}Al, *Geology, 24*, 47-51, doi: 101130/0091-7613(1996)024<0047:ETOIID>2.3.CO;2.

Andrew, J. E., and J. D. Walker (2009), Reconstructing late Cenozoic deformation in central Panamint Valley, California: Evolution of slip partitioning in the Walker Lane, *Geosphere, 5*, 172-198, doi: 10.1130/GES00178.1.

Argus, D. F., and R. G. Gordon (2001), Present tectonic motion across the Coast Ranges and San Andreas fault system in central California, *Geological Society of America Bulletin, 113*, 1580-1592, doi: 10.1130/0016-7606(2001)113<1580:PTMATC>2.0.CO;2.

Atwater, T., and J. Stock (1998), Pacific-North America plate tectonics of the Neogene southwestern United States, *International Geology Review, 40*, 375-402.

Avouac, J. P., and P. Tapponnier (1993), Kinematic model of the active deformation in central-Asia, *Geophysical Research Letters, 20*, 895-898.

Axen, G. J., J. M. Fletcher, E. Cowgill, M. Murphy, P. Kapp, I. MacMillan, E. Ramos-Velasquez, and J. Aranda-Gomez (1999), Range-front fault scarps of the Sierra El Mayor, Baja California: Formed above an active low-angle normal fault?, *Geology, 27*, 247-250, doi: 10.1130/0091-7613(1999)027<0247:RFFSOT>2.3.CO;2.

Bacon, S. N., and S. K. Pezzopane (2007), A 25,000 year record of earthquakes on the Owens Valley fault near Lone Pine, California: Implications for recurrence intervals, slip rates, and segmentation models, *Geological Society of America Bulletin, 119,* 823-847, doi: 10.1130/B25879.

Balco, G., J. O. Stone, N. A. Lifton, and T. J. Dunai (2008), A complete and easily accessible means of calculating surface exposure ages or erosion rates from ^{10}Be and ^{26} Al measurements, *Quaternary Geology, 3*, 174-195, doi: 10.1016/j.quageo.2007.12.001.

Bennett, R. A., B. P. Wernicke, N. A. Niemi, A. M. Friedrich, and J. L. Davis, Contemporary strain rates in the northern Basin and Range province from GPS data, *Tectonics, 22*, 1-31, doi: 10.1029/2001TC001355.

Bennett, R. A., A. M. Friedrich, and K. P. Furlong (2004), Codependent histories of the San Andreas and San Jacinto fault zones from inversion of fault displacement rates, *Geology, 32*, 961-964, doi: 10.1130/G20806.1.

Bierman, P. R., M. W. Caffee, P. T. Davis, K. Marsella, M. Pavich, P. Colgan, D. Mickelson, and J. Larsen (2002), Rates and timing of earth surface processes from in-situ-produced cosmogenic Be-10, in *Beryllium: Mineralogy, petrology, and geochemistry: Reviews in Mineralogy and Geochemistry*, v. 50, edited by E. S. Grew, pp. 147-205, doi: 10.2138/rmg.2002.50.4.

Bisdorf, R. J., and B. D. Smith (1976), Schlumberger soundings in Clayton Valley, Nevada, in *U.S.G.S Open-File Report 76-0017*, 19 p., Reston, Virginia.

Bull, W. B. (1991), *Geomorphic responses to climate change*, Oxford University Press, New York, 326 p.

Burchfiel, B. C. K. V. Hodges, and L. H. Royden (1987), Geology of Panamint Valley-Saline Valley pull-apart system, California: Palinspastic evidence for low-angle geometry of a Neogene range-bounding fault, *Journal of Geophysical Research, 92*, 10422-10426.

Burchfiel, B. C. (1979), Geologic history of the central western United States, *Nevada Bureau of Mines Geology Report, 33*, 1-11.

Caskey, S. J., S. G. Wesnousky, P. Zhang, and D. B. Slemmons (1996), Surface faulting of the 1954 Fairview Peak (M_s 7.2) and Dixie Valley (M_s 6.8) earthquakes, central Nevada, *Seismological Society of America Bulletin, 86*, 761-787.

Chevalier, M. L., F. J. Ryerson, P. Tapponier, R. C. Finkel, J. Van Der Woerd, L. Haibing, L. Qing (2005), Slip-rate measurements on the Karakoram fault may imply secular variations in fault motions, *Science, 307*, 411-414, doi: 10.1126/science.1105466.

Cichanski, M (2000), Low-angle, range-flank faults in the Panamint, Inyo, and Slate ranges, California: Implications for recent tectonics of the Death Valley region, *Geological Society of America Bulletin, 112*, 871-883, doi: 10.1130/0016-7606(2000)112<871:LRFITP>2.0.CO;2.

Cowgill, E. (2007), Impact of riser reconstruction on estimation of secular variation in rates of strike-slip faulting: Revisiting the Cherchen River site along the Altyn Tagh fault, NW China, *Earth and Planetary Science Letters, 254*, 239-255, doi: 10.1016/j.epsl.2006.09.015.

Cowgill, E., R. D. Gold, C. Xuanhua, W. Xiao-Feng, J. R. Arrowsmith, and J. Southon (2009), Low Quaternary slip rate reconciles geodetic and geologic rates along the Altyn Tagh fault, northwestern Tibet, *Geology, 37*, 647-650, doi: 10.1130/G25623A.1.

Davis, G. A., and B. C. Burchfiel (1973), Garlock fault: An intracontinental transform structure, southern California, *Geological Society of America Bulletin, 84*, 1407-1422.

Davis, J. R. (1979), Quaternary faulting in Clayton and Big Smoky Valleys, Nevada, *Abstracts with Programs- Geological Society of America, 11*, 74.

Davis, J. R., and J. D. Vine (1979), Stratigraphic and tectonic setting of the lithium brine field, Clayton Valley, Nevada, *Basin and Range Symposium*, 421-430.

Davis, J. R. (1981), Late Cenozoic geology of Clayton Valley, Nevada, and the genesis of a lithium-enriched brine, Ph.D. thesis, Dep. of Geological Sciences, University of Texas, Austin, Texas.

Desilets, D., and M. Zreda (2003), Spatial and temporal distribution of secondary cosmic-ray nucleon intensities and applications to in situ cosmogenic dating, *Earth and Planetary Science Letters, 206*, 21-42.

Desilets, D., M. Zreda, and T. Prabu (2006), Extended scaling factors for in situ cosmogenic nuclides: New measurements at low latitude, *Earth and Planetary Science Letters, 246*, 265-276, doi: 10.1016/j.epsl.2006.03.051.

Dixon, T. H., M. Miller, F. Farina, H. Wang, and D. Johnson (2000), Present day motion of the Sierra Nevada block and some tectonic implications for the Basin and Range province, North American Cordillera, *Tectonics, 19*, 1-24.

Dixon, T. H., E. Norabuena, L. Hotaling, (2003), Paleoseismology and Global Positioning System: Earthquake cycle effects and geodetic versus geologic slip rates in the eastern California shear zone, *Geology, 31*, 55-58, doi: 10.1130/0091-7613(2003)031<0055:PAGPSE>2.0.CO;2.

Dolan, J. F., D. D. Bowman, and C. G. Sammis (2007), Long-range and long-term fault interactions in Southern California, *Geology, 35*, 855-858, doi: 10.1130/G23789A.1.

Dokka, R. K. (1983), Displacements on late Cenozoic strike-slip faults of the central Mojave Desert, California, *Geology, 11*, 305-308, doi: 10.1130/0091-7613(1983)11<305:DOLCSF>2.0.CO;2.

Dokka, R. K., and C. J. Travis (1990), Role of the eastern California shear zone in accommodating Pacific-North American plate deformation, *Geophysical Research Letters, 17*, 1323-1326, doi: 10.1029/GLO17i009p01323.

Dunai, T. J. (2001), Influence of secular variation of the geomagnetic field on production rates of in situ produced cosmogenic nuclides, *Earth and Planetary Science Letters, 193*, 197-212.

England, P., and P. Molnar (2005), Late Quaternary to decadal velocity fields in Asia, *Journal of Geophysical Research, 110*, B12401, doi: 10.1029/2004JB003541.

Faulds, J. E., C. D. Henry, and N. H. Hinz (2005), Kinematics of the northern Walker Lane: An incipient transform fault along the Pacific- North American plate boundary, *Geology, 33*, 505-508, doi: 10.1130/G21274.

Flesch, L. M., W. E. Holt, A. J. Haines, and B. Shen-Tu (2000), Dynamics of the Pacific-North American plate boundary in the western United States, *Science, 287*, 834-836, doi: 10.1126/science.287.5454.834.

Foy, T. A., Z. M. Lifton, and K. L. Frankel (2011), Preliminary surficial geologic map of selected parts of Clayton Valley and the northwest Montezuma Range piedmont, Esmeralda County, Nevada, scale 1:10,000, *Nevada Bureau of Mines and Geology Open File Report*, Reno, Nevada, in review.

Frankel, K. L., and J. F. Dolan (2007), Characterizing arid-region alluvial fan surface roughness with airborne laser swath mapping digital topographic data, *Journal of Geophysical Research- Earth Surface, 112*, F02025, doi: 10.1029/2006JF000644.

Frankel, K. L., K. S. Brantley, J. F. Dolan, R. C. Finkel, R. E. Klinger, J. R. Knott, M. N. Machette, L. A. Owen, F. M. Phillips, J. L. Slate, and B. P. Wernicke (2007a), Cosmogenic ^{10}Be and ^{36}Cl geochronology of offset alluvial fans along the northern Death Valley fault zone: implications for transient strain in the eastern California shear zone, *Journal of Geophysical Research, 112*, B06407, doi: 10.1029/2006JB004350.

Frankel, K. L., J. F. Dolan, R. C. Finkel, L. A. Owen, and J. S. Hoeft (2007b), Spatial variations in slip rate along the Death Valley-Fish Lake Valley fault system determined from LiDAR topographic data and cosmogenic ^{10}Be geochronology, *Geophysical Research Letters, 34*, L18303, doi: 10.1029/2007GL030549.

Frankel, K. L., A. F. Glazner, E. Kirby, F. C. Monastero, M. D. Strane, M. E. Oskin, J. R. Unruh, J. D. Walker, S. Anandakrishnan, J. M. Bartley, D. S. Coleman, J. F. Dolan, R. C. Finkel, D. Greene, A. Kylander-Clark, S. Marrero, L. A. Owen, and F. Phillips (2008), Active tectonics of the eastern California shear zone, in *Field guide to plutons, volcanoes, reefs, dinosaurs, and possible glaciation in selected areas of Arizona, California, and Nevada: Geological Society of America Field Guide, 11*, edited by E. M. Duebendorfer and E. I. Smith, pp. 43-81, doi: 10.1130/2008.fld011(03).

Frankel, K. L., J. F. Dolan, L. A. Owen, P. N. Ganev, and R. C. Finkel (2011), Spatial and temporal constancy of seismic strain release along an evolving segment of the Pacific-North America plate boundary, *Earth and Planetary Science Letters,* in press.

Freed, A. M., and R. Burgmann (2004), Evidence of power-law flow in the Mojave desert mantle, *Nature, 430*, 548-551.

Freed, A. M., R. Burgmann, and T. Herring (2007), Far-reaching transient motions after Mojave earthquakes require broad mantle flow beneath a strong crust, *Geophysical Research Letters, 34*, L19302, doi: 10.1029/2007GL030959.

Friedrich, A. M., B. P. Wernicke, N. A. Niemi, R. A. Bennett, and J. L. Davis (2003), Comparison of geodetic and geologic data from the Wasatch region, Utah, and implications for the spectral character of Earth deformation at periods of 10 to 10 million years, *Journal of Geophysical Research, 108*, doi: 10.1029/2001JB000682.

Friedrich, A. M., J. Lee, B. P. Wernicke, K. Sieh (2004), Geologic context of geodetic data across a Basin and Range normal fault, Crescent Valley, Nevada, *Tectonics, 23*, TC2015, doi: 10.1029/2003TC001528.

Gan, W, J. L. Svarc, J. C. Savage, and W. H. Prescott (2000), Strain accumulation across the eastern California shear zone at latitude 36°30'N, *Journal of Geophysical Research, 105*, 16229-16236, doi: 10.1029/2000JB900105.

Gan, W., P. Zhang, Z. K. Shen, Z. Niu, M. Wang, Y. Wan, D. Zhou, and J. Cheng (2007), Present-day crustal motion within the Tibetan Plateau inferred from GPS measurements, *Journal of Geophysical Research, 112*, B08416, doi: 10.1029/2007JB005306.

Ganev, P. N., J. F. Dolan, K. L. Frankel, and R. C. Finkel (2010), Rates of extension along the Fish Lake Valley fault and transtensional deformation in the eastern California shear zone-Walker Lane belt, *Lithosphere, 2*, 33-49, doi: 10.1130/L51.1.

Glazner, A. F., and J. M. Bartley (1984), Timing and tectonic setting of Tertiary low-angle normal faulting and associated magmatism in the southwestern United States, *Tectonics, 3*, 385-396.

Glazner, A. F., J. D. Walker, J. M. Bartley, and J. M. Fletcher (2002), Cenozoic evolution of the Mojave block of southern California, in *Geologic Evolution of the Mojave Desert and Southwestern Basin and Range*, Geological Society of America Memoir 195, edited by A. F. Glazner, J. D. Walker, and J. M. Bartley, pp 19-41.

Glazner, A. F., J. Lee, J. M. Bartley, D. S. Coleman, A. Kylander-Clark, D. C. Greene, and K. Le (2005), Large dextral offset across Owens Valley, California from 148 Ma to 1872 A.D., in *Western Great Basin Geology, Vol. 99*, edited by C. Stevens and J. Cooper, pp. 1-35, The Pacific Section Society of Sedimentary Geology, Santa Fe Springs, CA.

Gold, R. D., and E. Cowgill (2011), Deriving fault-slip histories to test for secular variation in slip, with examples from the Kunlun and Awatere faults, *Earth and Planetary Science Letters, 301,* 52-64, doi: 10.1016/j.epsl.2010.10.001.

Gosse, J. C., and F. M. Phillips (2001), Terrestrial in situ cosmogenic nuclides: theory and application, *Quaternary Science Reviews*, *20*, 1475-1560.

Guest, B., T. L. Pavlis, H. Golding, and L. Serpa (2003), Chasing the Garlock: A study of tectonic response to vertical axis rotation, *Geology, 31*, 553-556, doi: 10.1130/0091-7613(2003)031<0553:CTGASO>2.0.CO;2.

Guest, B., N. Niemi, and B. Wernicke (2007), Stateline fault system: A new component of the Miocene-Quaternary eastern California shear zone, *Geological Society of America Bulletin*, *119*, 1,337-1,346, doi: 10.1130/0016-7606(2007)119[1337:SFSANC]2.0.CO;2.

Hammond, W. C., and W. Thatcher (2007), Crustal deformation across the Sierra Nevada, northern Walker Lane, Basin and Range transition, western United States measured with GPS, 2000-2004, *Journal of Geophysical Research-Solid Earth, 112*, B05411, doi: 10.1029/2006JB004625.

Hayman, N. W., J. R. Knott, D. S. Cowan, E. Nemser, and A. M. Sarna-Wojcicki (2003), Quaternary low-angle slip on detachment faults in Death Valley, California, *Geology, 31,* 343-346, doi: 10.1130/0091-7613(2003)031<0343:QLASOD>2.0.CO;2.

Hearn, E. H., and E. D. Humphreys (1998), Kinematics of the southern Walker Lane Belt and motion of the Sierra Nevada block, California, *Journal of Geophysical Research, 103*, 27033-27049, doi: 10.1029/98JB01390.

Hidy, A. J., J. C. Gosse, J. L. Pederson, J. P. Mattern, and R. C. Finkel (2010), A geologically constrained Monte Carlo approach to modeling exposure ages from profiles of cosmogenic nuclides: An example from Lees Ferry, Arizona, *Geochemistry, Geophysics, Geosystems, 11,* QOAA10, doi: 10.1029/2010GC003084.

Hilley, G.E., and J. R. Arrowsmith (2003), Scarp dater software: Scarp diffusion exercise from the International Quality Network Workshop: Potsdam, Germany, Potsdam University.

Hoeft, J. S. and K. L. Frankel (2010), Temporal variations in extension rate on the Lone Mountain fault and strain distribution in the eastern California shear zone-Walker Lane, *Geosphere, 6*, 917-936, doi: 10.1130/GES00603.1.

Hoeft, J. S., and K. L. Frankel (2011), Preliminary surficial geologic map of the Lone Mountain piedmont, Esmeralda County, Nevada, scale 1:10,000, *Nevada Bureau of Mines and Geology Open File Report*, Reno, Nevada, in review.

Humphreys, E. D., and R. J. Weldon (1994), Deformation across the western United States: A local estimate of Pacific-North America transform deformation, *Journal of Geophysical Research, 99,* 19975-20010, doi: 10.1029/94JB00899.

Kirby, E., J. D. Walker, J. Gosse, E. McDonald (2004), Late Quaternary-recent slip on a low-angle normal fault: Inferences from alluvial deposits along the Panamint Valley fault system, paper presented at 2004 Geological Society of America Annual Meeting, Geological Society of America, Denver, Colorado.

Kirby, E., D. W. Burbank, M. Reheis, and F. Phillips (2006), Temporal variations in slip rate of the White Mountains Fault Zone, Eastern California, *Earth and Planetary Science Letters, 248*, 168-185, doi: 10.1016/j.epsl.2006.05.

Kirby, E., S. Anandakrishnan, F. Phillips, and S. Marrero (2008), Late Pleistocene slip rate along the Owens Valley fault, eastern California, *Geophysical Research Letters, 35,* L01304, doi: 10.1029/2007GL031970.

Kohl, C. P., and K. Nishiizumi (1992), Chemical isolation of quartz for measurement of in situ-produced cosmogenic nuclides, *Geochimica et Cosmochimica Acta 56*, 3583-3587.

Kozaci, O., J. Dolan, R. Finkel, and R. Hartleb (2007), Late Holocene slip rate for the North Anatolian fault, Turkey, from cosmogenic ^{36}Cl geochronology: Implications for the constancy of fault loading and strain release rates, *Geology, 35*, 867-870, doi: 10.1130/G23187A.1.

Kreemer, C., G. Blewitt, and W. C. Hammond (2009), Geodetic constraints on contemporary deformation in the northern Walker Lane: 2. Velocity and strain rate tensor analysis, in *Late Cenozoic Structure and Evolution of the Great Basin-Sierra Nevada Transition*, Geological Society of America Special Paper 447, edited by J. S. Oldow and P. H. Cashman, pp. 17-31, doi: 10.1130.2009.2447(02).

Kylander-Clark, A. R. C., D. S. Coleman, A.F. Glazner, and J. M. Bartley (2005), Evidence for 65 km of dextral slip across Owens Valley, California, since 83 Ma, *Geological Society of America Bulletin, 117*, 962-968, doi: 10.1130/B25624.1.

Lal, D. (1991), Cosmic ray labeling of erosion surfaces: In situ nuclide production rates and erosion models, *Earth and Planetary Science Letters, 104*, 424-439, doi: 10.1016/0012-821X(91)90220-C.

Le, K, J. Lee, L. A. Owen, and R. Finkel (2007), Late Quaternary slip rates along the Sierra Nevada frontal fault zone: Slip partitioning across the western margin of the Eastern California Shear Zone-Basin and Range Province, *Geological Society of America Bulletin, 119*, 240-256, doi:10.1130/B25960.1.

Lee, J., C. M., Rubin, and A. Calvert (2001a), Quaternary faulting history along the Deep Springs fault, California, *Geological Society of America Bulletin, 113*, 855-869, doi: 10.1130/0016-7606(2001)113<0855:QFHATD>2.0.CO;2.

Lee, J., J. Q. Spencer, and L. A. Owen (2001b), Holocene slip rates along the Owens Valley fault, California: Implications for the recent evolution of the eastern California shear zone, *Geology, 29*, 819-822, doi: 10.1130/0091-7613(2001)029<0819:HSRATO>2.0.CO;2.

Lee, J., D. F. Stockli, L. A. Owen, R. C. Finkel, and R. Kislitsyn (2009a), Exhumation of the Inyo Mountains, California: Implications for the timing of extension along the western boundary of the Basin and Range Province and distribution of dextral fault slip rates across the eastern California shear zone, *Tectonics, 28*, TC1001, doi: 10.1029/2008TC002295.

Lee, J., J. Garwood, D. F. Stockli, and J. Gosse (2009b), Quaternary faulting in Queen Valley, California-Nevada: Implications for kinematics of fault slip transfer in the

eastern California shear zone-Walker Lane belt, *Geological Society of America Bulletin, 121*, 599-614, doi: 10.1130/B26352.1.

Leon, L. A., S. A. Christofferson, J. F. Dolan, J. H. Shaw, and T. L. Pratt (2007), Earthquake-by-earthquake fold growth above the Puente Hills blind thrust fault, Los Angeles, California: Implications for fold kinematics and seismic hazard, *Journal of Geophysical Research, 112*, B03S03, doi: 10.1029/2006JB004461.

Leon, L., J. F. Dolan, J. H. Shaw, and T. L. Pratt (2009), Evidence for large Holocene earthquakes on the Compton thrust fault, Los Angeles, California, *Journal of Geophysical Research, 114*, B12305, doi: 10.1029/2008JB006129.

Lifton, N. A., J. Bieber, J. Clem, M. Duldig, P. Evenson, J. Humble, and R. Pyle (2005), Addressing solar modulation and long-term uncertainties in scaling secondary cosmic rays for in situ cosmogenic nuclide applications, *Earth and Planetary Science Letters, 239*, 140-161, doi: 10.1016/j.epsl.2005.07.001.

Liu, M., H. Wang, and Q. Li (2010), Inception of the eastern California shear zone and evolution of the Pacific-North American plate boundary: From kinematics to geodynamics, *Journal of Geophysical Research, 115*, B07401, doi: 10.1029/2009JB007055.

Locke, A., P. Billingsley, and E. B. Mayo (1940), Sierra Nevada tectonic patterns, *Geological Society of America Bulletin, 51*, 513-540.

Loveless, J. P., and B. J. Meade (2011), Partitioning of localized and diffuse deformation in the Tibetan Plateau from joint inversions of geologic and geodetic observations, *Earth and Planetary Science Letters, 303*, 11-24, doi: 10.1016/j.epsl.2010.12.014.

Machette, M. N., J. L. Slate, and F. M. Phillips (2008), Terrestrial cosmogenic-nuclide dating of alluvial fans in Death Valley, California, *U.S. Geological Survey Professional Paper 1755*, 44 p.

McClusky, S. C., S. C. Bjornstad, B. H. Hager, R. W. King, B. J. Meade, M. M. Miller, F. C. Monastero, and B. J. Souter (2001), Present day kinematics of the eastern California shear zone from a geodetically constrained block model, *Geophysical Research Letters, 28*, 3369-3372.

McGill, S. F., S. G. Wells, S. K. Fortner, H. A. Kuzma, and J. D. McGill (2009), Slip rate of the western Garlock fault, at Clark Wash, near Lone Tree Canyon, Mojave Desert, California, *Geological Society of America Bulletin, 121,* 536-554, doi: 10.1130/B26123.1.

Meade, B. J. (2007), Present-day kinematics at the India-Asia collision zone, *Geology, 35*, 81-84, doi: 10.1130/G22924A.1

Miller, M. M., D. J. Johnson, T. H. Dixon, and R. K. Dokka (2001), Refined kinematics of the eastern California shear zone from GPS observations, 1993-1994, *Journal of Geophysical Research, 106*, 2245-2263.

Molnar, P, and P. Tapponnier (1975), Cenozoic tectonics of Asia: Effects of a continental collision, *Science, 189*, 419-426.

Molnar, P. (1988), Continental tectonics in the aftermath of plate tectonics, *Nature, 335*, 131-137.

Nielsen, R. L. (1965), Right-lateral strike-slip faulting in the Walker Lane, west-central Nevada, *Geological Society of America Bulletin, 76*, 1301-1308.

Niemi, N. A., B. P. Wernicke, A. M. Friedrich, M. Simons, R. A. Bennett, and J. L. Davis (2004), BARGEN continuous GPS data across the eastern Basin and Range province, and implications for fault systems dynamics, *Geophysical Journal International, 159*, 842-862, doi: 10.1111/j.1365-246X.2004.02454.x.

Numelin, T., E. Kirby, J. D. Walker, and B. Didericksen (2007), Late Pleistocene slip on a low-angle normal fault, Searles Valley, California, *Geosphere, 3*, 163-176, doi: 10.1130/GES00052.1.

Nur, A., H. Ron, and O. Scotti (1986), Fault mechanics and the kinematics of block rotations, *Geology, 14*, 746-749, doi: 10.1130/0091-7613(1986)14<746:FMATKO>2.0.CO;2.

Oldow, J. S. (1992), Late Cenozoic displacement partitioning in the northwestern Great Basin, in Graig, S. D., ed., Structure, tectonics, and mineralization of the Walker Lane: Reno, Nevada: Geological Society of Nevada, Walker Lane Symposium Proceedings, 17-52.

Oldow, J. S., G. Kohler, and R. A. Donelick (1993), Miocene to Holocene displacement transfer system linking the Furnace Creek and Walker Lane fault zones, western Great Basin, *Eos Trans. AGU, 74*, 66.

Oldow, J. S. G. Kohler, and R. A. Donelick (1994), Late Cenozoic extensional transfer in the Walker Lane strike-slip belt, Nevada, *Geology, 22*, 637-640, doi: 10.1130/0091-7613(1994)022<0637:LCETIT>2.3.CO;2.

Oldow, J. S., C. L. V. Aiken, J. L. Hare, J. F. Ferguson, and R. F. Hardyman (2001), Active displacement transfer and differential block motion within the central Walker Lane, western Great Basin, *Geology, 29*, 19-22, doi: 10.1130/0091-7613(2001)029<0019:ADTADB>2.0.CO;2.

Oldow, J. S. (2003), Active transtensional boundary zone between the western Great Basin and Sierra Nevada block, western U.S. Cordillera, *Geology, 31*, 1033-1036, doi: 10.1130/G19838.1.

Oldow, J. S., J. W. Geissman, and D. F. Stockli (2008), Evolution and strain reorganization within late Neogene structural stepovers linking the central Walker Lane and northern eastern California shear zone, western Great Basin, *International Geology Review, 50*, 270-290, doi: 10.2747/0020-6814.50.3.270.

Oldow, J. S., E. A. Elias, L. Ferranti, W. C. McClelland, and W. C. McIntosh (2009), Late Miocene to Pliocene synextensional deposition in fault-bounded basins within the upper plate of the western Silver Peak- Lone Mountain extensional complex, west-central Nevada, in *Late Cenozoic structure and evolution of the Great Basin- Sierra Nevada transition*, Geological Society of America Special Paper 447, edited by J. S. Oldow and P. H. Cashman, pp. 275-312, doi: 10.1130/2009.2447(14).

Oskin, M., and A. Iriondo (2004), Large-magnitude transient strain accumulation on the Blackwater fault, Eastern California shear zone, *Geology, 32*, 313-316, doi: 10.1130/G20223.1.

Oskin, M., L. Perg, D. Blumentritt, S. Mukhopadhyay, and A. Iriondo (2007), Slip rate of the Calico fault: Implications for geologic versus geodetic rate discrepancy in the eastern California shear zone, *Journal of Geophysical Research, 112*, B03402, doi: 10.1029/2006JB004451.

Oskin, M., L. Perg, E. Shelef, M. Strane, E. Gurney, B. Singer, and X. Zhang (2008), Elevated shear zone loading rate during an earthquake cluster in eastern California, *Geology, 36*, 507-510, doi: 10.1130/G24814A.1.

Oswald, J. A., and S. A. Wesnousky (2002), Neotectonics and Quaternary geology of the Hunter Mountain fault zone and Saline Valley region, southeastern California, *Geomorphology, 42*, 255-278, doi: 10.1016/S0169-555X(01)00089-7.

Owen, L. A., K. L. Frankel, J. R. Knott, S. Reynhout, R. C. Finkel, J. F. Dolan, and J. Lee (2011), Beryllium-10 terrestrial cosmogenic nuclide surface exposure dating of Quaternary landforms in Death Valley, *Geomorphology, 125*, 541-557, doi: 10.1016/j.geomorph.2010.10.024.

Peltzer, G., F. Crampe, S. Hensley, and P. Rosen (2001), Transient strain accumulation and fault interaction in the Eastern California shear zone, *Geology, 29*, 975-978, doi: 10.1130/0091-7613(2001)029<0975:TSAAFI>2.0.CO;2.

Petronis, M. S., J. W. Geissman, J. S. Oldow, and W. C. McIntosh (2002), Paleomagnetic and $^{40}Ar/^{39}Ar$ geochronologic data bearing on the structural evolution of the Silver Peak extensional complex, west-central Nevada, *Geological Society of America Bulletin, 114*, 1108-1130, doi: 10.1130/0016-7606(2002)114<1108:PAAAGD>2.0.CO;2.

Petronis, M. S., J. W. Geissman, J. S. Oldow, and W. C. McIntosh (2007), Tectonism of the southern Silver Peak Range: Paleomagnetic and geochronologic data bearing on the Neogene development of a regional extensional complex, central Walker Lane, Nevada, in *Exhumation associated with continental strike-slip fault systems*, Geological Society of America Special Paper 434, edited by S. M. Roeske et al., pp. 81-106, doi: 10.1130/2007.2434(05).

Petronis, M. S., J. W. Geissman, J. S. Oldow, and W. C. McIntosh (2009), Late Miocene to Pliocene vertical-axis rotation attending development of the Silver Peak- Lone Mountain displacement transfer zone, west-central Nevada, *in* Oldow, J. S., and P. H. Cashman, eds., Late Cenozoic structure and evolution of the Great Basin-Sierra Nevada transition: Geological Society of America Special Paper 447, 215-253, doi: 10.1130/2009.2447(12).

Phillips, F. M., and L. Majkowski (2011), The role of low-angle normal faulting in active tectonics of the northern Owens Valley, California, *Lithosphere, 3*, 22-36, doi: 10.1130/L73.1.

Pigati, J. S., and N. A. Lifton (2004), Geomagnetic effects on time-integrated cosmogenic nuclide production with emphasis on in situ ^{14}C and ^{10}Be, *Earth and Planetary Science Letters, 226*, 193-205, doi: 10.1016/j.epsl.2004.07.031.

Reheis, M. C., J. C. Goodmacher, J. W. Harden, L. D. McFadden, T. K. Rockwell, R. R. Schroba, J. M. Sowers, J. M. Taylor, and E. M. Taylor (1995), Quaternary soils and dust deposition in southern Nevada and California, *Geological Society of America Bulletin, 107*, 1003-1022, doi: 10.1130/0016-7606(1995)107<1003:QSADDI>2.3.CO;2.

Reheis, M. C., and T. H. Dixon (1996), Kinematics of the eastern California shear zone: Evidence for slip transfer from Owens and Saline Valley fault zones to Fish Lake Valley fault zone, *Geology, 24*, 339-342, doi: 10.1130/0091-7613(1996)024<0339:KOTECS>2.3.CO;2.

Reheis, M. C., and T. L. Sawyer (1997), Late Cenozoic history and slip rates of the Fish Lake Valley, Emigrant Peak, and Deep Springs fault zones, Nevada and California, *Geological Society of America Bulletin, 109*, 280-299, doi: 10.1130/0016-7606(1997)109<0280:LCHASR>2.3.CO;2.

Reheis, M. C. (2006), A 16-year record of eolian dust in southern Nevada and California, USA: Controls on dust generation and accumulation, *Journal of Arid Environments, 67*, 487-520, doi: 10.1016/j.jaridenv.2006.03.006.

Ritter, J. B., J. R. Miller, Y. Enzel, S. D. Howes, G. Nadon, M. D. Grubb, K. A. Hoover, T. Olsen, S. L. Reneau, D. Sack, C. L. Summa, I. Taylor, K. C. N. Touysinhthiphonexay, E. G. Yodis, N. P. Schneider, D. F. Ritter, and S. G. Wells (1993), Quaternary evolution of Cedar Creek alluvial fan, Montana, *Geomorphology, 8*, 287-304, doi: 10.1016/0169-555X(93)90025-W.

Rockwell, T. K., S. Lindvall, M. Herzberg, D. Murbach, T. Dawson, and G. Berger (2000), Paleoseismology of the Johnson Valley, Kickapoo, and Homestead Valley faults: Clustering of earthquakes in the eastern California shear zone, *Bulletin of the Seismological Society of America, 90*, 1200-1236.

Savage, J. C., M. Lisowski, and W. H. Prescott (1990), An apparent shear zone trending north-northwest across the Mojave Desert into Owens Valley, California, *Geophysical Research Letters, 17*, 2113-2116, doi: 10.1029/GLO17i012p02113.

Scotti, O., A. Nur, and R. Estevez (1991), Distributed deformation and block rotation in three dimensions, *Journal of Geophysical Research, 96*, 12225-12243.

Sella, G. F., T. H. Dixon, and A. Mao (2002), REVEL: A model for recent plate velocities from space geodesy, *Journal of Geophysical Research, 107*, 2081, doi: 10.1029/2000JB000033.

Shen, Z. K., J. N. Lu, M. Wang, and R. Burgmann (2005), Contemporary crustal deformation around the southeast borderland of the Tibetan Plateau, *Journal of Geophysical Research, 110,* B11409, doi: 10.1029/2004JB003421.

Sieh, K. E., and R. H. Jahns (1984), Holocene activity of the San Andreas fault at Wallace Creek, California, *Geological Society of America Bulletin, 95,* 883-896, doi: 10.1130/0016-7606(1984)95<883:HAOTSA>2.0.CO;2.

Sieh, K. E., and 18 others (1993), Near-field investigations of the Landers earthquake sequence, April to July, 1992, *Science, 260*, 171-176.

Staiger, J., J. Gosse, R. Toracinta, B. Oglesby, J. Fastook, and J. V. Johnson (2007), Atmospheric scaling of cosmogenic nuclide production; climate effect, *Journal of Geophysical Research, 112,* B02205, doi: 10.1029/2005JB003811.

Stewart, J. H. (1988), Tectonics of the Walker Lane belt, western Great Basin: Mesozoic and Cenozoic deformation in a zone of shear, in Ernst, W. G., ed, *Metamorphism and Crustal Evolution, Rubey Volume VII*, 683-713, Prentice Hall, Englewood Cliffs.

Stockli, D. F., T. A. Dimitru, M. O. McWilliams, and K. A. Farley (2003), Cenozoic tectonic evolution of the White Mountains, California and Nevada, *Geological Society of America Bulletin, 115*, 788-816, doi: 10.1130/0016-7606(2003)115<0788:CTEOTW>2.0.CO;2.

Stone, J. O. (2000), Air pressure and cosmogenic isotope production, *Journal of Geophysical Research, 105,* 23753-23759, doi: 10.1029/2000JB900181.

Tincher, C. R., and D. F. Stockli (2009), Cenozoic volcanism and tectonics in the Queen Valley area, Esmeralda County, western Nevada, *in* Oldow, J. S., and P. H. Cashman eds., Late Cenozoic structure and evolution of the Great Basin- Sierra Nevada transition: Geological Society of America Special Paper 447, 255-274, doi: 10.1130/2009.2447(13).

Thatcher, W. (1995), Microplate versus continuum descriptions of active tectonic deformation, *Journal of Geophysical Research, 100*, 3885-3894.

Thatcher, W., G. R. Foulger, B. R. Julian, J. Svarc, E. Quilty, and G. W. Bawden (1999), Present-day deformation across the Basin and Range province, western United States, *Science, 283*, 1714-1718.

Thatcher, W. (2007), Microplate model for the present-day deformation of Tibet, *Journal of Geophysical Research, 112*, B01401, doi: 10.1029/2005JB004244.

Thatcher, W. (2009), How the continents deform: Evidence from tectonic geodesy, *Annual Review of Earth and Planetary Sciences, 37*, 237-262, doi: 10.1146/annurev.earth.031208.100035.

Wald, D. J., and T. H. Heaton (1994), Spatial and temporal distribution of slip for the 1992 Landers, California, earthquake, *Bulletin of the Seismological Society of America, 84*, 668-691.

Walker, J. D., E. Kirby, and J. E. Andrew (2005), Strain transfer and partitioning between the Panamint Valley, Searles Valley, and Ash Hill fault zones, California, *Geosphere, 1*, 111-118, doi: 10.1130/GES00014.1.

Weldon, R. J., K. M. Scharer, T. E. Fumal, G. Biasi (2004), Wrightwood and the earthquake cycle; what a long recurrence record tells us about how faults work, *GSA Today, 14*, 4-10.

Wernicke, B (1981), Low-angle normal faults in the Basin and Range Province: nappe tectonics in an extending orogen, *Nature, 291*, 645-648.

Wernicke, B., G. J. Axen, and J. K. Snow (1988), Basin and Range extensional tectonics at the latitude Las Vegas, Nevada, *Geological Society of America Bulletin, 100*, 1738-1757, doi: 10.1130/0016-7606(1988)100<1738:BARETA>2.3.CO;2.

Wernicke, B., and J. K. Snow (1998), Cenozoic tectonism in the central Basin and Range: Motion of the Sierran-Great Valley block, *International Geology Review, 40*, 403-410.

Wernicke, B., A. M. Friedrich, N. A. Niemi, R. A. Bennett, and J. L. Davis (2000), Dynamics of plate boundary fault systems from Basin and Range Geodetic Network (BARGEN) and geologic data, *GSA Today, 10*, 1-7.

Wernicke, B., J. L. Davis, N. A. Niemi, P. Luffi, and S. Bisnath (2008), Active megadetachment beneath the western United States, *Journal of Geophysical Research- Solid Earth, 113,* doi: 10.1029/2007B005375.

Wesnousky, S. G. (1988), Seismological and structural evolution of strike-slip faults, *Nature, 335,* 340-343.

Wesnousky, S. G. (1990), Seismicity as a function of cumulative geologic offset: Some observations from southern California, *Bulletin of the Seismological Society of America, 80,* 1374-1381.

Wesnousky, S. G. (2005a), Active faulting in the Walker Lane, *Tectonics, 24*, TC3009, doi: 10.1029/2004TC001645.

Wesnousky, S. G. (2005b), The San Andreas and Walker Lane fault systems, western North America: transpression, transtension, cumulative slip, and the structural evolution of a major transform plate boundary, *Journal of Structural Geology, 27*, 1505-1512.

Wilcox, R. E., T. P. Harding, and D. R. Seely (1973), Basic wrench tectonics, *American Association of Petroleum Geologists Bulletin, 57*, 74-96.

Wilson, C. W. (1975), Bouguer gravity map of Clayton Valley, Nevada, *United States Geological Survey Open-File Report, 75-333*.

Wright, L. A., and B. W. Troxel (1970), Summary of regional evidence for right-lateral displacement in the western Great Basin: Discussion, *Geological Society of America Bulletin, 81,* 2167-2174.

Yin, A (1989), Origin of regional, rooted low-angle normal faults: A mechanical model and its tectonic implications, *Tectonics, 8*, 469-482.

Zampirro, D. (2005), Hydrogeology of Clayton Valley brine deposits, Esmeralda County, Nevada, *The Professional Geologist, 42,* 46-54.

Zechar, J. D., and K. L. Frankel (2009), Incorporating and reporting uncertainties in fault slip rates, *Journal of Geophysical Research, 114*, B12407, doi: 10.1029/2009JB006325.